Reconstruction of the Holocene monsoon climate variability in the Arabian Sea based on alkenone sea surface temperature, primary productivity and denitrification proxies

Dissertation

zur Erlangung des Doktorgrades an der Fakultät für Mathematik, Informatik und Naturwissenschaften

Fachbereich Geowissenschaften

der Universität Hamburg

vorgelegt von

Anna Böll

aus

Hamburg

Hamburg, 2014

Tag der Disputation: 4. November 2014

Folgende Gutachter empfehlen die Annahme der Dissertation:

Prof. Dr. Kay-Christian Emeis

und

Dr. Birgit Gaye

Zusammenfassung

Der Indische Monsun beeinflusst weite Teile unserer Weltbevölkerung. Allerdings sind kurzfristige Monsunschwankungen auf für den Menschen relevanten Zeitskalen (Jahrzehnte bis Jahrhunderte) bisher wenig untersucht. Ziel dieser Arbeit ist es, holozäne Schwankungen in der Entwicklung des Sommer- und des Wintermonsuns in hoher Auflösung zu rekonstruieren. Hierfür wurden verschiedene Sedimentkerne aus unterschiedlichen Gebieten im Arabischen Meer analysiert. Die Ozeanographie des Arabischen Meeres und die dort vorherrschenden biogeochemischen Prozesse, wie Oberflächenwassertemperaturen (SST), Primärproduktion, Intensität der Zwischenwasser-Sauerstoffminimumzone sowie Denitrifizierung in der Wassersäule sind eng an den saisonalen Monsunzyklus gekoppelt.

Primärproduktion und SST im nordwestlichen Arabischen Meer werden hauptsächlich durch Auftriebsprozesse gesteuert, die mit dem Sommermonsun einhergehen, wohingegen niedrige SST und erhöhte Primärproduktion im nordöstlichen Arabischen Meer vor Pakistan an die nordöstlichen Winde des Wintermonsuns gekoppelt sind. In dieser Arbeit wurde ein fein laminierter Sedimentkern vom Pakistanischen Kontinentalhang genutzt, um die Intensität des Wintermonsuns während des späten Holozäns in hoher Auflösung zu rekonstruieren. Hierfür habe ich verschiedene Primärproduktions-Indikatoren (organischer Kohlenstoff, Karbonate/Opal, $\delta^{15}N$) sowie Alkenone zur Bestimmung von SST-Änderungen analysiert (Kapitel 3). Die rekonstruierten SST nehmen während der letzten 2400 Jahre ab, wohingegen die Primärproduktion zunimmt, was auf eine lang anhaltende Verstärkung des Wintermonsuns zurückzuführen ist. Ein Vergleich meiner Wintermonsun-Rekonstruktion mit Aufzeichnungen zur Sommermonsunaktivität zeigt, dass es in der asiatischen Monsunregion während des späten Holozäns einen inversen Zusammenhang zwischen Sommermonsunstärke und Wintermonsunintensität gegeben hat. Dieser Zusammenhang zwischen Sommer- und Wintermonsunaktivität wird höchstwahrscheinlich durch langfristige Verschiebungen in der Breitengradposition der Intertropischen Konvergenz Zone (ITCZ) verursacht, die wiederum durch Änderungen in der solaren Einstrahlung angetrieben werden.

Der Vergleich von zwei SST-Rekonstruktionen, die anhand von Alkenon-Analysen an einem Sedimentkern aus dem Sommermonsun dominierten nordwestlichen Arabischen Meer und an einem Sedimentkern aus dem vom Wintermonsun beeinflussten nordöstlichen Arabischen Meer durchgeführt wurden, zeigt, dass dieses antagonistische Verhalten von Sommer- und Wintermonsunstärke auch während der letzten 25000 Jahre existiert hat (Kapitel 4). Starker Auftrieb vor der Küste des nördlichen Oman spiegelt eine verstärkte

Aktivität des Sommermonsuns während des frühen Holozänen Klimaoptimums wider. Zeitgleich dazu lassen ansteigende SST vor Pakistan auf eine Abnahme der Wintermonsunstärke schließen. Die seit dem frühen Holozän einsetzende Verstärkung der Wintermonsunaktivität wurde höchst wahrscheinlich durch eine südwärts gerichtete Verschiebung der ITCZ angetrieben.

Die Alkenone-SST-Rekonstruktion des späten Holozäns aus dem nordöstlichen Arabischen Meer zeigt eine enge Korrelation zu den Klimaaufzeichnungen des asiatischen Kontinents und der höheren Breiten der Nordhemisphäre auf Zeitskalen von Jahrzehnten und Jahrhunderten. Dabei führen kältere Klimabedingungen, wie sie z. B. während der kleinen Eiszeit beobachtet wurden, zu einer Verstärkung der nordöstlichen Monsunwinde und zu einer Abnahme der SST im nordöstlichen Arabischen Meer.

Kapitel 5 befasst sich mit der zeitlichen und räumlichen Variabilität der Sauerstoffminimumzone (OMZ) im Arabischen Meer während des Holozäns. Weiterhin wurde der Zusammenhang zwischen OMZ-Intensität und Änderungen in der Monsunstärke untersucht. Hierfür wurde ein Sedimentkern vom Kontinentalhang vor Nord-Oman, der das späte und mittlere Holozän umfasst, auf unterschiedliche Indikatoren zur Zwischenwasser-Sauerstoffanreicherung und Südwestmonsunstärke analysiert. Der Vergleich meiner $\delta^{15}N$ und Mn/Al Daten mit anderen Datensätzen zur Denitrifizierung und Sauerstoffversorgung aus dem nördlichen Arabischen Meer zeigt, dass sich der Kern der OMZ während des Holozäns von Nordwestern (frühes Holozän) nach Nordosten (spätes Holozän) verlagert hat. Diese Verschiebung wird zum einem durch eine Reorganisation der Zwischenwasser-Zirkulation (Sauerstoffzufuhr) im nördlichen Arabischen Meer verursacht, die durch den Anstieg des Meeresspiegels hervorgerufen wurde. Hinzu kommen Änderungen in der Monsunintensität, die sich regional unterschiedlich auf die Primarproduktion (Sauerstoffbedarf) des Arabischen Meeres ausgewirkt haben.

Abstract

The Indian monsoon climate influences large parts of the world's population. But relatively little is known about its decadal to centennial scale variation at time scales of societal relevance. The aim of this study was to reconstruct the Holocene history of summer and winter monsoon variability in high-resolution by analyzing sediment cores from different locations in the Arabian Sea (northern Indian Ocean). Oceanic properties and biogeochemical processes in the Arabian Sea, such as sea surface temperature (SST), primary productivity and the intensity of the mid-water oxygen minimum zone and water column denitrification are closely coupled to the seasonal monsoon cycle.

While primary productivity and SST in the northwestern Arabian Sea are mainly impacted by upwelling processes associated with the summer monsoon, in the northeastern Arabian Sea off Pakistan low SST and high primary productivity are driven by the northeasterly winds of the winter monsoon. Based on this modern setting, I analyzed alkenone-derived SST changes together with proxies of primary productivity (organic carbon, carbonate/opal, $\delta^{15}N$) in a well-laminated sediment core from the Pakistan continental margin to establish a high-resolution record of winter monsoon strength for the late Holocene (chapter 3). Over the last 2400 years reconstructed SST decreased whereas productivity increased, reflecting a long-term trend of winter monsoon strengthening. A comparison of my winter monsoon record with records of summer monsoon strength shows that an inverse relationship of summer and winter monsoon strength exists in the Asian monsoon region over the late Holocene. The linked variation of summer and winter monsoon strength most likely was caused by shifts in the long-term latitudinal position of the Intertropical Convergence Zone (ITCZ), forced by changes in solar output.

Reconstruction and comparison of alkenone-derived SST patterns from two sediment cores, one from the summer monsoon dominated northwestern Arabian Sea and one from the winter monsoon influenced northeastern Arabian Sea, reveal that this antagonistic behavior of summer and winter monsoon strength was also evident over the last 25,000 years (chapter 4). Strong upwelling at the coast of northern Oman reflects intensified summer monsoon activity during the early Holocene climate optimum, contemporaneous with a decline in winter monsoon strength as indicated by increasing SST off Pakistan. Strengthening of winter monsoon activity since the early Holocene was forced by a southward displacement of the ITCZ throughout the Holocene.

The late Holocene alkenone-based SST record from the northeastern Arabian Sea shows a close correlation to decadal to centennial scale climate variability recorded on the Asian continent and the high-latitude Northern Hemisphere. Colder climate conditions (as observed during the Little Ice Age) increase the strength of northeast monsoonal winds and lower SST in the northeastern Arabian Sea.

Chapter 5 deals with the temporal and spatial variability of the Arabian Sea oxygen minimum zone (OMZ) over the Holocene and its relation to varying monsoon strength. Proxies of mid-water oxygenation and southwest monsoon strength were analyzed in a sediment core from the northern Oman Margin representing the late and mid Holocene. The comparison of my $\delta^{15}N$ and Mn/Al records with other records of denitrification and oxygenation from the northern Arabian Sea shows that the location of the core OMZ has shifted from the northwest (early Holocene) to the northeast (late Holocene) throughout the Holocene. This shift was caused by a reorganization of mid-water circulation (oxygen supply) in the northern Arabian Sea due to sea level rise together with spatial differences in the response of primary productivity (oxygen demand) to varying monsoon activity.

Table of contents

CHAPTER 1

1. Introduction

1.1. The Indian monsoon system

The Indian monsoon is a major component of our global climate system that affects large parts of the world's population. In the monsoon region almost 80% of the total annual precipitation is supplied during the summer monsoon season with far-reaching consequences for the environment, economy and society of southern and southeast Asia. Variations in the onset of summer monsoon rains but also in the amount of precipitation can seriously affect the livelihood of people living in countries influenced by a monsoon climate (e.g., Clift and Plumb, 2008). Thus, it is important to understand the controls of the monsoon and how it has changed in the past.

The monsoon circulation is driven by solar triggered differential heating of land and ocean and the resultant development of atmospheric pressure gradients. Increased solar insolation in spring forces the Asian continent to heat faster than the Indian Ocean due to differences in heat capacity and specific heat of water and land (Webster, 1987). The warm air over the continent starts to rise and a low atmospheric pressure cell develops over the continent and a cell of high pressure over the southern Indian Ocean, marking the onset of the summer monsoon with low-level winds blowing from the southwest (SW) (Figure 1.1a). Near the equator the low-level trade winds converge into a band of low pressure, forming the Intertropical Convergence Zone (ITCZ) that shifts seasonally with the course of the sun. Northward migration of the ITCZ at the beginning of the summer monsoon supplies moisture from the Indian Ocean to the Asian continent where it causes heavy rainfall. The cross-equatorial monsoon circulation and rainfall pattern are further strengthened by the orography and high elevation of the Himalayan mountains (Prell and Kutzbach, 1992). In boreal winter

the atmospheric pressure gradient reverses due to low solar insolation and faster cooling of the Asian continent than the southern Indian Ocean. The ITCZ migrates to the south and dry, continental, north-easterly winds prevail over large parts of India and the northern Indian Ocean (Figure 1.2b).
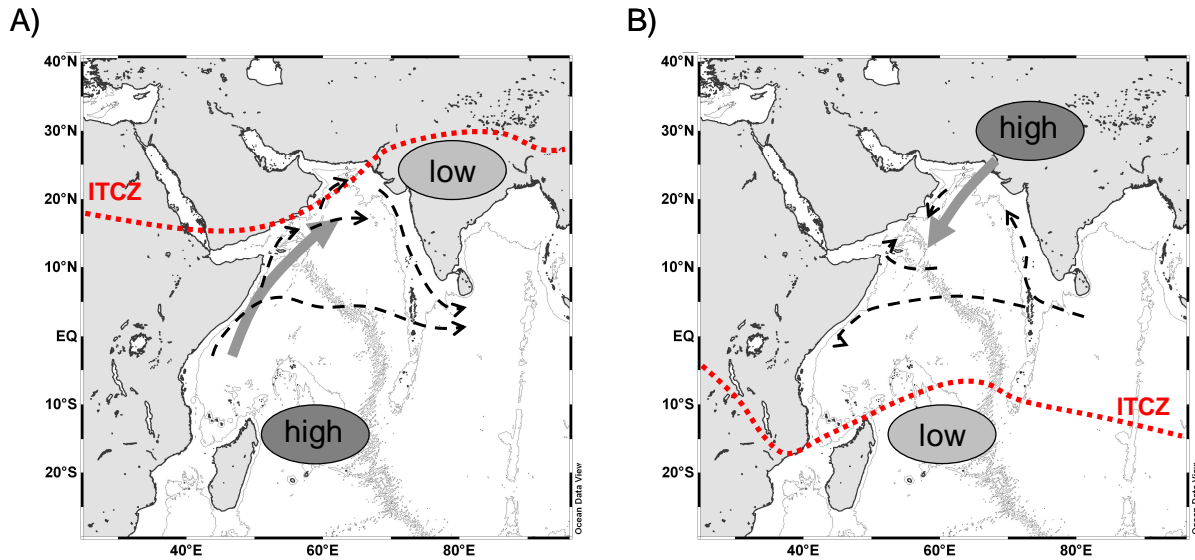

Figure 1.1: The Indian monsoon system during (a) Northern Hemisphere summer and (b) Northern Hemisphere winter. Differences in atmospheric pressure force an annual reversal of low-level winds (gray arrows) and seasonal shifts in the Intertropical Convergence Zone (red dotted line). This drives the seasonal reversal of surface circulation in the Arabian Sea (dashed black arrows; redrawn from Schott and McCreary (2001)).

1.2. The northern Arabian Sea and the seasonal monsoon cycle

The Arabian Sea is a semi-enclosed oceanic basin in the northern Indian Ocean, bordered by the African continent in the west, the Arabian Peninsula in the north and Pakistan and India in the east. Oceanic properties and biogeochemical processes in the Arabian Sea are closely coupled to the seasonal monsoon cycle. The south-westerly winds of the summer monsoon cause that the surface circulation in the Arabian Sea is clockwise during summer while it reverses; now being anti-clockwise, during the northeast monsoon in winter (Figure 1.1). The main monsoon driven oceanic properties of the Arabian Sea will be described below.

Sea surface temperature – Sea surface temperature (SST) changes in the northern Arabian Sea are mainly governed by upwelling processes in summer and convective mixing in winter (Figures 1.2a and 1.2c). The summer low-level jet stream over the northwestern

(NW) Arabian Sea (Findlater Jet; Findlater, 1969) induces upwelling of cold and nutrient rich waters along the coast of Somalia and Oman, so that SST in this region is low from July to August (Hastenrath and Lamb, 1979). While the northeastern (NE) Arabian Sea is not influenced by upwelling processes and SST remains warm during summer, low solar insolation together with enhanced evaporation due to dry and continental winds from the northeast cause convective deepening of the mixed layer and sea surface cooling off Pakistan during the winter monsoon season (Prasanna Kumar and Prasad, 1996).

Primary productivity – The Arabian Sea is one of the most productive oceanic regions worldwide. Primary productivity is highly seasonal and closely coupled to the seasonal monsoon cycle (Figures 1.2b and 1.2d). In the coastal region of the NW Arabian Sea primary production is elevated during the summer monsoon, when upwelling of mid-waters associated to south-westerly winds provides nutrients to fuel high rates of biological productivity. Sediment trap studies from this region show that particle fluxes reach values of up to 600 mg m^{-2} day^{-1} from June to September (Haake et al., 1993; Nair et al., 1989; Rixen et al., 1996). In the NE Arabian Sea, on the other hand, primary productivity is most pronounced during the winter monsoon (Banse and McClain, 1986; Madhupratap et al., 1996). This second peak in primary productivity is supported by the additional supply of nutrients into the euphotic zone through convective winter mixing.

Oxygen minimum zone – High rates of primary production and the subsequent oxygen-consuming mineralization of sinking organic matter together with sluggish intermediate water circulation (and thus low oxygen supply) favor a stable mid-water oxygen minimum zone (OMZ) between 200 and 1200 m water depth in the northern Arabian Sea (e.g., Olson et al., 1993). Although primary productivity is highest in the NW Arabian Sea, oxygen concentrations at intermediate water depth are lowest in the NE basin due to the inflow of saline and warm water masses from the Red Sea and Persian Gulf and resultant weak ventilation of the NE Arabian Sea.

Nitrogen cycle – Stable and year-round oxygen deficient conditions at intermediate water depth make the Arabian Sea to one of the major denitrification regions of the world ocean (Bange et al., 2000; Bulow et al., 2010; Ward et al., 2009). Denitrification reduces nitrate (NO_3^-) to nitrite (NO_2^-) and gaseous nitrogen (N_2) and thus accounts for the main loss of fixed nitrogen from the biosphere with implications for carbon cycling and the biological pump (Altabet et al., 2002). The Arabian Sea, furthermore, contributes to the oceanic loss of nitrous oxide (N_2O) to the atmosphere since N_2O, an important green house gas, is produced as a by-product of denitrification (Bange et al., 2001). Overall, nitrogen cycling in the

Arabian Sea is primarily dominated by denitrification (nitrogen loss) and advective input of nitrogen from the south (major nitrogen source) (Bange et al., 2000).
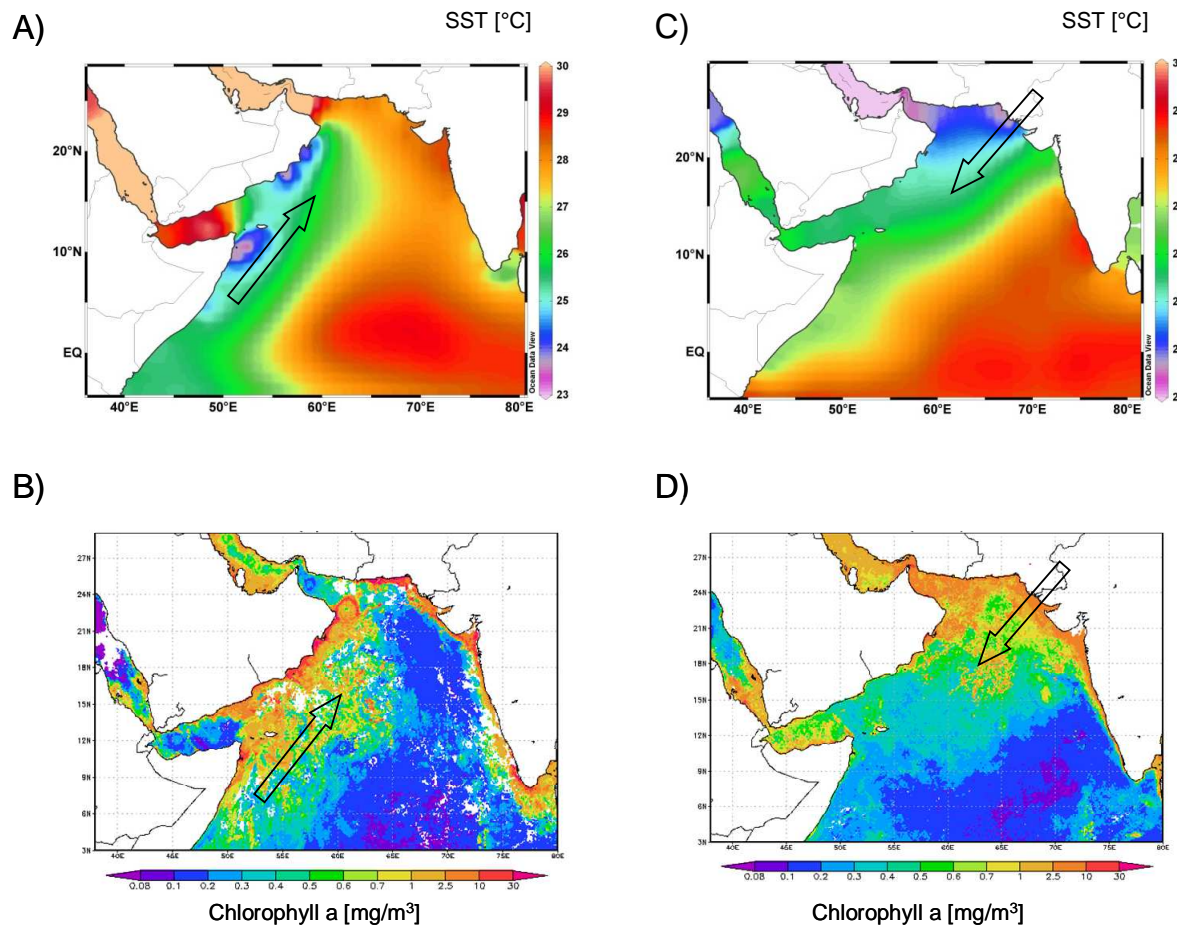

Figure 1.2: Sea surface temperature (SST) and primary productivity in the northern Arabian Sea during summer (left panels) and winter monsoon (right panels), respectively. SST data are obtained from the World Ocean Atlas 2009 (Locarnini et al., 2010). Primary productivity changes are indicated by the chlorophyll a distribution (satellite observations, available from http://gdata1.sci.gsfc.nasa.gov/daac-bin/G3/gui.cgi?instance_id=ocean _month). Black arrows indicate prevailing wind directions.

1.3. Past climate variability and the Indian monsoon system

The strength of the Indian monsoon system was not stable through time but changed in line with past global climate variability. Past changes in the Earth climate, such as the occurrence of glacial/interglacial cycles, were triggered by changes in the seasonal distribution of solar radiation driven by long-term variations in the Earth's orbit (eccentricity, obliquity and precession), known as Milankovitch cycles. Glaciation of the Northern

Hemisphere high-latitudes due to varying solar radiation has also affected the intensity of the Indian summer monsoon through internal climate feedback mechanisms including snow cover, surface albedo, land-sea thermal contrast and the long-term position of the ITCZ (Figure 1.3). Thus, monsoon strength has varied on glacial/interglacial cycles as a response to changes in Northern Hemisphere solar insolation and glacial boundary conditions (Clemens et al., 1991; Prell and Kutzbach, 1992). Climate over the last 100 kyrs fluctuated not only on orbital time scales, but exhibits several abrupt warming events (Dansgaard-Oeschger events) that were followed by more gradual cooling (Heinrich event) on sub-orbital time scales (Dansgaard et al., 1993), and that were also reflected in the intensity of the Indian summer monsoon.
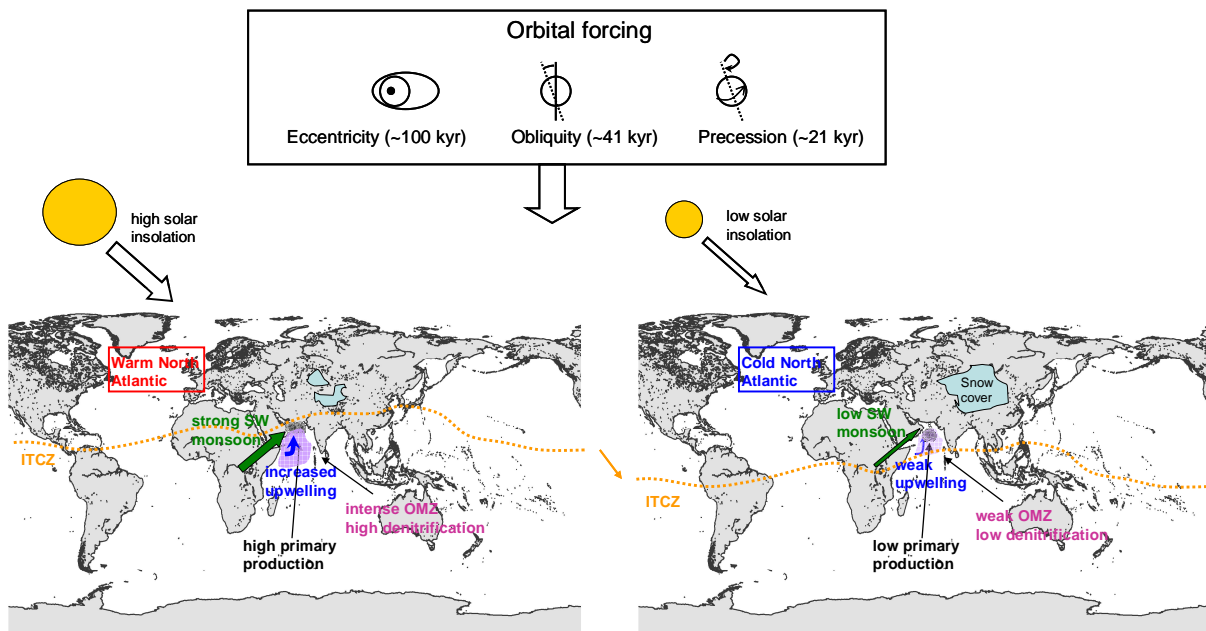

Figure 1.3: Simplified overview of climate variability in the Arabian Sea region as a function of changing solar radiation driven by long-term variations in the Earth's orbit.

Summer monsoon intensity over southern Asia was strengthened during periods of high solar insolation and warm climate conditions on the Northern Hemisphere (interglacial, interstadial), while times of low solar insolation and relatively colder climate on the Northern Hemisphere (glacial, stadial) were linked to weak summer monsoon winds (Clemens and Prell, 1990; Schulz et al., 1998). Strong SW monsoonal winds have driven intense upwelling, high primary production and a pronounced OMZ and elevated denitrification in the Arabian

Sea over interglacial and interstadial periods (e.g., Emeis et al., 1995; Reichart et al., 1998; Rostek et al., 1997). On the other hand, denitrification was nearly absent (Altabet et al., 1999; Suthhof et al., 2001) and primary production was low during glacial and stadial periods (Figure 1.3).

Recent studies have further shown that Holocene climate was far from stable: Centennial scale variations in the Asian summer monsoon seem to be linked to cold, ice-rafting events in the North Atlantic ('Bond event'; Bond et al., 2001) that occurred with a cyclicity of about 1500 years (Gupta et al., 2003; Hong et al., 2003). The initial forcing for the centennial to decadal scale climate fluctuations over the Holocene is still unclear but may be related to solar activity associated with sunspot cycles (Bond et al., 2001; Neff et al., 2001).

1.4. Arabian Sea sediments – a recorder for monsoon variability

Arabian Sea sediments provide a unique climate archive of past monsoon variability. The composition of sediments records the environmental and climate conditions that prevailed during their deposition. Elevated (monsoon driven) primary productivity and a pronounced OMZ cause high sedimentation rates and well preserved sediments at the continental margins that enable the reconstruction of monsoon strength at decadal to centennial scale resolution. To reconstruct past variations in the oceanic environment of the Arabian Sea, I used different sediment cores (Table 1.1) and analyzed different paleoceanographic proxies, which are described below (Figure 1.4).

1.4.1. Alkenones as an indicator for sea surface temperature variations

Long-chain alkenones (C_{37}-C_{39}), synthesized by haptophyte algae, provide a well-established proxy to estimate present and past sea surface temperatures in the ocean (Brassell et al., 1986; Prahl and Wakeham, 1987). The alkenone-SST proxy is based on the ratio of di- and tri-unsaturated C_{37}-alkenones that changes as a function of growth temperature. The alkenone-producing coccolithophorids *Emiliania huxleyi* and *Geophyrocapsa oceanica* respond to an increase of growth temperature by producing relatively higher amounts of di-unsaturated C_{37}-alkenones, which is expressed in the alkenone unsaturation index $U_{37}^{K'} = C_{37:2}/(C_{37:2} + C_{37:3})$. The $U_{37}^{K'}$-SST relationship can vary between oceanic regions and is determined through culture, water column and sediment core top calibrations (Herbert, 2003). For this PhD thesis, I used a sediment core top calibration from the Indian Ocean (Sonzogni et

al., 1997b) to translate the $U_{37}^{K'}$-index to sea surface temperature (SST = ($U_{37}^{K'}$-0.043)/0.033)). In Arabian Sea sediments alkenones reflect an annual mean temperature signal of the upper mixed layer (Sonzogni et al., 1997b).

1.4.2. The estimation of primary productivity changes

Several approaches exist to reconstruct past changes in oceanic primary production (contents and fluxes of biogenic remnants, organic marker molecules, elements like Ba, Cd, Cu, species composition of phytoplankton, proxies of surface nutrient concentrations), each on them having their own limitations and advantages (Berger et al., 1994). Applicability of the respective primary productivity proxies strongly depend on the studied oceanic region and the prevailing environmental conditions.

One direct indicator of primary productivity is based on the production of organic matter by phytoplankton growth under the availability of nutrients and light at the sea surface and the subsequent flow of particulate organic matter through the water column to the seafloor. However, only a small fraction of the organic matter produced by phytoplankton is preserved in marine sediments. The content of organic matter that is buried in marine sediments is further influenced by organic matter remineralization in the water column and sediment-water interface and by its preservation in the sediments; both processes primarily being a function of oxygen availability and sedimentation rate (Müller and Suess, 1979; Paropkari et al., 1992). Nevertheless, sedimentary contents and fluxes of biogenic components, such as organic carbon, opal and carbonate, trace past variations in primary productivity in the highly productive and oxygen poor waters of the Arabian Sea (e.g., Emeis et al., 1995; Schulz et al., 1998).

1.4.3. Stable nitrogen isotopes

Nitrogen consists of the two stable isotopes ^{14}N and ^{15}N that occur with an natural abundance of 99.64% and 0.36%, respectively (Hoefs, 2009). The ratio of the two stable isotopes of nitrogen ($^{15}N/^{14}N$) is expressed as $\delta^{15}N$, which is given as the per mil difference from the N-isotope composition of atmospheric N_2 that has a $\delta^{15}N$ values of 0‰: $\delta^{15}N$ = [(R_{Sample}-$R_{Standard}$)/$R_{Standard}$)]*1000, where R_{Sample} is the $^{15}N/^{14}N$ ratio of the sample and $R_{Standard}$ is the $^{15}N/^{14}N$ ratio of atmospheric N_2.

Incomplete transformation of nitrogen in the marine nitrogen cycle (including nitrogen fixation, ammonium and nitrate assimilation, ammonification, nitrification, denitrification, anammox) is often associated with a kinetic fractionation of stable nitrogen isotopes because marine organisms usually prefer the lighter stable isotope ^{14}N over the heavier ^{15}N isotope. Thus, measurements of $\delta^{15}N$ are used to study fluxes and processes in the marine nitrogen cycle (e.g., Ganeshram et al., 2000; Gaye et al., 2013; Naqvi et al., 1998). In this study, sedimentary $\delta^{15}N$ is used as a tracer for denitrification that primarily reflects the intensity of the OMZ. In oxygenated waters of the open ocean nitrate has an average $\delta^{15}N$ value of about 5‰ (Sigman et al., 2000). Under low oxygen concentrations denitrification fractionates nitrogen isotopes leaving the remaining nitrate enriched in $\delta^{15}N$. This isotopically enriched nitrate is transported into the euphotic zone via upwelling and mixing, gets assimilated by phytoplankton uptake and sinks to the seafloor, enhancing the $\delta^{15}N$ signature of marine sediments (Altabet et al., 1995; Naqvi et al., 1998).
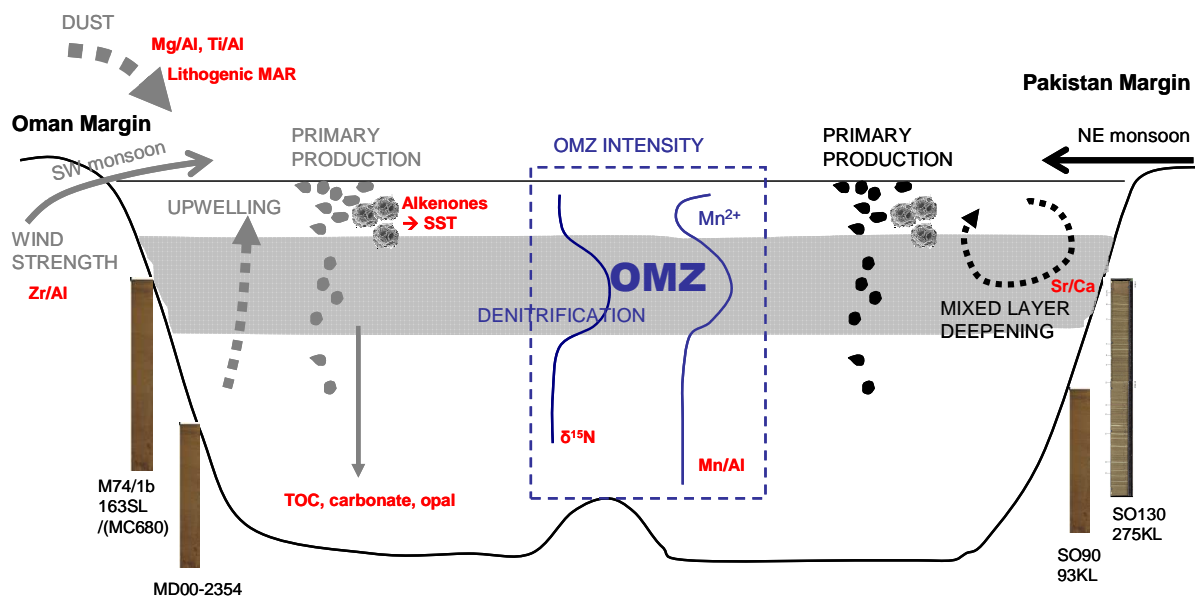

Figure 1.4: Overview of the different paleo-proxies (red) that are used in this study to reconstruct monsoon driven processes in the northern Arabian Sea. Processes that are mainly driven by the SW monsoon are illustrated in gray (Oman Margin) and NE monsoon induced processes are marked in black (Pakistan Margin). Biogeochemical processes related to oxygen minimum zone intensity are shown in blue. Further shown is the location of sediment cores that are investigated in this study.

1.4.4. Elemental composition of sediments

Most of the major and trace metals in the ocean are involved in biogeochemical cycles and thus provide information about the climatic and oceanic processes they are linked to. The elemental composition of sediments is often expressed as the element to aluminium ratio in order to account for possible dilution with $CaCO_3$. In Arabian Sea sediments major and trace elements can be attributed to mainly three sources and thus can be used as provenance indicators: (1) terrigenous sources (eolian and fluviatil), (2) biogenic carbonates and (3) primary productivity (Reichart et al., 1997; Shimmield and Mowbray, 1991; Sirocko et al., 2000). Elements such as Mn, Mo and V are further sensitive to redox processes that occur at the boundary of the OMZ and trace changes in the Arabian Sea oxygen minimum zone (e.g., Reichart et al., 2002b; Suthhof et al., 2001). In this study, I used the elemental composition of sediments to gain information about past variations in dust input (Mg/Al, Ti/Al), monsoon wind strength (Zr/Al), OMZ intensity (Mn/Al) and winter mixing (Sr/Ca). A detailed description of the respective element indicator is given in chapters 3 and 5.

Table 1.1: Basic information of the sediment cores investigated in this study.

Core	Latitude N°	Longitude E°	water depth [m]	depth interval [cm]	time period [yrs BP]	Resolution [yrs]
SO90-39KG	24°50.01	65°55.01	695	15	-38 - 56	6-8
SO130-275KL	24°49.31	65°54.60	782	188	60 - 2400	5-80
SO90-93KL	23°35	64°13	1802	245	1000 - 24 600	~100
M74/1b-163SL	21°55.97	59°48.15	650	400	160 - 2700	100-300
					5700 - 8000	10-50
MD00-2354	21°02.55	61°28.51	2740	400	1300 - 24 900	100-300
MC680	22°37.16	59°41.50	789	50	80 - 1000	25 -150
					5700 - 6100	60 - 120

KG = box core, KL = piston core, SL = gravity core, MC = multicorer

CHAPTER 2

2. Project, objectives and thesis outline

Project - The research presented in this PhD thesis is part of the BMBF funded Research Unit CARIMA (Natural versus anthropogenic controls of past monsoon variability in central Asia recorded in marine archives) that involves five German and one Indian Research Groups. As a subproject of the research program CAME (Central Asia and Tibet: Monsoon dynamics and geo-ecosystems), CARIMA provides the 'marine part' of CAME by studying monsoon impacts on the marine environment. The main aim of CARIMA is to quantify the natural monsoon variability at inter-annual to centennial time scales over the Holocene to gain a better understanding of monsoon dynamics at time scales of societal relevance. In my study, I used different sediment cores from two regions in the Arabian Sea that are differentially impacted by the SW and NE monsoon as unique monsoon archives. I analyzed and reconstructed monsoon driven oceanic processes such as primary productivity, upwelling and winter mixing, denitrification and OMZ intensity and the input of lithogenic material to Arabian Sea sediments.

Objectives – The key objectives that are addressed in this dissertation are the following:

- I aim to investigate and reconstruct monsoon variability over the late Holocene (last 2000 years) in high-resolution. Therefore, I reconstructed SST and primary productivity variations that are mainly driven by changing NE monsoon activity on the Pakistan continental margin (chapter 3).

- Past variations in summer and winter monsoon strength revealed an antagonistic relationship over glacial/interglacial and stadial/interstadial cycles (Rostek et al., 1997; Schulte and Müller, 2001; Schulz et al., 1998). I aim to disentangle signals of SW and NE monsoon in order to investigate if this antagonistic relationship of summer and winter monsoon strength has also existed throughout the Holocene (chapters 3 and 4).

- Past studies have shown that the monsoon was impacted by North Atlantic climate change over sub-Milankovitch time scales (Gupta et al., 2003; Schulz et al., 1998). I aim to investigate if centennial scale changes in monsoon activity over the Arabian Sea were also linked to Northern Hemisphere climate change over the last 2000 years (chapters 3 and 4).

- I will discuss possible forcing mechanisms (solar activity, position of the ITCZ) that link SW and NE monsoon strength on the one hand, and monsoon activity to global climate variability on the other hand (chapters 3 and 4).

- Future climate scenarios predict a strengthening SW monsoon and resultant enhancement of primary production in the Arabian Sea under global warming conditions (Goes et al., 2005). This scenario implies an expanding OMZ with possible feedback mechanisms for global climate change through N_2O emissions. In this context, I aim to investigate the past variability and spatial extension of the Arabian Sea OMZ and its relation to short-term (decadal to centennial scale) fluctuations of monsoon intensity over the Holocene (chapter 5).

Thesis outline – The following chapters present the results of this PhD thesis and correspond to 3 manuscripts that are accepted in, submitted to or will be submitted to peer-reviewed scientific journals.

Chapter 3

Late Holocene primary productivity and sea surface temperature variations: implications for winter monsoon variability

Böll, A., Lückge, A., Munz, P., Forke, S., Schulz, H., Ramaswamy, V., Rixen, T., Gaye, B., Emeis, K.-C. (Paleoceanography 29, 778-794. doi:10.1002/2013PA002579)

Chapter 4

Contrasting sea surface temperature of summer and winter monsoon variability in the northern Arabian Sea over the last 25 ka

Böll, A., Schulz, H., Munz, P., Rixen, T., Gaye, B., Emeis, K.–C. (submitted to Palaeogeography, Palaeoclimatology, Palaeoecology)

Chapter 5

Spatial and temporal variability of the Arabian Sea oxygen minimum zone over the Holocene

Böll, A., Munz, P., Lückge, A., Schulz, H., Gaye, B., Emeis, K.-C. (submitted to Quaternary Science Reviews)

CHAPTER 3

3. Late Holocene primary productivity and sea surface temperature variations: implications for winter monsoon variability

Abstract

Variability in the oceanic environment of the Arabian Sea region is strongly influenced by the seasonal monsoon cycle of alternating wind directions. Prominent and well studied is the summer monsoon, but much less is known about late Holocene changes in winter monsoon strength with winds from the northeast that drive convective mixing and high surface ocean productivity in the northeastern Arabian Sea. To establish a high-resolution record of winter monsoon variability for the late Holocene, we analyzed alkenone-derived sea surface temperature (SST) variations and proxies of primary productivity (organic carbon and $\delta^{15}N$) in a well-laminated sediment core from the Pakistan continental margin. Weak winter monsoon intensities off Pakistan are indicated from 400 B.C. to 250 A.D. by reduced productivity and relatively high SST. At about 250 A.D., the intensity of the winter monsoon increased off Pakistan as indicated by a trend to lower SST. We infer that monsoon conditions were relatively unstable from ~500 to 1300 A.D., because primary production and SST were highly variable. Declining SST and elevated biological production from 1400 to 1900 A.D. suggest invigorated convective winter mixing by strengthening winter monsoon circulation, most likely a regional expression of colder climate conditions during the Little Ice Age on the Northern Hemisphere. The comparison of winter monsoon intensity with records of summer monsoon intensity suggests that an inverse relationship between summer and winter monsoon strength exists in the Asian monsoon system during the late Holocene, effected by shifts in the Intertropical Convergence Zone.

3.1. Introduction

The Asian monsoon system is one of the most important components of global climate. Although variations in the Asian monsoon have a great impact on climatological and biogeochemical processes in the ocean as well as on land, there are yet few high-resolution studies recording monsoon variability during the last 2000 years. One opportunity to establish such high-resolution records of late Holocene climate change comes from laminated sediments deposited on the Makran continental margin in the northeastern Arabian Sea (Doose-Rolinski et al., 2001; Lückge et al., 2001; von Rad et al., 1999a).

Primary productivity in the Arabian Sea is high and is tightly linked to the seasonal dynamics of the Asian monsoon system. Forced by reversing atmospheric pressure gradients between central Asia and the southern Indian Ocean and accompanied by shifts in the Intertropical Convergence Zone (ITCZ) (Clemens et al., 1991), low-level winds reverse direction in the course of the year. Strong south-westerly winds during the summer months caused by differential land-ocean heating in spring (Hastenrath and Lamb, 1979) induce clockwise surface water circulation in the Arabian Sea. As a consequence, upwelling of nutrient-rich waters along the coast off Somalia, Oman, and southwest India supports high biological productivity during the months June to September (Haake et al., 1993; Nair et al., 1989; Rixen et al., 1996). A secondary primary productivity peak in the northern basin is initiated when the wind direction reverses due to faster cooling of the continent in fall (Rixen et al., 2005). Prevailing moderate and dry north-easterly winds in winter drive a counterclockwise surface circulation and cool Arabian Sea surface waters (Wyrtki, 1973), thereby initiating convective winter mixing that provides nutrients for seasonally and regionally enhanced biological productivity (Banse and McClain, 1986; Madhupratap et al., 1996).

Whereas most sediment trap studies in the central Arabian Sea indeed indicate highest biological productivity during the summer monsoon (Broerse et al., 2000; Prahl et al., 2000; Wakeham et al., 2002); highest particle fluxes in the northeastern Arabian Sea are observed during the winter monsoon season (Andruleit et al., 2000; Lückge et al., 2002; Rixen et al., 2005; Schulz et al., 2002b) and are associated with sea surface cooling down to about 23°C. Hence, periods of low sea surface temperatures (SSTs) in the northeastern Arabian Sea are linked to the cool northeast monsoonal winds during winter.

We know today that monsoon activity varied not only on Milankovitch time scales but also during the late Holocene, as evident in Arabian Sea sediments (Agnihotri et al., 2008; Anderson et al., 2010, 2002; Chauhan et al., 2010; Gupta et al., 2011, 2003; Lückge et al.,

2001; von Rad et al., 1999a) and in various cave records from Oman (Burns et al., 2002; Fleitmann et al., 2004), Yemen (Van Rampelbergh et al., 2013), India (Berkelhammer et al., 2010; Sinha et al., 2011b, 2007), and China (Zhang et al., 2008). Similarly, primary productivity in the Arabian Sea was not uniform on time scales of a few hundred thousand years but tracked monsoon variations caused by glacial/interglacial cycles (Rostek et al., 1997; Schulte and Müller, 2001; Schulte et al., 1999; Schulz et al., 1998). Although some knowledge exists about summer monsoon related changes in primary productivity over the last 2000 years from the Oman Margin (Anderson et al., 2010, 2002; Gupta et al., 2003) and the southwestern coast off India (Agnihotri et al., 2008), paleoceanographic responses to late Holocene winter monsoon variability in the northeastern Arabian Sea are unknown.
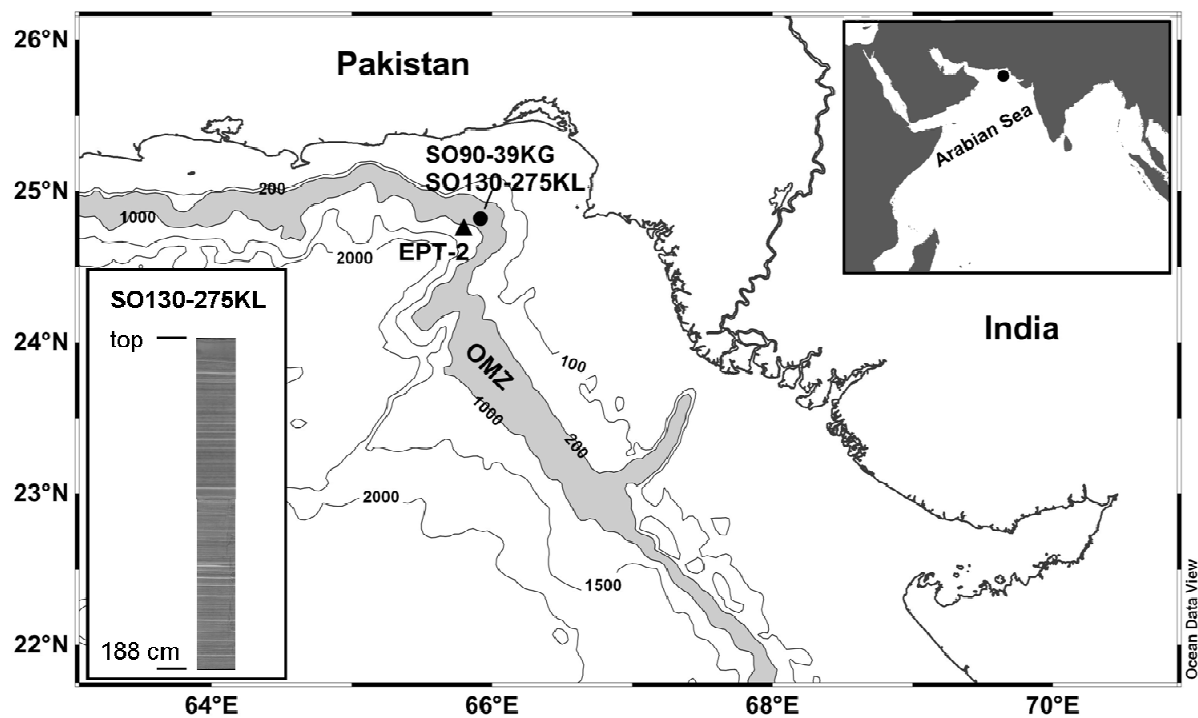
Figure 3.1: Study area in the northeastern Arabian Sea off Pakistan with core locations 275KL and 39KG and sediment trap station EPT-2. The shaded area indicates OMZ impinging on the continental slope. Bathymetry is shown in meters. Inset: vertical profile of core 275KL showing varve-like lamination. This map is produced by using Ocean Data View (Schlitzer, 2013).

Here we report a high-resolution record of winter monsoon variability for the late Holocene discerned from changes in primary productivity and sea surface temperature for the mainly winter monsoon dominated northeastern Arabian Sea. We analyzed a 188 cm long section of a well-laminated sediment core from the Pakistan Margin (Figure 3.1) for bulk

components (organic carbon, carbonate, and opal), stable nitrogen isotopes, and alkenone unsaturation ratios to reconstruct the productivity and monsoon variability throughout the last 2400 years. A key proxy for the winter monsoon intensity is the alkenone-derived SST estimate, which we validate by analyzing the seasonality of the alkenone-based SST signal at eastern PAKOMIN sediment trap station (EPT-2) close to our core location. Our detailed objectives are to (1) examine the relationship between SST and alkenone unsaturation ratios in sediment trap material for the northeastern Arabian Sea, (2) reconstruct late Holocene (winter monsoon dominated) SST and paleoproductivity changes for the northeastern Arabian Sea, (3) compare the winter monsoon dominated record with records of summer monsoon variability to learn about the dynamics of the monsoon low-level wind system, and (4) examine possible links in the regional wind and surface ocean system to Northern Hemisphere climate change in historical time.

3.2. Study Area

Unlike offshore the coast of Somalia, Oman, and southeast India, upwelling does not occur during the southwest (SW) monsoon season on the Pakistan Margin, so that SSTs are warm during summer (27.8 to 29.3°C). In the northeastern Arabian Sea, high productivity during the SW monsoon in summer is partly supported by the lateral advection of nutrient-rich surface waters from the upwelling area off Oman (Schulz et al., 1996). Cool winter SSTs (~23°C) during the northeast (NE) monsoon season are accompanied by a deepening of the mixed layer through convective mixing (Figure 3.2) that stimulates a second peak in primary production (Banse and McClain, 1986; Madhupratap et al., 1996). During this season reduced solar insolation together with enhanced evaporation lead to density increase of surface waters and convective deepening of the mixed layer over the Pakistan Margin. Concentrations of nitrate and chlorophyll *a* and primary production in the surface layer here correlate with mixed layer depth and wind speeds (Madhupratap et al., 1996; Prasanna Kumar and Prasad, 1996; Prasanna Kumar et al., 2001). Increased particle fluxes during the months of January and February indicate even higher production during the NE monsoon season than during the SW monsoon season over the Pakistan Margin (Andruleit et al., 2000; Schulz et al., 2002b; see Figure 3.2).

In the northern Arabian Sea, a stable mid-water oxygen minimum zone (OMZ) between 200 and 1200 m water depth is maintained by high organic matter (OM) fluxes and subsequent oxygen consumption during mineralization of organic matter, combined with

reduced vertical mixing caused by the input of warm, saline water masses from the Persian Gulf and the Red Sea to intermediate water depths (Olson et al., 1993; Schulz et al., 1996). High organic matter fluxes from the euphotic zone raise rates of denitrification in the OMZ, which in turn raise the $\delta^{15}N$ values of thermocline nitrate mixed into the surface layer and assimilated by phytoplankton. Intensification of the OMZ thus results in high sedimentary $\delta^{15}N$ values upon burial of particulate N, whereas weakening of the OMZ and reduced denitrification intensity lead to low sedimentary $\delta^{15}N$ values (e.g., Altabet et al., 1995; Gaye-Haake et al., 2005; Naqvi et al., 1998; Suthhof et al., 2001).
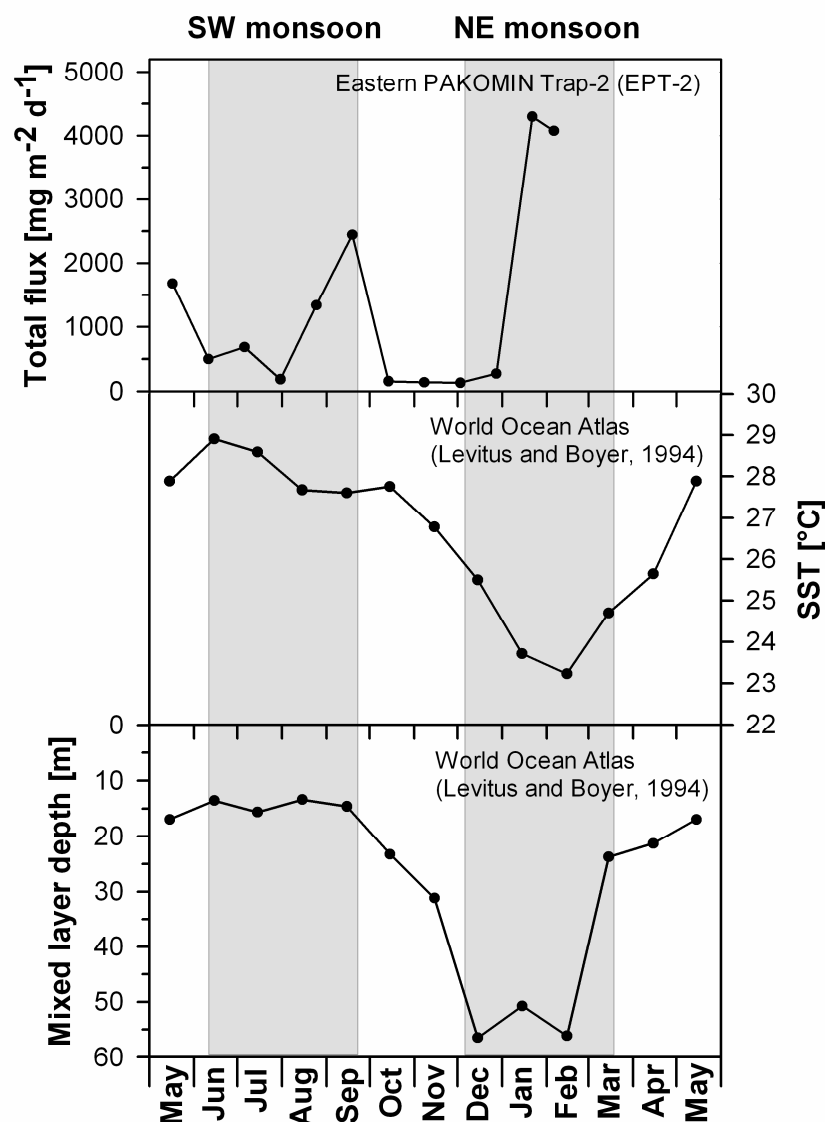
Figure 3.2: Annual variability of mixed layer depth and SST for site 275KL extracted from the World Ocean Atlas (Levitus and Boyer, 1994) and total particle flux measured in sediment trap EPT-2 after Andruleit et al. (2000). Increased particle fluxes occur during the NE monsoon season when strong convective winter mixing deepens the mixed layer and SST decreases.

Sediments deposited within the OMZ depth interval on the Pakistan Margin are laminated with alternating dark and light sediment layers and record high input of lithogenic material originating from dust storms and/or river runoff (Schulz et al., 1996; von Rad et al., 1999a, 1995). Lückge et al. (2002) showed that dark laminae are deposited over large parts of the year and reflect primary production of marine organic matter, whereas light-colored laminae contain almost exclusively land-derived materials which are deposited in the winter season during short-term heavy rainfall events.

3.3. Methods

3.3.1. Sample collection and stratigraphy

In this study we investigated piston core 275KL and box core 39KG, both located within the center of the OMZ off the Pakistan coast (Figure 3.1). The box core 39KG (24°50.01'N, 65°55.01'E; 695 m water depth) was collected in 1993 during SONNE cruise 90, and results were published by Doose-Rolinski et al. (2001), Lückge et al. (2001), and von Rad et al. (1999a). The piston core 275KL was retrieved from the same position in 1998 during SONNE cruise 130 (24°49.31'N, 65°54.60'E; 782 m water depth). We studied the top 188 cm interval of core 275KL and the top 15 cm of core 39KG, which together yield a continuous record of environmental conditions on the Pakistan Margin over the last 2400 years. Core 275KL was continuously sampled in 0.5 cm intervals (sample resolution of 5 to 80 years) for bulk analyses (organic carbon and carbonate), and every third or fourth sample (of this sample series) was analyzed for opal concentrations and stable nitrogen isotope measurements. Alkenones were measured at continuous 2 cm intervals in core 275KL. In core 39KG, all parameters were analyzed on 1 cm intervals (6 to 8 year resolution). All samples were freeze dried and homogenized with mortar and pestle prior to chemical treatment and analyses.

In addition to seasonal varves, core 275KL exhibits reddish brown silt turbidites up to 9 cm thick and light gray short event deposits (>1 mm thick) consisting of allochthonous lithotypes interpreted as "plume deposits" by episodically heavy river floods that transport mud suspensions across the narrow shelf onto the steep upper slope (Lückge et al., 2002; von Rad et al., 2002b). Sediments containing these event deposits or turbidites were excluded from our sample set.

Varves, turbidites, and event layers in our core are equivalent to the lithostratigraphy observed in core 56KA from the same position. Core 56KA has been dated by von Rad et al. (1999a) by varve counting and several conventional and accelerated mass spectrometry

(AMS) ^{14}C datings. Our age model is based on the visual correlation of event deposit layers from both cores as stratigraphic tie points and interpolation between these tie points.

We also analyzed alkenones and calculated alkenone fluxes as well as the $U^{K'}_{37}$-index of samples from the Eastern PAKOMIN sediment trap mooring station (EPT-2; 24°45.6'N, 65°48.7E; 590 m water depth) to ascertain the validity of sea surface temperatures estimated in sediment core samples. The EPT-2 trap was deployed from May 1995 to February 1996 and was previously studied by Andruleit et al. (2000) and Schulz et al. (2002b).

3.3.2. Bulk components (organic carbon, carbonate, and opal)

Total carbon was analyzed on a Carlo Erba 1500 elemental analyzer (Milan, Italy) with a precision of 0.2%. Total organic carbon (TOC) was measured with the same instrument after samples were treated with 1 M hydrochloric acid (HCl) to remove inorganic carbon. Analytical precision for organic carbon was 0.02%. Carbonate carbon was calculated as the difference between total carbon and organic carbon.

Biogenic opal was determined by wet alkaline extraction of biogenic silica (BSi) using a variation of the DeMaster method (DeMaster, 1981). About 30 g sediment per sample was digested in 40 mL of 1% sodium carbonate solution (Na_2CO_3) in a shaking bath at 85°C. After 3 h, the supernatant was withdrawn and neutralized in 0.021 M HCl. The concentration of dissolved silica in subsamples was determined photometrically. Biogenic opal was calculated by multiplying the BSi concentrations with a factor of 2.4. The mean standard deviation based on duplicate measurements of samples is 0.17%. To ensure that BSi is not overestimated by mineral dissolution at low BSi concentrations, we analyzed representative samples after 3, 4, and 5 h and used a slope correction for the determination of BSi concentrations (Conley, 1998). The amount of BSi was then estimated from the intercept of the line through the time course aliquots (DeMaster, 1981). Results of slope-corrected opal estimates showed that our method slightly overestimated opal concentrations by a mean of 0.13%. All bulk components are presented as weight percent.

Mass accumulation rates of organic carbon were calculated by multiplying the dry bulk densities of the sediments (measured at the Department of Geosciences, University of Tübingen) with calculated sedimentation rates and the weight fraction of organic carbon.

3.3.3. X-ray elemental analysis

X-ray fluorescence (XRF) core scanner data were collected by XRF core scanner I at MARUM-Center for Marine Environmental Sciences (University of Bremen) using a Kevex Psi Peltier cooled silicon detector and a Kevex X-ray tube with the target material molybdenum (Mo). Counts were acquired directly at the split core surface of the archive half every 2 mm down-core over an area of 0.2 cm^2 with an instrument slit size of 2 mm using a generator setting of 20 kV, 0.087 mA, and a sampling time of 30 s. The split core surface was covered with a polypropylene foil to avoid contamination of the XRF measurement unit and desiccation of the sediment.

3.3.4. Nitrogen stable isotope ratios

The ratio of the two stable isotopes of nitrogen ($^{15}N/^{14}N$) is expressed as $\delta^{15}N$, which is given as the per mil deviation from the N-isotope composition of atmospheric N_2 ($\delta^{15}N = 0‰$): $\delta^{15}N = [(R_{Sample}-R_{Standard})/R_{Standard}]*1000$, where R_{Sample} is the $^{15}N/^{14}N$ ratio of the sample and $R_{Standard}$ is the $^{15}N/^{14}N$ ratio of atmospheric N_2. $\delta^{15}N$ values were determined using a Finnigan MAT 252 gas isotope mass spectrometer after high-temperature flash combustion in a Carlo Erba NA-2500 elemental analyzer at 1100°C. Pure tank N_2 calibrated against the International Atomic Energy Agency reference standards IAEA-N-1 and IAEA-N-2, which were, in addition to an internal sediment standard, also used as working standards. Analytical precision based on replicate measurements of a reference standard was better than 0.1‰. Duplicate measurements of samples resulted in a mean standard deviation of 0.07‰.

3.3.5. Alkenones

Freeze-dried and homogenized sediment samples (1 to 3g) were extracted twice for 5 min with methylene chloride (DCM) using an accelerated solvent extractor (Dionex; temperature 75°C, pressure 70 bar). Directly after extraction, a known amount of internal standard (14-heptacosanone) was added to the extracts. The extracts were then rotary evaporated until near dryness and saponified with 5% methanolic potassium hydroxide (KOH) solution overnight. The KOH solution was dried under a nitrogen flow, dissolved in DCM, and cleaned over a silica gel column using DCM as eluent. The clean fraction containing the alkenones was dried under N_2 and taken up in n-hexane (50-150μL) prior to

analysis. Alkenones were analyzed by gas chromatography on an Agilent 6850 gas chromatograph (GC) equipped with a split-splitless inlet system and flame ionization detector (310°C). Separation was achieved on a silica column (30 m x 0.1 µm film thickness x 0.32 mm ID; Optima1; Macherey-Nagel) using hydrogen as carrier gas (1 mL min^{-1}). The GC oven maintained 50°C for the first minute and was then programmed from 50° to 230°C at 20°C min^{-1}, from 230° to 260°C at 4.5°C min^{-1}, and from 260° to 320°C at 1.5°C min^{-1} followed by an isothermal period of 15 min. $C_{37:2}$- and $C_{37:3}$- alkenones were identified by comparing peak retention times between sediment samples and a working sediment standard. Quantification of alkenones was achieved by integrating the peak areas of the C_{37}-alkenones and that of the internal standard (14-heptacosanone). Since both the C_{37}-alkenones and the internal standard are very similar in structure, no different response factors between the C_{27}-ketone and the C_{37}-alkenones are assumed. Alkenones were translated into sea surface temperature using the core top calibration for the Indian Ocean from Sonzogni et al. (1997b): $SST = (U_{37}^{K'} - 0.043)/0.033$ with $U_{37}^{K'} = C_{37:2}/(C_{37:2} + C_{37:3})$. Replicate extraction and measurement of a working sediment standard resulted in a mean standard deviation of estimated SST of 0.5°C.

3.4. Results

3.4.1. Alkenone fluxes and $U_{37}^{K'}$ in sediment traps

Alkenone fluxes in EPT-2 between May 1995 and February 1996 ranged from 0.15 µg m^{-2} d^{-1} to 1.21 µg m^{-2} d^{-1} (Figure 3.3a). Peak fluxes occurred in May 1995 (1.21 µg m^{-2} d^{-1}) and during the late NE monsoon in January 1996 (0.92 µg m^{-2} d^{-1}) and February 1996 (0.94 µg m^{-2} d^{-1}). Alkenone fluxes for the months September and October could not be determined due to low amounts of sample material. Alkenone fluxes on the Pakistan continental margin track coccolith fluxes during the seasonal cycle (Andruleit et al., 2000) with maxima at the onset of the summer and of the winter monsoon. This underscores a strong link between primary and alkenone production. Alkenone (C_{37}) fluxes on the Pakistan Margin match those from the Oman Margin (Wakeham et al., 2002) but are slightly lower than the total alkenone (C_{37}, C_{38} and C_{39}) fluxes in the central Arabian Sea (Prahl et al., 2000). Sediment trap studies from different parts of the Arabian Sea thus showed a strong coupling between coccolithophore (and alkenone) production and the seasonal cycle in this area (Andruleit et al., 2000; Broerse et al., 2000; Prahl et al., 2000; Wakeham et al., 2002).

This seasonality may bias the SST signal in sediments toward seasonal flux maxima, so that it may not be representative of the annual mean SST (AM-SST). In our set of trap samples covering the period from May 1995 to February 1996, the seasonal variability of alkenone-derived SST (26.1°C to 28.1°C; $U_{37}^{K'}$ from 0.904 to 0.971; Figure 3.3b) is attenuated compared to observed SSTs which vary from 23.0°C to 29.2°C (Reynolds et al., 2002). The observed mismatch between alkenone-based SST in sediment trap samples and regional seasonal SST patterns seems to be a general phenomenon independent on oceanic region (central Arabian Sea (Prahl et al., 2000); Sea of Okhotsk, northwest Pacific (Seki et al., 2007), subtropical oligotrophic North Pacific (Prahl et al., 2005)). In general, these studies found that alkenone-based SST produces a warm SST bias in winter and a cold SST bias in summer concordant with our observations from the northeastern Arabian Sea, where monthly average alkenone-based SSTs deviate most from modern observed SSTs during the cold winter months of the trapping period in 1995/1996. The overestimation of winter SST by alkenones may be explained by a change in the coccolithophore community to alkenone-producing species that exhibit a different response to growth temperature, thus altering the relationship of $U_{37}^{K'}$ ratio to SST (Prahl et al., 2005). At the Pakistan Margin, changes in the coccolithophore assemblage (including the alkenone-producing species *Emiliania huxleyi* and *Gephyrocapsa oceanica*) are mainly controlled by variations in the mean mixed layer depth and total nutrient availability (Andruleit et al., 2004). A change in the alkenone-producing coccolithophore community due to mixed layer deepening at site EPT-2 is well reflected in the ratio of *G. oceanica* to *E. huxleyi* that show an increasing abundance of *G. oceanica* relative *to E. huxleyi* in winter (see Figure 3.4; coccolithore flux data were taken from Andruleit et al. (2000)). Although relative species composition of the two alkenone-producing coccolithophorides seems to be stable in the Indian Ocean sedimentary record (spatially (Sonzogni et al., 1997b) as well as through time (Doose-Rolinski et al., 2001)), we suggest that it might be of importance for $U_{37}^{K'}$ calibration on a seasonal scale on the Pakistan continental margin. If we use a linear offset of 0.085 (instead of 0.043) to calibrate the $U_{37}^{K'}$ index to SST as suggested by Prahl et al. (2005) for the deeply mixed wintertime, alkenone-based SST were much closer to observed SST at 10 m water depth (Figure 3.4). On the other hand, the slight cold bias of alkenone-based SST in our trap samples during summer is best explained by alkenone production in the upper mixed layer between 0 to 30 m water depths.
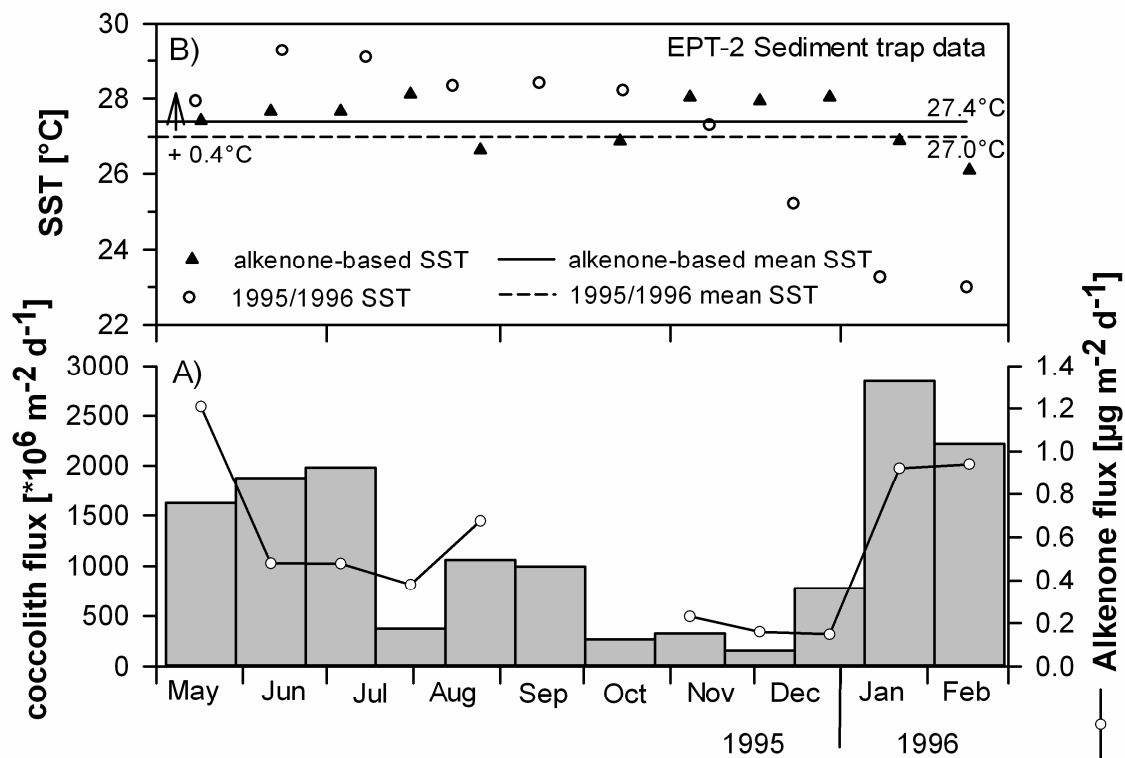
Figure 3.3: (a) Total coccolith (gray bars; Andruleit et al., 2000) and alkenone fluxes (open circles) at trap EPT-2 in the northeastern Arabian Sea off Pakistan. (b) Alkenone-derived SST measured in EPT-2 samples (triangle) compared to 1995/1996 monthly SST (circle; extracted from the web-site http://ingrid.ldgo.columbia.edu). Mean alkenone-based SST is about 0.4°C higher than mean temperature over May 1995 to February 1996.

Albeit the complexity of processes that plays a role in seasonal alkenone-based SST estimates, we state that sedimentary $U^{K'}_{37}$ measurements on the Pakistan Margin are best approximated by AM-SST. The average alkenone-derived SST of the sampling period is 27.4°C, which (considering an uncertainty of 0.5°C) matches well with the mean modern SST (27.0°C; see Figure 3.3b), which in turn is very close to the average mean SST from May to February obtained from the Levitus climatology (26.9°C (Levitus and Boyer, 1994)). Climatological annual mean SST (including the months missing in the trap investigation) is 26.4°C (Levitus and Boyer, 1994). But because alkenones reflect an integrated signal of the upper 0 to 50 m of the water column (Sonzogni et al., 1997b), small deviations from actual sea surface temperature measurements are to be expected.

Our interpretation of sedimentary $U^{K'}_{37}$ measurements as an AM-SST signal is supported by $U^{K'}_{37}$ estimates for sediment trap samples from the central Arabian Sea (Prahl et al., 2000)

and by a compilation of sediment trap time series distributed over different oceanic regions worldwide (Rosell-Melé and Prahl, 2013). Furthermore, measurements of sediment core tops, which were used to develop an alkenone calibration equation for the Indian Ocean, showed no significant differences between calculated production-weighted temperature and AM-SST (Sonzogni et al., 1997a, 1997b). According to Doose-Rolinski et al. (2001), alkenone-derived SSTs measured in a Holocene section of a sediment core from the Pakistan Margin were best approximated by annual mean temperature as well.
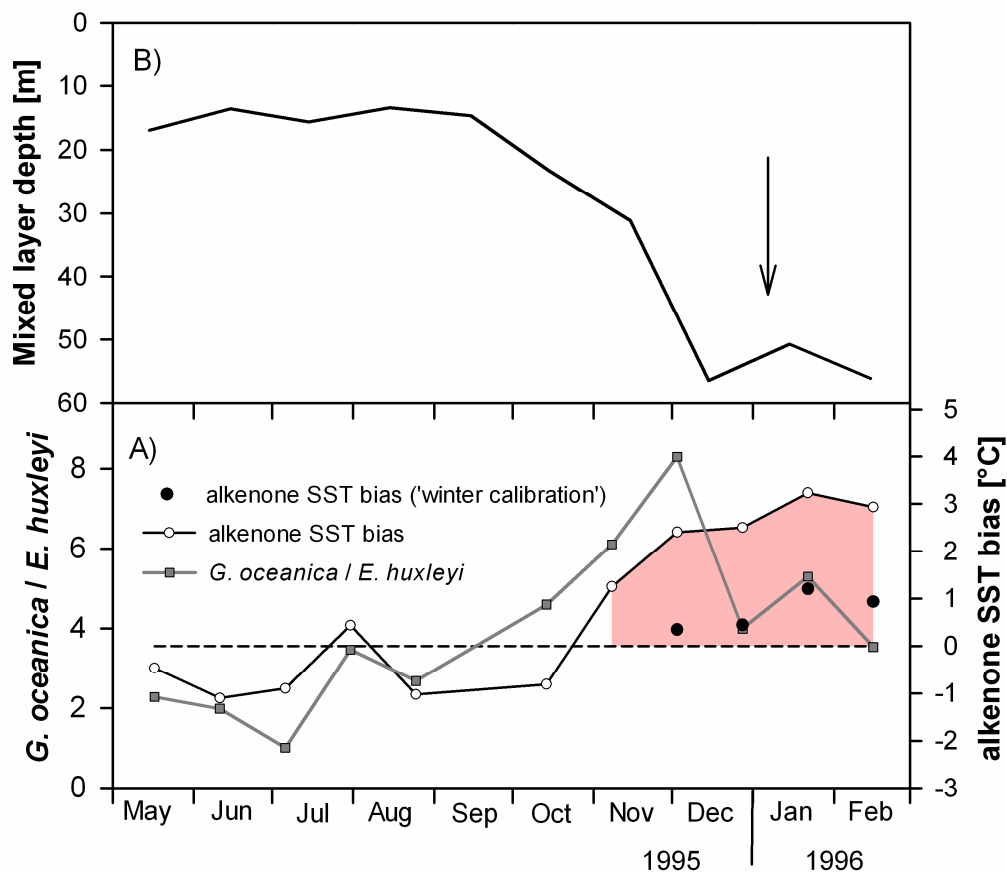
Figure 3.4: (a) Alkenone SST bias (circle; difference between monthly observed SST at 10 m water depth (Levitus and Boyer, 1994) and alkenone-derived SST measured in EPT-2 samples) compared to the ratio of *G. oceanica* to *E. huxleyi* (square, data were taken from Andruleit et al. (2000)) at trap EPT-2. Red shaded area indicates overestimation of SST by alkenones in winter. This overestimation is significantly reduced by the use of a different SST calibration (filled circle; SST = (U_{37}^{K} - 0.085)/0.033). (b) Seasonal variations of mixed layer depth at site 39KG/275KL showing a strong mixed layer deepening during winter.

3.4.2. Alkenone SST record in core 39KG/275KL

Alkenone SST vary between 26.9°C and 28.4°C ($U_{37}^{K'}$ from 0.932 to 0.981) over the last 2400 years and thus lie well above the modern annual mean of 26.4°C (Levitus and Boyer, 1994). Conte et al. (2006) stated that a positive offset of reconstructed core top temperature (27.6°C for SO90-39KG) compared to atlas temperature is observed in several areas worldwide. It is alternatively explained by diagenetic alteration of alkenone ratios in the water column and/or surficial sediments, by lateral advection, or by variations in the seasonality and depth of alkenone production. In our view, diagenesis can be ruled out as a significant process affecting our $U_{37}^{K'}$ estimates, because the offset was also observed between trap alkenone SST and modern AM-SST and was furthermore confirmed by Mg/Ca temperatures (Dahl and Oppo, 2006). Biasing of the alkenone signal by alkenones produced and advected from the upwelling area off Oman may be a factor (Andruleit et al., 2000), but coccolithophore fluxes on the Pakistan Margin are only slightly enhanced during the SW monsoon season, and the associated bias in the alkenone signal must be of minor importance. As SSTs in the southeastern Arabian Sea remain relatively high during winter, lateral advection of water masses and alkenones from the southwest Indian coast (following the counterclockwise surface current established during the NE monsoon) on the other hand would result in a warm bias of alkenone SST on the Pakistan Margin during the winter. However, based on a comparison of coccolith fluxes with coccosphere fluxes (which should present a vertical flux signal), Andruleit et al. (2000) suggested that coccolithophore assemblages were not influenced by resuspension processes during this time of the year.

Regardless of the absolute SST, Figure 3.7 illustrates relative SST variations around the overall mean of 27.7°C over the last 2 millennia. Although the amplitude of the alkenone-derived SST signal is small in our record, our SST reconstruction exhibits statistical significant periods of long-term SST changes. SSTs were high at around 28.2°C until 250 A.D., rapidly decreased and outlined a time period of low SST that lasted from 400 to 1000 A.D. After a rebound to >28°C between 1000 and 1300 A.D., the decline in SST continued until minimum temperatures (26.9°C) are registered during the 18th century. The minimum of our SST reconstruction at this time agrees with the results obtained from a global climate proxy network, which suggests 0.3°C cooler SSTs than present during the Little Ice Age in the northeastern Arabian Sea (Mann et al., 2009). Our SST estimates, after this minimum, suggest a northern Arabian Sea warming tendency that persists to the present.

3.4.3. Records of Productivity

Our analytical approach to trace the past productivity changes were based on TOC concentrations, $\delta^{15}N$ values, and the ratio of carbonate to opal. The range of TOC concentrations (1.0 and 2.0%) and $\delta^{15}N$ values (7.1 to 8.5‰) in the sediment cores at sites 39KG/275KL (Figure 3.6) is a characteristic of high-productivity areas with a well-developed OMZ and water column denitrification (e.g., Altabet et al., 1999; Gaye-Haake et al., 2005; Naqvi et al., 1998) such as the northern Arabian Sea (Cowie et al., 1999). Organic carbon concentrations in sediments on the Pakistan Margin (and elsewhere) are influenced by surface productivity but also by dilution with lithogenic material, bottom water oxygen concentrations, bulk accumulation rate, sediment texture, refractory of organic matter, and the mineral surface area (e.g., Keil and Cowie, 1999; Paropkari et al., 1992; Suthhof et al., 2000; van der Weijden et al., 1999).

At our core site the use of organic carbon mass accumulation rates (TOC MAR) as a productivity indicator that theoretically remove an influence of dilution is complicated by strongly fluctuating sedimentation rates (SR) (ranging from 87 to 212 cm kyr^{-1}). Sediment mass accumulation rates (71 to 203 g cm^{-2} kyr^{-1}; event deposits excluded) calculated from SR and bulk densities are even higher than glacial/interglacial variations reported from the western (SR ranging from 6 to 38 cm kyr^{-1} and MAR ranging from 5 to 50 g cm^{-2} kyr^{-1} (Emeis et al., 1995)) and eastern Arabian Sea (SR ranging from 4 to 9 cm kyr^{-1} (Rostek et al., 1997)). SR and MAR at our study site are caused by highly variable input of lithogenic matter (range from 81 to 86%) from river runoff and/or dust storms (Schulz et al., 1996; von Rad et al., 1999a). Even though sedimentary OM in our core mainly consists of marine OM ($\delta^{13}C$ measured in core 275KL ranges from -21.5 to -19.5‰), significant positive correlations between TOC MAR and SR ($R^2=0.56$) and TOC MAR and sedimentary mass accumulation rates ($R^2=0.76$) indicate a dominant influence of bulk MAR (and thus alternating input of organic matter transported with mineral matter on its passage across the shelf) on organic carbon accumulation rates (Emeis et al., 1995; Müller and Suess, 1979). This conclusion is supported by the good agreement between down-core variations in TOC MAR and varve thickness, which is an indicator for precipitation and river runoff (von Rad et al., 1999a; see Figure 3.5b). Thus, we infer that in our study area, TOC contents can be used as a tracer for the past primary productivity changes rather than the organic carbon accumulation rates. Although measured TOC contents during the period 400 to 900 A.D. might partly be affected by dilution as indicated by visual comparison of organic carbon concentrations with MAR (Figure 3.5a), no significant correlation between TOC contents and mass accumulation rates

(R^2=0.008) could be observed indicating no significant control of the dilution on down-core variations in TOC concentrations.
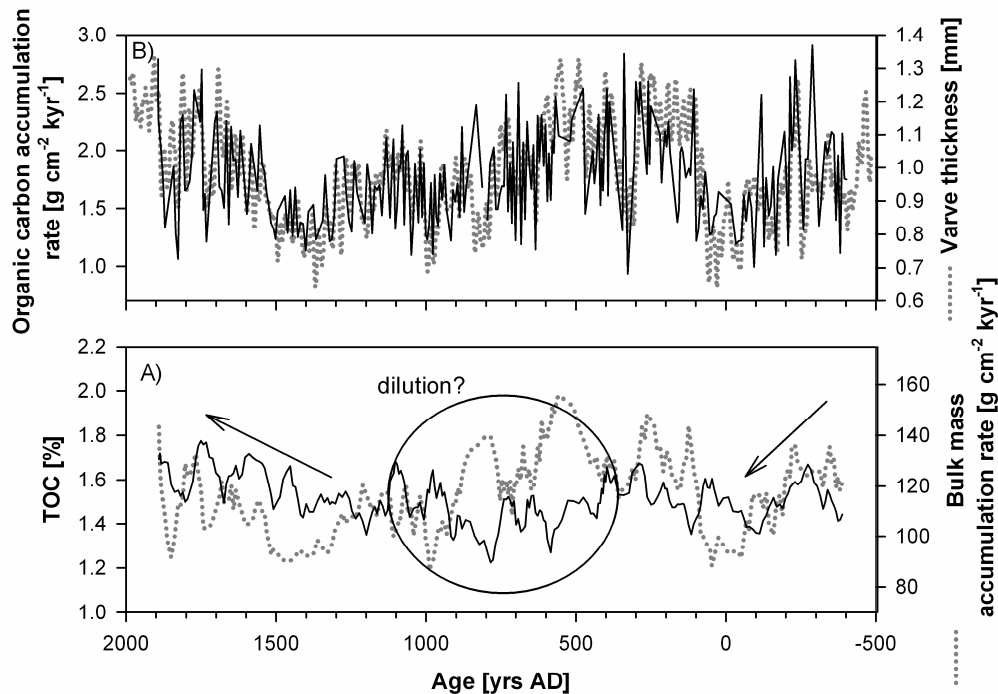

Figure 3.5: (a) Late Holocene variability of TOC contents compared to bulk mass accumulation rates in core SO130-275KL. (b) Down-core variations of organic carbon mass accumulation rates for core SO130-275KL compared to varve thickness data (dotted line) measured in core SO90-56KA (von Rad et al., 1999a) from the same location (both turbidite/event deposit free).

Over the last 2400 years of our record, elevated TOC concentrations coincide with increased $\delta^{15}N$ values and vice versa, a relationship described for Holocene sediments (Agnihotri et al., 2003) and over glacial/interglacial cycles (Altabet et al., 1995; Ganeshram et al., 2000; Suthhof et al., 2001) in the northern Indian Ocean. Parallel changes in TOC concentrations and $\delta^{15}N$ are both related to the productivity variations caused by variable access to the subthermocline nitrate pool. That nitrate pool has a high $\delta^{15}N$ resulting from denitrification within the upper part of the OMZ (Gaye et al., 2013). Upwelling does not occur at our core location, so that variable deepening of the mixed layer due to convective winter mixing during the NE monsoon season is the most likely process transporting the ^{15}N-enriched nitrate to the ocean surface and enabling productivity. Together, $\delta^{15}N$ values and TOC concentrations in our sediment cores thus reflect productivity changes associated with mixed layer deepening due to NE monsoon conditions. A third indirect signal of productivity

is the ratio of the biogenic constituents carbonate (ranging from 6 to 15.5%) and opal (ranging from 0.5 to 0.9%), because high nutrient availability induces diatom blooms and high flux rates or organic matter, whereas high carbonate rain rates indicate low nutrient availability. The carbonate to opal ratio ranges from 14 to 29 and indicates a dominance of carbonate primary producers (coccolithophores) at our study site that decreases over time relative to opal from diatoms (Ramaswamy and Gaye, 2006). In this general trend, declining carbonate to opal ratios indicate a shift to higher productivity around 1400 A.D. (Figure 3.6).
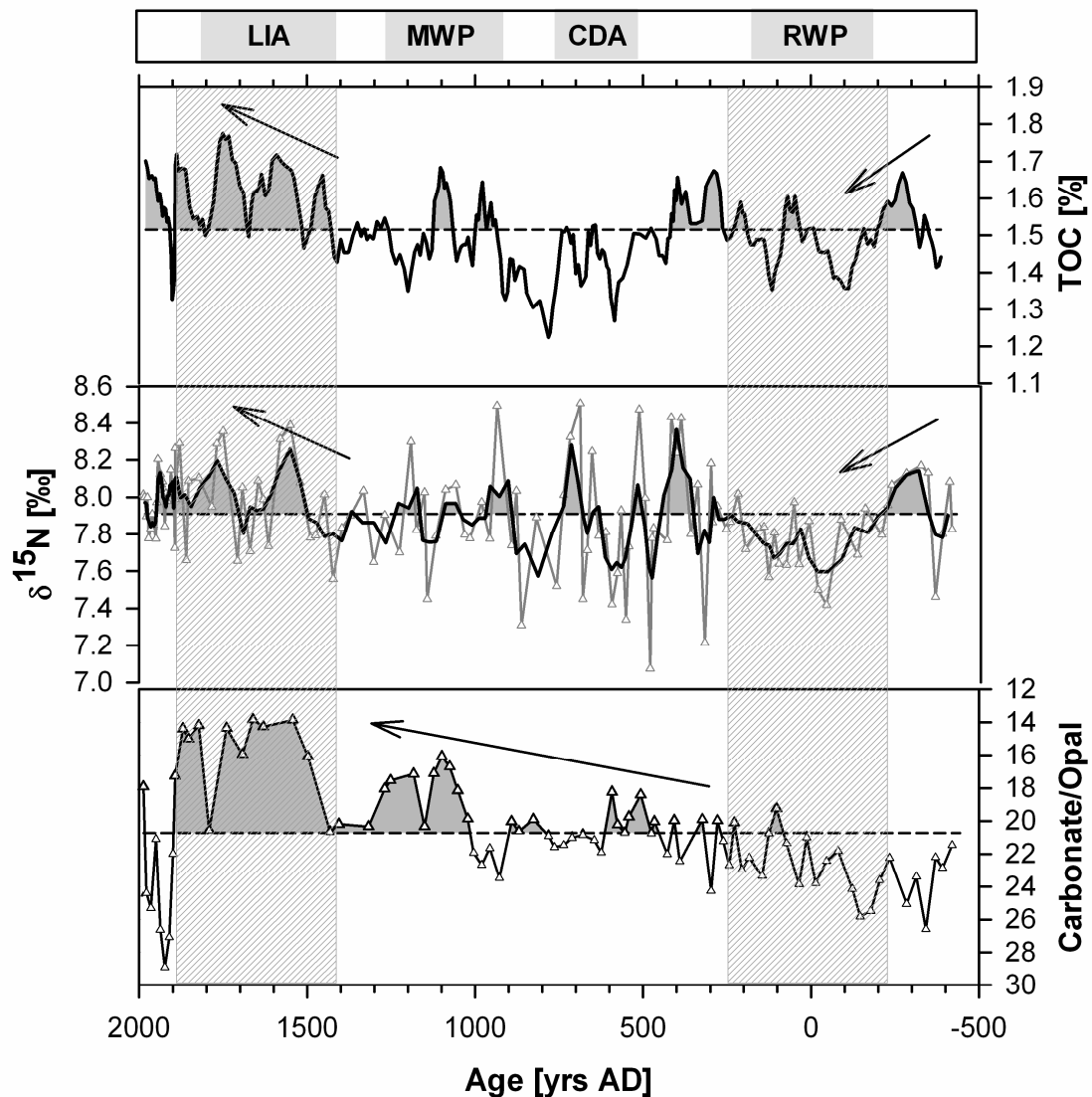
Figure 3.6: Late Holocene productivity record for cores 39KG and 275KL from the northeastern Arabian Sea. Carbonate/opal ratios, $\delta^{15}N$ values (bold line: running mean of 3) and smoothed TOC contents (running average of 5) were used as productivity indicators. The gray shaded areas indicate good agreement between productivity proxies. The dashed lines indicate the respective mean over the complete dataset. Further illustrated are characteristic climate periods known from the Northern Hemisphere: Little Ice Age (LIA), Medieval Warm Period (MWP), Cold Dark Ages (CDA), and Roman Warm Period (RWP).

As discussed above, proxies indicative of productivity changes are influenced by a lot of processes. To minimize the effect of processes not related to productivity variations and to better filter out the signal caused by productivity changes, a productivity index (combining TOC, δ^{15}N, and carbonate/opal) was calculated. First, the range of values for all three parameters was standardized to values between 0 and 1, so that the respective productivity indicators were equally weighted and comparable to each other. The sum of the standardized values was calculated and again standardized to values between 0 (low productivity) and 1 (high productivity). High productivity from 1400 to 1950 A.D. and periods of decreased productivity from about 200 B.C. to 250 A.D., as recorded by all individual productivity parameters (Figure 3.6, indicated by the gray shaded areas), are well reflected by our productivity index (Figure 3.7, not reverse y axis). In addition, superimposed on short-term variability, the productivity index shows a gradual trend to increasing primary production in the northeastern Arabian Sea over the late Holocene.

3.4.4. Variability in Sr/Ca ratios

The relationship between elevated Sr/Ca ratios and increased winter monsoon activity was first proposed for glacial/interglacial intervals by Reichart et al. (1998) and was later adapted for Holocene sediments by Lückge et al. (2001). These authors proposed that elevated Sr/Ca ratios image variations in mixed layer depths. Because aragonite has a higher Sr content than calcite, variations in Sr/Ca track the depth interval of the aragonite compensation depth (ACD), and the deepening of the ACD and higher Sr/Ca ratios indicate intensified deep winter mixing due to elevated winter monsoon activity (Reichart et al., 1998). A different mechanism for changes in Sr/Ca on millennial time scales was proposed by Böning and Bard (2009), who attributed the variations in Sr/Ca in the northeastern Arabian Sea to changes in the formation of Antarctic Intermediate Waters. Today, Antarctic Intermediate Water in the Arabian Sea can only be traced up to 5°N (You, 1998), so that for the 2400-year record here, this long-term variability is most likely irrelevant.

The Sr/Ca ratio in the sediment cores vary between 0.023 and 0.032 at sites 39KG/275KL (Figure 3.7), which are in the range of previously measured values for Holocene sediments from the Makran area (Lückge et al., 2001). The increase in Sr/Ca ratios indicates a shift to winter monsoon conditions on the Pakistan Margin around 700 A.D.

3.5. Discussion

3.5.1. Productivity and SST variability: evidence for monsoonal change

Winter monsoon activity affects both sea surface temperature and mixed layer depth over the Pakistan Margin and thus controls the amount of thermocline nutrients entrained into the mixed layer (Figure 3.2). As a result, primary productivity changes in the northeastern Arabian Sea are strongly coupled to the intensity of the NE monsoon season. Whereas primary production is unambiguously related to monsoon strength, SST in the northeastern Arabian Sea, although primarily controlled by monsoon related processes, can also be impacted by global temperature variations. A decrease in the alkenone-based SST signal at sites 39KG/275KL can thus be caused either by local strengthening of NE monsoon conditions or by globally lowered atmospheric temperature. If SST was changing as a response to varying NE monsoon intensity, then this should also be noted in our primary productivity reconstruction because intensified NE monsoon strength induces high rates of primary production at the Pakistan continental margin. The general trend of decreasing SST and increasing productivity seen in our record over the last 2400 years (Figure 3.7) confirms that alkenone SST primarily reflect changes in the NE monsoon strength. This coupling of SST and productivity is particularly pronounced during the periods from 400 B.C. to 300 A.D. and from 1400 A.D. until the present, while it is less clear between ~500 and 1300 A.D. Furthermore, alkenone SSTs follow the same pattern as reconstructed winter SSTs (based on planktic foraminifera transfer functions measured in the same sediment core; unpublished data) confirming the strong influence of the winter season on alkenone SST in this region.

A link between NE monsoon conditions, decreasing SSTs, and increasing productivity can be observed not only on a seasonal scale and over the last 2400 years but also on time scales of several hundreds of thousands of years. In the northeastern Arabian Sea, relatively high productivity and sea surface cooling appear to correspond to glacial stages due to elevated NE monsoon activity (e.g., Rostek et al., 1997; Schulte and Müller, 2001; Schulte et al., 1999).

3.5.2. Local monsoon dynamics in the northeastern Arabian Sea during the last 2400 years

On the basis of the above-mentioned considerations, our multi-proxy study from the northeastern Arabian Sea indicates three main periods of changing monsoon intensities

throughout the late Holocene (Figure 3.7). Winter monsoon intensity was low before about 250 A.D. and is recorded by high SSTs and generally low primary production due to diminished north-easterly winds and reduced convective winter mixing in the northeastern Arabian Sea. Winter monsoon mixing strengthened after 250 A.D., which caused a cooling of the sea surface and slightly increased primary production. Finally, winter monsoon conditions started to predominate off Pakistan at about 700 A.D., as indicated by a shift to higher Sr/Ca ratios in core 275KL (Figure 3.7, note reverse Sr/Ca y axis). Weak correlation between SST and primary productivity from ~500 to 1300 A.D. suggests a "transition period" from weak to strengthening NE monsoon, characterized by unstable and fluctuating environmental conditions on the Pakistan Margin. Strong winter monsoon activity prevailed during the Little Ice Age (LIA) from 1400 to 1900 A.D., as indicated by low SSTs and a peak in biological productivity due to strong convective winter mixing. Low SSTs during the LIA as well as relatively high SSTs due to diminished NE monsoon conditions occurring 2000 years ago agree with another northeastern Arabian Sea (alkenone-based) SST reconstruction (Doose-Rolinski et al., 2001). Although both SST records differ in detail, possibly as a result of proxy uncertainty, they display similar trends of warming at around 0 A.D. and cooling during the LIA. This small-scale variability between both records might further be caused by the analysis of different core sections and thus variations in the time interval which is integrated by the alkenones.

The dynamics of the monsoon low-level wind system on the Pakistan Margin throughout the last 2400 years affect marine processes as well as moisture changes in this area. Variable but relatively low-salinity values after 500 A.D. probably reflect diminished SW monsoon and/or enhanced NE monsoon conditions (Doose-Rolinski et al., 2001). Lückge et al. (2001) proposed a shift from SW monsoon dominated precipitation to NE monsoon precipitation in the Makran area around 500 A.D. These findings match our interpretation of predominating NE monsoon conditions since ~700 A.D.

Enhanced NE monsoonal activity during the LIA was most likely induced by an increased influence of westerlies in the Makran area during this period. Today, winter rainfall brought by westerly winds and connected to cyclonic storms originating in the Mediterranean significantly contributes to the total annual precipitation in the study area (Lückge et al., 2001; von Rad et al., 2002c, and references therein). Higher precipitation implicating stronger westerlies on the coast off Pakistan after 1600 A.D. and during the LIA was deduced from varve thickness data from the nearby core SO90/56KA (von Rad et al., 1999a) and in a cave record from the central Kumaun Himalaya (Sanwal et al., 2013). A significant feature

preceding the LIA in the northeastern Arabian Sea is a distinct phase of increased SST (1050
to 1300 A.D.; see Figure 3.7) that coincides with the Medieval Warm Period (MWP), a time
of generally warm climate conditions observed in the Northern Hemisphere.
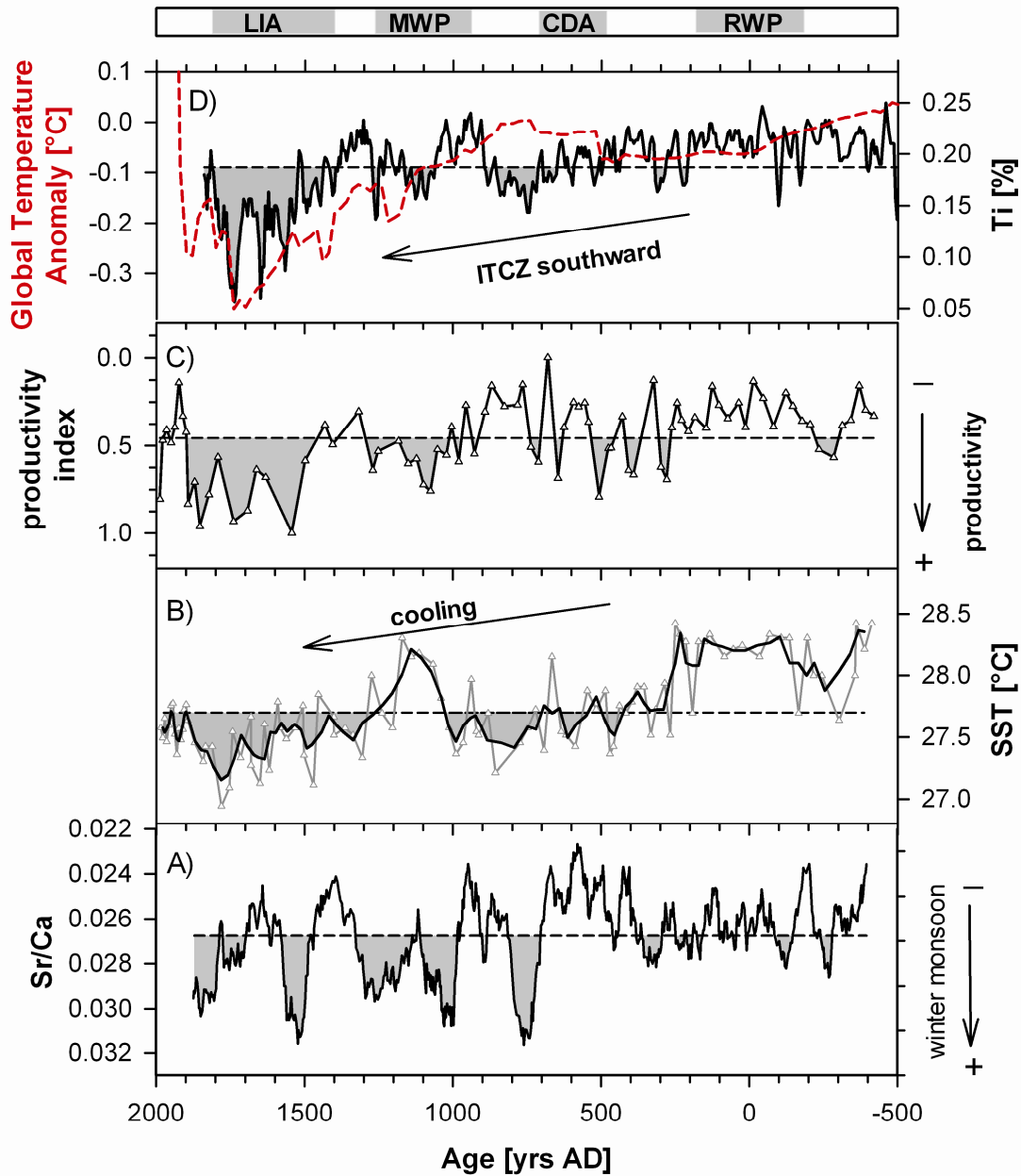
Figure 3.7: Reconstruction of winter monsoon variability in the northeastern Arabian Sea over the last 2400
years compared to long-term movements of the Intertropical Convergence Zone (ITCZ). (a) Smoothed Sr/Ca
ratios (21 point running mean), (b) alkenone SST record (bold line: 3 point running mean), and (c) productivity
index for cores 39KG/275KL. (d) Titanium content of Cariaco Basin sediments as an indicator for latitudinal
shifts in the ITCZ (Haug et al., 2001) compared to global temperature anomalies (Marcott et al., 2013). The
dashed lines indicate the respective mean over the studied time interval.

The response of the marine system to regional monsoon dynamics is best explained by the reactions of the surface ocean to seasonal shifts in the ITCZ. The reversal of low-level winds in the Arabian Sea during the seasonal cycle is accompanied by a shift in the location of the ITCZ. Core sites 39KG/275KL are located at the average northern latitudinal position of the ITCZ, and thus, surface ocean processes in this area are sensitive to the long-term movements of the annual mean position of the ITCZ and the associate change in prevailing low-level winds. Northward migration of the ITCZ in spring (SW monsoon) and southward retreat in autumn (NE monsoon) differentially impact on surface ocean salinity and temperature and thus thermocline depth in the northeastern Arabian Sea. At times when the northern position of the ITCZ slightly shifts south of the average position, the duration of NE monsoon influence at site 275KL during winter is prolonged. This would enhance the influence of the winter monsoon on surface ocean conditions in this area.

Different studies widely distributed over the low-latitude region (e.g., Fleitmann et al., 2007; Haug et al., 2001; Russell and Johnson, 2005) indicate a general southward shift of the annual mean position of the ITCZ over the late Holocene in response to global climate variability. We argue that long-term southward movement of the ITCZ throughout the late Holocene is responsible for the long-term trends of declining sea surface temperature and rising productivity seen in our record (Figure 3.7). In this long-term trend, times of the southernmost ITCZ displacements were contemporaneous with the periods of highest primary productivity and lowest SST on the Pakistan continental margin. Both reflect an increasing regional influence of the NE monsoon and a reaction of the surface ocean by progressive winter deepening of convective mixing. This argument is supported by Jung et al. (2004), who attributed coherent basin-wide decadal to century scale temperature variations in the Arabian Sea during the Holocene (based on a correlation between SST variations off Somalia and Pakistan) to a shift in the mean position of the ITCZ throughout the Holocene. Such a connection between a southward migrating annual mean position of the ITCZ and monsoon as well as precipitation changes throughout the Holocene was proposed by several authors (Fleitmann et al., 2007, 2003; Haug et al., 2001; Lückge et al., 2001; Russell and Johnson, 2005; Sinha et al., 2011b; Wang et al., 2005b; Yancheva et al., 2007).

3.5.3. Reversed behavior between summer and winter monsoon strength during the late Holocene

The mechanism above argues for an inverse relationship between summer and winter monsoon strength throughout the Indian and East Asian monsoon domain in the time-variant location of the ITCZ, expressed by the decreasing summer monsoon intensity with increasing winter monsoon activity and vice versa (e.g., Reichart et al., 2002b; Yancheva et al., 2007). Is this inverse relationship evident in a comparison of our winter monsoon record with records of summer monsoon strength? The regions influenced most drastically by the SW monsoon are the Oman and the Somalia upwelling systems, that both registered a gradual warming of sea surface temperatures during the last 2400 years (Huguet et al., 2006), in contrast to decreasing SST on the Pakistan Margin over this period. This points to a general antagonistic behavior in the millennial trend of summer and winter monsoon strength over the late Holocene. However, summer and winter monsoons were more variable on centennial time scales, particularly during the time intervals of greatest climate contrast over the last 2000 years on the Northern Hemisphere, namely, the MWP (950 to 1250 A.D.) and the LIA (1400 to 1800 A.D.). Evidence for increased summer monsoon intensity during the MWP comes from the northwestern Arabian Sea (Anderson et al., 2010, 2002; Gupta et al., 2003), from Oman (Fleitmann et al., 2004), India (Sinha et al., 2011b, 2007), as well as from China (Zhang et al., 2008). Changes in winter monsoon strength off Pakistan during this time are less pronounced. While higher SST argues for diminished NE monsoon activity over the northeastern Arabian Sea, slightly enhanced primary production and relatively higher Sr/Ca ratios might be indicative of NE monsoon intensification. One possible explanation for this mismatch might be that primary productivity on the Pakistan Margin during this time is fueled by lateral advection of nutrients from the upwelling area off Oman due to intensified summer monsoon circulation. On the other hand, most studies reconstructed diminished SW monsoon strength during the LIA (Fleitmann et al., 2004; Sinha et al., 2011a; Zhang et al., 2008), when our record suggests increased NE monsoon activity over the Pakistan Margin.

During the last 400 years, however, SW monsoon strengthens again in the northwestern Arabian Sea, probably as a result of a general warming trend (Anderson et al., 2002). Speleothem $\delta^{18}O$ from Kahf Defore in southern Oman indicates summer monsoon rainfall generally above the long-term average since 1660 A.D. and supports this hypothesis (Fleitmann et al., 2004). However, in the Pakistan Margin record, winter monsoon indicators continue to dominate over the last 400 years. Only most recently (since 1900 A.D.), primary productivity on the Pakistan Margin appears to decrease and SSTs increase slightly,

suggestive of diminished NE monsoon conditions in the northeastern Arabian Sea. The Oman cave record on land may be more sensitive to summer monsoon changes than the marine record in the Makran area, which is dominated by winter monsoon variability.
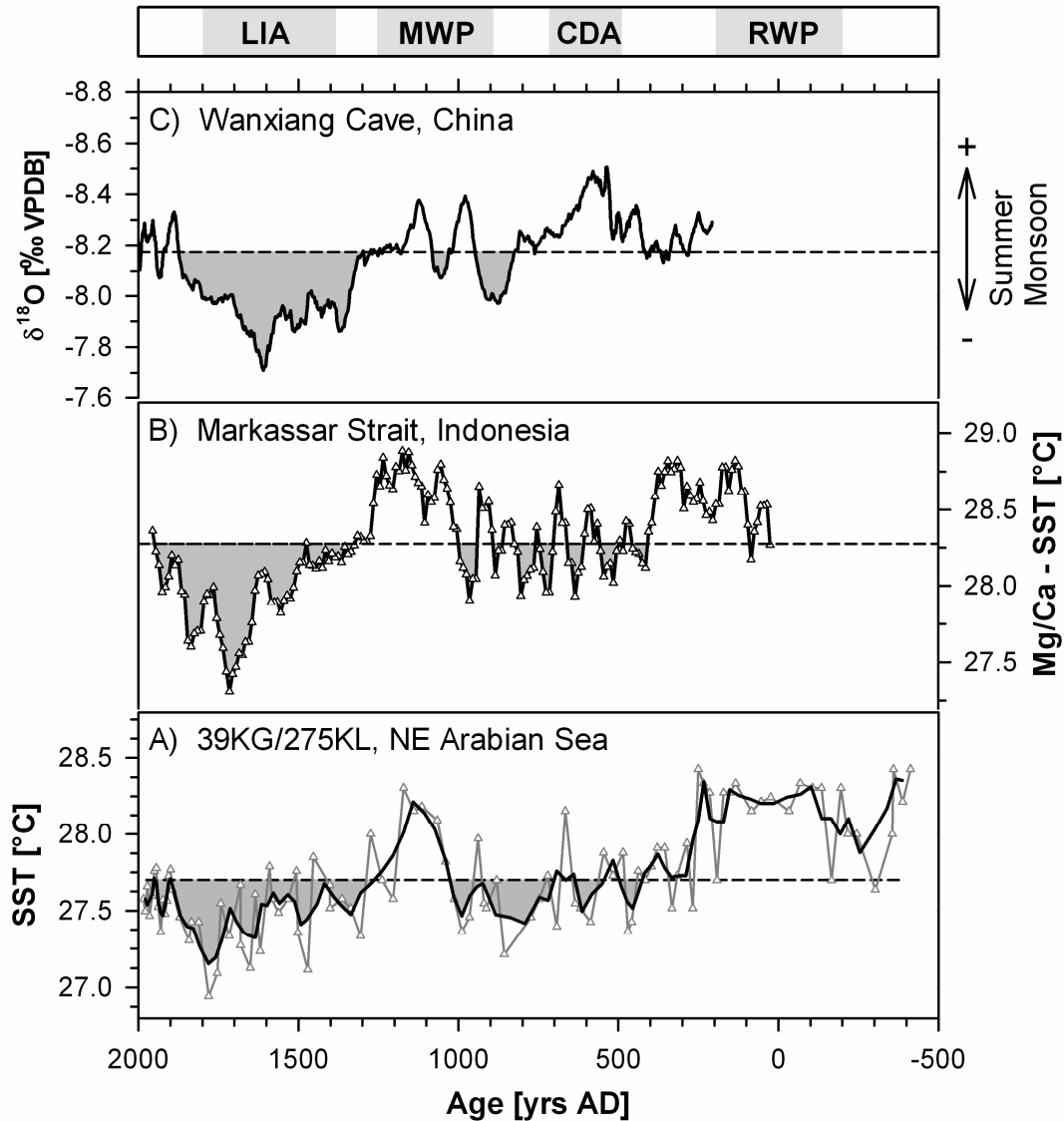
Figure 3.8: (a) Late Holocene alkenone-derived SST variations (cores 39KG and 275KL) from the northeastern Arabian Sea compared to (b) Mg/Ca-SST variations reconstructed for the Markassar Strait (Indonesia) by Oppo et al. (2009) and (c) a smoothed $\delta^{18}O$ record (15-point moving average) of Wanxiang Cave (China) as an indicator for summer monsoon intensity from Zhang et al. (2008). Dashed lines indicate the respective mean over the studied time interval.

The antagonism of SW and NE monsoon is evidenced by the comparison of our winter monsoon record with other monsoon reconstructions in the Arabian Sea and beyond. Based on the assumption that the $\delta^{18}O$ signal measured in speleothems from Wanxiang Cave is mainly influenced by summer monsoon precipitation, Zhang et al. (2008) compiled a 1810 year long record of summer monsoon intensity for central China. Their $\delta^{18}O$ variations show a strong resemblance to our reconstructed SST curve with lower SST in the northeastern Arabian Sea, coinciding with a decline in summer monsoon rainfall in central China due to weaker East Asian summer monsoon intensity (Figure 3.8). Furthermore, SST variations in the northeastern Arabian Sea are not only related to changes in East Asian summer monsoon over central China but also to changes in SSTs from the Indo-Pacific warm pool (Oppo et al., 2009, Figure 3.8). In accordance with our interpretation, Oppo et al. (2009) suggested that strong sea surface cooling in the Markassar Strait during the LIA was caused by intensified winter monsoon conditions rather than by monsoon induced upwelling. We thus conclude that a linkage between summer and winter monsoon strength exists over the whole Asian monsoon system during the late Holocene, reflecting long-term and short-term shifts in the ITCZ.

3.5.4. Global connections: The LIA climate feature

The monsoon record from the Pakistan Margin is in phase with characteristic, northern hemispheric climate periods of the late Holocene, such as the Little Ice Age, the Medieval Warm Period, and the Roman Warm Period (RWP). It reveals a consistent pattern of diminished winter monsoon activity in the northeastern Arabian Sea during northern hemispheric warm periods (MWP and RWP) and strengthened winter monsoon activity during hemispheric colder periods (LIA). Our high-resolution record implies that this consistent link between the North Atlantic and the Indian Ocean, which was described for glacial/interglacial (e.g., Schulte and Müller, 2001; Schulz et al., 1998; Sirocko et al., 1993) to climatological (Gupta et al., 2003) time scales, appears to operate during historical times as well. It causes the SW monsoon to weaken and the NE monsoon to gain strength during colder climate conditions over the North Atlantic.

One of the most prominent climate features in the northeastern Arabian Sea over the last 2400 years was the sharp decrease in SST due to the strengthening NE monsoon conditions between 1400 and 1850 A.D., contemporaneous with the LIA. Once described as a climate period restricted only to the northern extratropical hemisphere (e.g., Keigwin, 1996), LIA

climate conditions appear to have impacted on SST in low-latitude regions as well (Black et al., 2007; DeMenocal, 2000; Oppo et al., 2009). A recently published global data set of proxy records indeed confirms a global cooling trend between 1580 and 1880 A.D. (PAGES 2k Consortium, 2013) that is preceded by a phase of low solar irradiance between 1450 and 1750 A.D. (Bard et al., 2000), suggesting that LIA climate conditions may at least partly be influenced by solar forcing. Solar radiation has been proposed as a forcing mechanism controlling both North Atlantic climate (Bond et al., 2001) as well as variations in monsoon intensity during the Holocene (Agnihotri et al., 2002; Fleitmann et al., 2003; Gupta et al., 2005; Neff et al., 2001; Wang et al., 2005b). We thus infer that the decline in SST and increased NE monsoonal wind strength in the northeastern Arabian Sea during the LIA were triggered by global colder climate conditions (as a response to radiative forcing such as solar output, aerosols, and greenhouse gases), accompanied by southward displacement of the ITCZ.

3.6. Conclusions

Our high-resolution reconstruction of primary productivity and alkenone-derived SST from the northeastern Arabian Sea provides a unique record of winter monsoon variability throughout the late Holocene. In this area, primary production and sea surface temperatures are linked to winter monsoon intensity that cools the sea surface and increases its salinity so that thermocline deepening entrains more nutrients into the mixed layer and raises productivity. Because core 275KL is located in a sensitive region at the modern northern mean latitudinal position of the ITCZ, observed changes in surface ocean properties in response to the monsoonal wind regime on the Pakistan Margin track long-term and short-term movements of the ITCZ throughout the late Holocene. Reconstructed SST decreased whereas productivity increased over the last 2400 years, imaging a long-term trend of NE monsoon strengthening in response to insolation-induced southward migration of the ITCZ. Comparison of our winter monsoon record with records of summer monsoon intensity confirms an antagonistic relationship between summer and winter monsoon strength during the last 2400 years.

Reconstructed monsoon variability supports the growing body of evidence that significant climate variability occurs not only on time scales of several hundred of thousand years but also through the late Holocene. Before 250 A.D., winter monsoon activity in the northeastern Arabian Sea was generally weak, and convective winter mixing was shallow,

indicated by high SSTs (~28.3°C) and reduced primary productivity. Winter monsoon conditions started to predominate off Pakistan at about 700 A.D., in response to the overall southward movement of average ITCZ location during the late Holocene. While winter monsoon activity was relatively unstable from ~500 to 1300 A.D., strong sea surface cooling down to 26.9°C and a peak in primary productivity indicated strong and prevailing winter monsoon activity during the LIA from 1400 to 1900 A.D. The coherence between monsoon-induced variations over the Pakistan Margin with other monsoon records indicates a strong linkage of climate variability in the entire Asian monsoon system during the late Holocene, caused by migration of the ITCZ.

CHAPTER 4

4. Contrasting sea surface temperature of summer and winter monsoon variability in the northern Arabian Sea over the last 25 ka

Abstract

The seasonal monsoon cycle with winds from the southwest (SW) in summer and from the northeast (NE) in winter strongly impacts on modern regional sea surface temperature (SST) patterns in the Arabian Sea (northern Indian Ocean). To reconstruct the temporal and spatial variation in the dynamically coupled winter and summer monsoon strength over the last 25 ka, we analyzed alkenone-derived SST variations in one sediment core from the northwestern Arabian Sea, that is influenced by the summer monsoon (SST affected by upwelling processes), and in one core from the northeastern Arabian Sea, where SST is mainly governed by the winter monsoon (no upwelling). Comparison of the SST records reveals an antagonistic relationship of summer and winter monsoon strength throughout the late deglaciation and the Holocene. Upwelling along the Arabian Peninsula associated with peak SW monsoonal wind strength was strongest during the early Holocene climate optimum between 11 to 8 ka, and coincided with the northernmost position of the Intertropical Convergence Zone (ITCZ) marked by maximum precipitation over northern Oman. The SW monsoon weakened over the middle to late Holocene, while the NE monsoon gained strength. This different evolution was caused by the southward displacement of the ITCZ throughout the Holocene. Superimposed over the long-term trend are variations in northeast monsoon wind strength at time scales of centuries that were synchronous with late Holocene climate variations recorded on the Asian continent and in the high-latitude Northern Hemisphere. Their likely driving forces are insolation changes associated with sunspot cycles. Enhanced

by feedback mechanisms (e.g. land-sea thermal contrast) they enforced centennial scale fluctuations in wind strength and temperature in the northern Arabian Sea monsoon system.

4.1. Introduction

The oceanic environment and surface ocean properties of the Arabian Sea are directly coupled to the seasonal monsoon cycle. Alternating wind directions with low-level winds from the southwest in summer and from the northeast in winter cause regional differences in Arabian Sea sea surface temperature patterns. South-westerly winds are generated by the atmospheric pressure difference between the cold southern Indian Ocean and the heat low over central Asia in spring and summer. They drive upwelling of cold, nutrient-rich waters along the coasts of Somalia, Oman and southwest India and wind-stress curl-driven upwelling offshore (Hastenrath and Lamb, 1979; Rixen et al., 2000). These upwelling regions exhibit sea surface cooling during Northern Hemisphere (NH) summer (Levitus and Boyer, 1994) and high rates of primary production by upwelled nutrients (Haake et al., 1993; Rixen et al., 1996). In the northeastern Arabian Sea off Pakistan, on the other hand, no upwelling occurs and SST remains warm during NH summer. The seasonal SST pattern in the northern Arabian Sea is furthermore governed by the NE monsoon in NH winter. During this part of the year moderately strong, cold and dry north-easterly winds (caused by the reversal of atmospheric pressure gradients between central Asia and the southern Indian Ocean in fall (Clemens et al., 1991)) prevail in this region. The resultant increase in evaporation rates together with a reduction in solar insolation lower SST and increase the density of surface waters (Madhupratap et al., 1996; Prasanna Kumar and Prasad, 1996). Thus, while SSTs on the Pakistan Margin show a clear seasonal signal with high SST in summer (~28.5°C) and low SST (~23.5°C) in winter (Figure 4.1c; Levitus and Boyer, 1994), this seasonal pattern is less pronounced on the Oman Margin due to upwelling induced cooling during the summer monsoon season (Figure 4.1b).

The seasonally variable SST pattern of the Arabian Sea thus reflects monsoon dynamics and relative monsoon strength, so that SST changes determined in sediment records track past variations in monsoon strength over glacial/interglacial cycles (Emeis et al., 1995; Rostek et al., 1997; Schulte and Müller, 2001) and during the Holocene (e.g., Anand et al., 2008; Dahl and Oppo, 2006; Huguet et al., 2006; Naidu and Malmgren, 2005; Saher et al., 2007a; Saraswat et al., 2013). From these reconstructions, a general pattern emerged of increased NE monsoon strength during cold glacial stages and stadials, and vigorous SW monsoon strength

during warm interglacials and interstadial periods (e.g., Reichart et al., 1998; Rostek et al., 1997; Schulte and Müller, 2001; Schulz et al., 1998; Wang et al., 2001). This change in wind patterns had consequences beyond SST: Interglacials and interstadials also marked productivity maxima and an expanded oxygen minimum zone (OMZ) with intense denitrification in the Arabian Sea sub-thermocline, as reflected in maxima of organic carbon burial and $\delta^{15}N$ in sediments (Altabet et al., 2002; Suthhof et al., 2001). Monsoon activity in the Arabian Sea region varied not only on Milankovitch and millennial time scales during the Pleistocene, but also (with smaller amplitude) during the Holocene (e.g., Anderson et al., 2010, 2002; Fleitmann et al., 2004; Gupta et al., 2003; Lückge et al., 2001; Overpeck et al., 1996; Sirocko et al., 1993). Strongest SW monsoon activity was recorded in the early Holocene insolation maximum when air temperatures (Marcott et al., 2013) and summer precipitation in Asia were high (Fleitmann et al., 2003; Herzschuh, 2006). Most of these studies aimed to reconstruct summer monsoon strength, that determines the state of the upwelling system in the western Arabian Sea (Anderson et al., 2010, 2002; Gupta et al., 2003; Naidu and Malmgren, 1996). Much less attention has been given to the response of the NE monsoon to changing mid-latitude glacial/interglacial boundary conditions, and the dynamic evolution of the coupled winter and summer monsoon throughout the Holocene (Liu et al., 2009; Reichart et al., 2002b; Yancheva et al., 2007).

Since SST provide a signal for both monsoon seasons (i.e., determined by the intensity of summer upwelling versus deep winter mixing), several authors reconstructed time series of seasonal SST variations to distinguish between summer and winter monsoon strength (Anand et al., 2008; Naidu and Malmgren, 2005; Saher et al., 2007b). An alternative approach was used by Dahl and Oppo (2006), who investigated the spatial SST history of the Arabian Sea basin for different time slices. These authors showed that comparing SST variations in areas today affected by upwelling with areas not affected by upwelling is a viable approach to distinguish sea surface cooling caused by SW monsoonal upwelling from cooling caused by the northeasterly winds of the winter monsoon.

Here we add to this knowledge by presenting two new high-resolution alkenone-based SST records, one from the northern Oman Margin and one from the Pakistan Margin, spanning the last deglaciation and Holocene period. Alkenones are a robust and well studied indicator for past SST changes, but there are yet only a few alkenone-based SST records that document the Holocene SST history of the Arabian Sea (Huguet et al., 2006; Schulte and Müller, 2001; Sonzogni et al., 1998), and none of them with sufficient resolution or location to track Holocene changes in upwelling intensity. By comparing our high-resolution

alkenone-based SST record from the northern Oman Margin (SST affected by upwelling processes, Figure 4.1b) with that from the Pakistan Margin (no upwelling, Figure 4.1c) we aim to disentangle SST signals of the SW and NE monsoon to examine the relationship between both monsoon seasons over the last 25 ka. We furthermore seek for SST signals that (1) would document a response of the NE monsoon to changing glacial/interglacial boundary conditions and (2) would imply an influence of Asian and high-latitude Northern Hemisphere climate on northeast monsoonal wind strength during the Holocene epoch. To these ends, we compared our SST record of the last 25 ka (this study) together with our previously published high-resolution SST record of the late Holocene (Böll et al., 2014), both from the northeastern Arabian Sea, with records of air temperature variability from Asia and the NH, as well as with records of NH solar insolation.
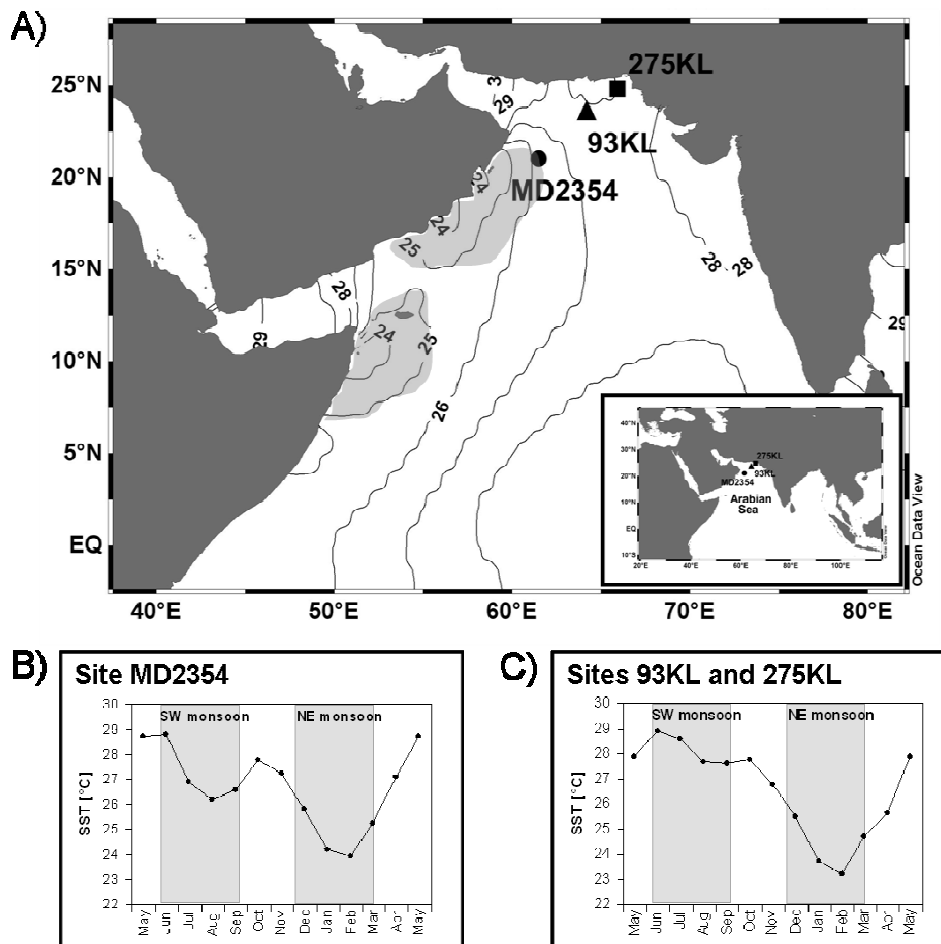
Figure 4.1: (a) Study area with core location MD00-2354 from the northwestern (NW) Arabian Sea and 93KL and 275KL from the northeastern (NE) Arabian Sea. Illustrated is the sea surface temperature pattern during the summer monsoon season (Jul-Sep). Shaded areas indicate regions of upwelling. This map was produced by using Ocean Data View (Schlitzer, 2013). (b) Annual SST variability for site MD2354 and (c) sites 93KL and 275KL extracted from the Wold Ocean Atlas (Levitus and Boyer, 1994).

4.2. Material and Methods

4.2.1. Sediment cores and stratigraphy

Piston core 93KL (23°35'N, 64°13'E; 1802 m water depth) was collected in 1993 during SONNE cruise 90 from the northern Murray Ridge near the coast of Pakistan (Schulz et al., 2002a, 1998; von Rad et al., 2002a). Calypso core MD00-2354 (21°02.55'N, 61°28.51'E; 2740 m water depth) was obtained from the northernmost section of the Owen Ridge, ~210 km offshore the Oman Margin by the research vessel MARION DUFRESNE in 2000. Both cores were sampled in 2.5 cm intervals (sample resolution of 100 to 300 years in core MD2354 and ~100 years in core 93KL) and alkenone unsaturation ratios were measured at the Institute for Baltic Sea Research Warnemünde (see below). Core SO130-275KL representing the late Holocene was analyzed at the Institute of Geology in Hamburg and results were published by (Böll et al., 2014).

Pronounced sediment facies changes between laminated, organic carbon rich and bioturbated, hemipelagic sediments are observed in the northern Arabian Sea at shallow to intermediate water depths within the oxygen minimum zone off Pakistan. Their relative dominance varied in phase with Northern Hemisphere climate depicted by the Greenland ice cores (e.g., Grootes and Stuiver, 1997). The change in depositional conditions is also seen in cores from deeper water and is represented by various sediment properties, such as sediment color, sediment geochemistry, or physical properties. A detailed chronology of core SO90-93KL, based on a correlation of sediment facies to the GISP2 ice core record has been published by Schulz et al. (1998, 2002a) for the past 110,000 years. Following this correlation a series of events (Table 4.1) has been recognized and dated by AMS ^{14}C and by high-resolution planktonic δ^{18}O records of the northern Indian Ocean (Sirocko et al., 1993). For the present study, that stratigraphic framework (using these parameters in addition to δ^{18}O stratigraphy) has been adopted. 5 to 25 specimens of *Globigerinodes ruber* white were picked from the 315-400 µm size fraction. Tests were cracked and cleaned in methanol and ultrasonic bath and were analyzed at the Kiel University Leibniz Institute for isotope research. The stable planktic isotope record for the Arabian Sea displays the established scheme of the two-step deglaciation with rapid shifts in δ^{18}O centered at ~15.0 and 11.0 kyr BP, framing a ~3 kyr-long plateau of δ^{18}O values of -0.7‰ (MD2354) and -1.0‰ (93KL). We estimate that the precision of our approach is less than 1 kyr, and thus comparable to individual AMS ^{14}C dating (where available) of stratigraphic match points.

Benthic stable isotope records in the Indopacific region show more divergent results (Skinner and Shackleton, 2005; Waelbroeck et al., 2006) and imply that distant and/or regional circulation changes occurred during the last deglaciation. A deep hydrological front at about 2000 m water depth, for instance, may have existed in the Indian Ocean (Kallel et al., 1988). Our two cores from 2740 m and 1802 m water depth are close to that inferred interface between a deep water and an intermediate-shallow water mass (Labeyrie et al., 2005) and benthic $\delta^{18}O$ records could be diachronous by up to 3000 years.

Table 4.1: Age models (0-25 Kyr) for Arabian Sea cores SO90-93KL* and MD00-2354.

GISP 2 AGE (Kyr BP)	SO90-93KL Depth (cm)	MD00-2354 Depth (cm)	Comment
1.00 [#]	0.0	0.0	Core Top
9.7 [5]	58.0	80.0	Start Early Holocene
11.45 [4]	70.0	115.0	Start Termination IB
12.6	76.0	130.0	Younger Dryas Maximum
12.9	82.0	142.5	Younger Dryas Start
14.5	97.5	165.0	IS1=B/A Maximum
16.1 [3]	124.0	197.5	H 1 Maximum
17.2 [2]	137.5	227.5	H 1 Base
23.3	159.0	297.5	IS 2
24.0	221.0	375.0	H 2 Maximum
24.7	233.0	390.0	H 2 Midpoint

* Schulz et al., 1998.

suggested age of intact core top, indicated by bronish-colored top layer.

5, 4, 3, 2 correlative isotope events to Sirocko (Table I, 1993).

B/A=Bølling/Allerød Epoch, IS=Interstadial, H=Heinrich chronozones.

4.2.2. Alkenone analysis

Sample preparation and analytical methods for alkenone analysis of cores SO90-93KL and MD2354 are detailed in Emeis et al. (2000). Sample preparation and analytical methods for core 275KL are those in Böll et al. (2014). Replicate extraction and measurement of a working sediment standard resulted in a mean standard deviation of estimated SST of 0.5°C. The alkenone index for all cores was translated to SST using the Indian Ocean core top equation of (Sonzogni et al., 1997b): $SST = (U_{37}^{K'} - 0.043)/0.033$ with $U_{37}^{K'} = C_{37:2}/(C_{37:2} + C_{37:3})$.

4.3. Results

Alkenone-derived SST estimates agree well with modern annual mean SST in the Indian Ocean (Sonzogni et al., 1997b), and in our records the SST at site 93KL (NE Arabian Sea off Pakistan) ranged between 23.2°C and 28.0°C over the last 25 ka (Figure 4.2b). In the interval representing the last glacial in core 93KL in the NE Arabian Sea, SST were high (25 to 26°C) during the Bølling-Allerød and Dansgaard-Oeschger events 1 and 2 and low (23 to 24°C) during Heinrich events 1 and 2 (H1, H2). The Last Glacial Maximum (LGM) to Holocene transition started at about 17 ka and is marked by a temperature increase of 4°C, which is slightly higher than the temperature increase found in other Arabian Sea alkenone-SST reconstructions (Emeis et al., 1995; Rostek et al., 1997; Sonzogni et al., 1998). After a maximum at 8 ka during the early Holocene SW monsoon maximum, SST were relatively stable and showed a slight decrease until today. The general Holocene SST trend seen in core 93KL is similar to the SST reconstruction of the nearby core 136KL (Schulte and Müller, 2001). Since the SST history of the last 2.5 ka is not very well resolved in core 93KL, alkenone-SST data from the recently published, nearby high-resolution core 275KL (Böll et al., 2014) were used to better resolve the late Holocene SST evolution. That record reveals a late Holocene SST cooling trend in the NE Arabian Sea, in line with the long-term temperature trend seen in core 93KL.

The range of SST at site MD2354 in the NW Arabian Sea (between 22.7°C and 26.1°C) is smaller than SST variations observed in core 93KL (Figure 4.2b). SST at both study sites was similar low during the LGM and H1, but showed a different evolution over Interstadial 1, when SST increased at site 93KL but remained low at site MD2354. On the other hand, SST at site MD2354 evolved simultaneously with SST at site 93KL during the transition to Holocene conditions and increased by up to 3°C from 17 to 15 ka. But whereas SST continued to rise until 8 ka at site 93KL, SST at site MD2354 reached maximum temperatures at ~14 ka, followed by a SST decrease to 24.5°C at around 9.5 ka. This SST decrease signal intensified upwelling caused by enhanced SW monsoon strength during the early Holocene (e.g., Gupta et al., 2003; Naidu and Malmgren, 1996; Sirocko et al., 1993). Following peak intensity during the Holocene climate optimum, upwelling and, by inference, wind strength weakened and SST gradually increased at site MD2354 off northern Oman.
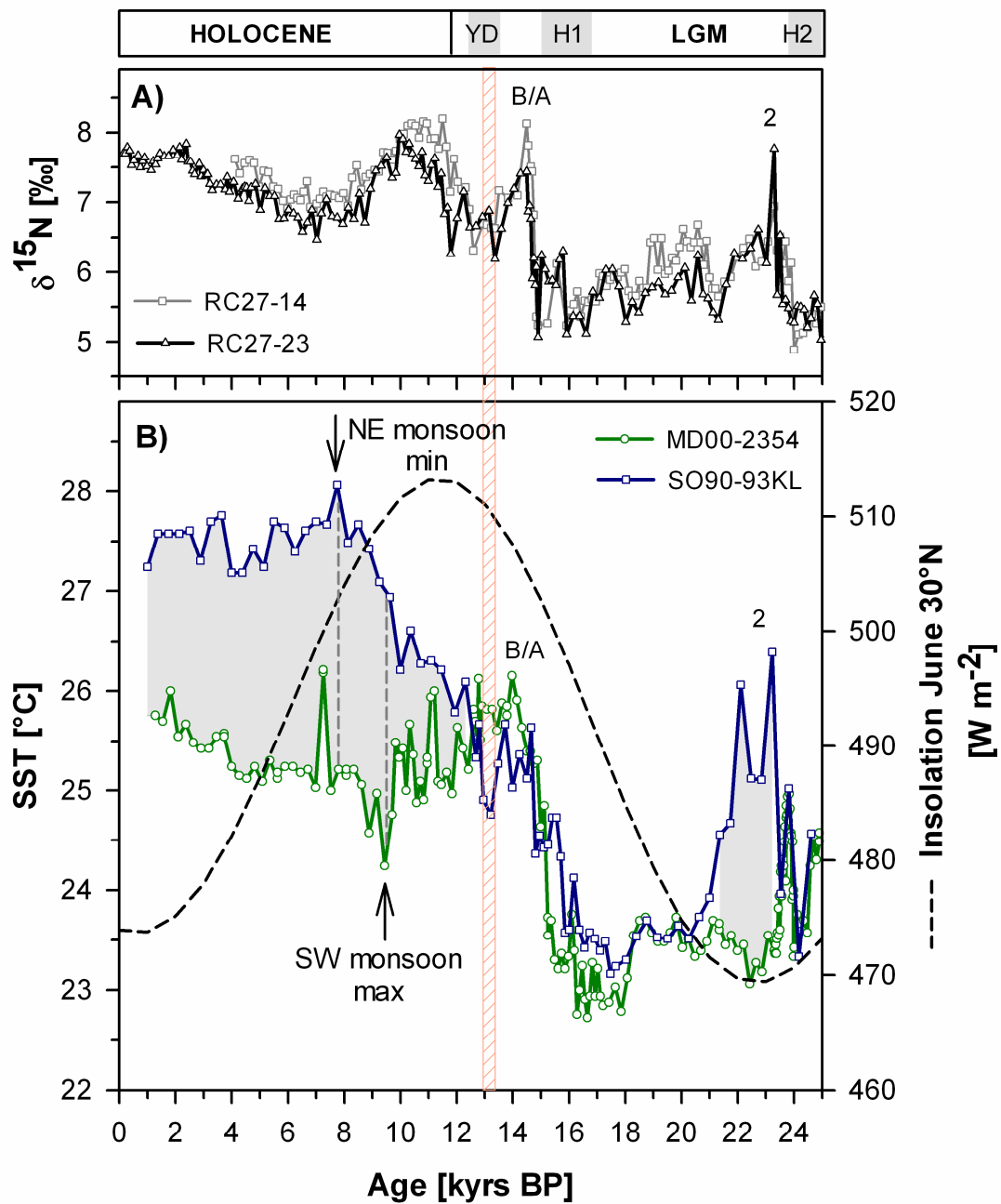
Figure 4.2: (a) δ15N record of cores RC27-23 and RC27-14 from the Oman Margin (Altabet et al., 2002), (b) alkenone-derived SST reconstruction for the northwestern Arabian Sea (core MD2354) and for the northeastern Arabian Sea (core 93KL). Both SST records are equally affected by winter cooling but only SST at site MD2354 is influenced by upwelling-induced cooling. Gray shading indicates the occurrence of upwelling at site MD2354. Dashed gray lines indicate the timing of maximum SW and minimum NE monsoon strength, respectively. Further illustrated are Heinrich events (H1 and H2), Dansgaard-Oeschger event 2 and the Younger Dryas (YD; stippled area).

4.4. Discussion

4.4.1. Dynamic evolution of SW and NE monsoon intensity during the last 25 ka

Both the NE (site 93KL) and NW Arabian Sea (site MD2354) sites experienced low SSTs during the LGM compared to Holocene values (Figure 4.2b). Other late Quaternary reconstructions of temperatures in the Arabian Sea mixed layer (Anand et al., 2008; Dahl and Oppo, 2006; Huguet et al., 2006; Naidu and Malmgren, 2005; Rostek et al., 1997; Saher et al., 2007a, 2007b; Saraswat et al., 2013; Schulte and Müller, 2001) also evidence basin-wide low SSTs during the LGM. Similar annual mean SST of sites 93KL and MD2354 indicates that this cooling was controlled by glacial boundary conditions and intensified NE monsoon strength, and not by intense upwelling (Emeis et al., 1995; Schulte and Müller, 2001; Schulz et al., 1998). SST at both of our study sites today are equally affected by the NE monsoon in winter, but SW monsoonal upwelling lower annual mean (AM) SST at site MD2354 compared to site 93KL (Figure 4.1b,c). The past onset of upwelling processes in the northern Arabian Sea thus should be reflected in an AM SST difference between our two study sites (i.e. lower AM SST at site MD2354 compared to site 93KL; see also gray shaded areas in Figure 4.2b).

One further argument against intensified upwelling and high primary production during the LGM is the variation in δ^{15}N, an indicator for the extent of denitrification in the OMZ. Low δ^{15}N values were recorded from 21 to 15 ka at the upwelling sites RC 27/23 and 14 and suggest a less intense OMZ and significant reduction or even absence of mid-water denitrification than in the modern situation (Altabet et al., 2002), most likely associated with reduced particle export from the mixed layer (Figure 4.2a).

The strong SST contrast between sites 93KL and MD2354 from 23 to 21.5 ka together with high δ^{15}N reveal that this glacial situation was interrupted by upwelling processes in the northern Arabian Sea during IS 1 (Figure 4.2a, b). While diminished north-easterly winds caused a SST increase at site 93KL off Pakistan during this period, the SST increase was suppressed at site MD2354 due to the intensification of SW monsoon winds and the accompanied onset of upwelling offshore northern Oman.

The northern Arabian Sea began to warm at about 17 ka, most likely as a result of weakening NE monsoon forcing together with strengthening SW monsoon winds. This SST rise lagged the increase of NH solar insolation by about 5000 years and can be attributed to glacial boundary conditions and NE monsoon forcing (Figure 4.2b). The overall increase in SST was interrupted by a short-term period of SW monsoon weakening (and/or NE monsoon

strengthening) induced by NH cooling during the Younger Dryas, which is expressed in decreased precipitation in Oman (Fuchs and Buerkert, 2008) and northeast Asia (Dykoski et al., 2005; Wang et al., 2001), and also by reduced upwelling (relatively low $\delta^{15}N$, see Figure 4.2a (Altabet et al., 2002)) and low organic carbon flux rates in the Arabian Sea (e.g., Ivanochko et al., 2005; Schulte and Müller, 2001). Whereas SST in the NE Arabian Sea (site 93KL) gradually increased until 8 ka due to weakening NE monsoon strength, SST off Oman (site MD2354) decreased after its maximum during the Bølling-Allerød at ~14 ka. Significant lower SST at site MD2354 than at site 93KL since 13 ka mark the onset of oceanic conditions in the northern Arabian Sea that are characterized by SW monsoon induced upwelling offshore Somalia and Oman (gray shaded area in Figure 4.2b). Thus, the SST decrease from 14 to 9.5 ka at site MD2354 tracks intensified upwelling offshore Oman caused by invigorated SW monsoon winds. Our alkenone-derived SST record is the first one to confirm an early Holocene upwelling increase with a SST minimum. The SST estimate of 24.5°C at ~9 ka suggests that upwelling was much more vigorous than today, because modern annual average SST are around 26°C in the Oman upwelling area (Levitus and Boyer, 1994). Other evidence, such as peak abundances of *G. bulloides* (Gupta et al., 2003; Naidu and Malmgren, 1996) and maximum $\delta^{15}N$ (Altabet et al., 2002; Suthhof et al., 2001) also suggest that upwelling was intense during the early Holocene. Terrestrial records, moreover, indicate an early Holocene SW monsoon maximum throughout the Asian monsoon domain: Wet climate conditions with high rates of summer monsoonal rainfall were recorded in southern China (Dykoski et al., 2005), India (Kessarkar et al., 2013), Oman (Fleitmann et al., 2007, 2003; Fuchs and Buerkert, 2008) and Yemen (Lézine et al., 2007). Fleitmann et al. (2007) and Van Rampelbergh et al. (2013) pointed out that maximum rainfall in southern and northern Oman cave records is related to a shift of the northernmost position of the Intertropical Convergence Zone (ITCZ) to northern Oman. We believe that this has not only intensified, but also led to a longer duration of seasonal upwelling.

The early Holocene upwelling intensification indicated by SST cooling at site MD2354 is in line with the $\delta^{15}N$ record from the Oman Margin during the period from 12 to 10 ka (Figure 4.2a). High $\delta^{15}N$ values during this time indicate intensified denitrification in an expanding OMZ caused by enhanced particle export from the mixed layer due to increased upwelling strength. But this period was followed by an interval of decreasing $\delta^{15}N$ from 10 to 9 ka that is embedded in the decreasing temperature trend (Figure 4.2a,b). The deviation from the long-term (glacial-interglacial) antagonistic pattern of SST and $\delta^{15}N$ is in our interpretation due to adjustments in intermediate water mass origin and circulation in the northern Arabian Sea.

Pichevin et al. (2007) pointed out that the extension and position of the OMZ is the expression of an interplay between productivity and ventilation, and Rixen et al. (2013) showed that enhanced upwelling is accompanied with enhanced inflow of well-ventilated Indian Central Water into the OMZ from the south. Furthermore, sea level rise in the early Holocene triggered the outflow of Persian Gulf intermediate water into the thermocline of the Arabian Sea, which today adds to OMZ ventilation (Lambeck, 1996).

Temperatures in the sea surface of the NE Arabian Sea (site 93KL) evolved differently. Over the time of maximum upwelling and SW monsoon strength in the NW Arabian Sea from 12 to 9 ka, SSTs here continue to rise and indicate waning NE monsoon strength. This decoupling of conditions in the mixed layers over the Oman and Pakistan margins on sub-Milankovitch time scales has been previously observed in productivity records (Reichart et al., 2002b).

SST at site MD2354 increased again over the middle to late Holocene (since ~8 ka) but slightly decreased at site 93KL pointing to a decline in SW monsoon strength (weakened upwelling) at invigorated NE monsoon conditions as a response to decreasing NH summer solar insolation (e.g., Fleitmann et al., 2003; Gupta et al., 2005; Neff et al., 2001). Over this period intense (weak) winter monsoon activity in the northern Arabian Sea coincides with strong (weak) East Asian winter monsoons (Yancheva et al., 2007). Minimum NE monsoon intensity (~8 ka), however, occurred 1500 years later than peak SW monsoon strength (~9.5 ka) and the general opposing trend of summer and winter monsoon activity was less clear between 9.5 to 8 ka (Figure 4.2b). This antagonistic pattern of summer and winter monsoon variability is best explained by long-term movements of the annual mean position of the ITCZ (Yancheva et al., 2007), as proposed previously by Böll et al. (2014) for the late Holocene. Northern Hemisphere cooling in response to decreasing solar irradiance moves the mean position of the ITCZ southward (Broccoli et al., 2006), thus reducing the northward extent of the Asian SW monsoon and reducing summer monsoon precipitation over the Asian continent (Yancheva et al., 2007). The NE Arabian Sea is located within the northern limit of the long-term annual mean position of the ITCZ, so that long-term southward displacement of the ITCZ throughout the Holocene (Haug et al., 2001) shortens the summer monsoon season and strengthens or prolongs the influence of NE monsoon winds over the northern Arabian Sea, causing low annual mean SST off Pakistan (site 93KL). Insolation-triggered ITCZ movements thus do not only affect the rainfall patterns over land, but apparently also influence upper ocean properties in the northern Arabian Sea by modulating monsoon strength.

4.4.2. Monsoon variability in the NE Arabian Sea and Asian air temperature variations during the last deglaciation and over the last 2500 years

SST offshore Pakistan today is strongly influenced by ocean-atmosphere interaction. Comparison of our northern Arabian Sea SST record (site 93KL) with records of air temperature variability from Asia (Peterse et al., 2011; Thompson et al., 1997; Wen et al., 2010) shows that this relationship was less pronounced during the last deglaciation (Figure 4.3b,c). Whereas air temperatures recorded on the Asian continent closely tracked NH summer solar insolation during the last deglaciation (Figure 4.3b), maximum SST at site 93KL (and thus minimum NE monsoon strength) in the NE Arabian Sea lagged air temperature and maximum solar insolation by about 3.5 ka (Figure 4.3c). Longer records have shown that the timing of maximum summer monsoon strength lagged peak NH summer solar insolation by ~8 ka at the precession band over the last 350,000 years (e.g., Clemens and Prell, 2003; Clemens et al., 2010; Wang et al., 2005a). However, high-resolution records indicate a phase lag of about 2-3 ka between maximum summer monsoon strength and peak summer solar insolation for the last glacial to Holocene transition (Dykoski et al., 2005; Fleitmann et al., 2007; Overpeck et al., 1996), that is in line with our SST data from the northern Arabian Sea. This lag has been attributed to internal climate forcing by glacial boundary conditions, such as North Atlantic temperature and global ice coverage and to the extent of latent heat export from the southern subtropical Indian Ocean associated with the precession and obliquity band (Clemens and Prell, 2003).

Monsoon intensity off Pakistan (site 93KL) apparently was still influenced by glacial boundary conditions during the last deglaciation that suppressed direct insolation forcing on monsoon intensity and thus SST. Slightly decreasing SST at site 93KL indicative of increased NE monsoon strength off Pakistan from about 8 to 4 ka (Figure 4.3c), on the other hand, match very well with contemporaneous cooling on the Tibetan Plateau as indicated by a depletion of ice core $\delta^{18}O$ in the Guliya ice cap (Figure 4.3; Thompson et al., 1997). This would imply that during the mid to late Holocene, when glacial boundary conditions were negligible, NE monsoon intensity in the NE Arabian Sea may have directly (and without a time lag) responded to atmospheric forcing, such as air temperature and solar insolation. To test this hypothesis for centennial scale climate variability, below we compared our previously published, high-resolution SST reconstruction of core 275KL (Böll et al., 2014) with air temperature variations recorded in Asia over the last 2000 years (Figure 4.4).
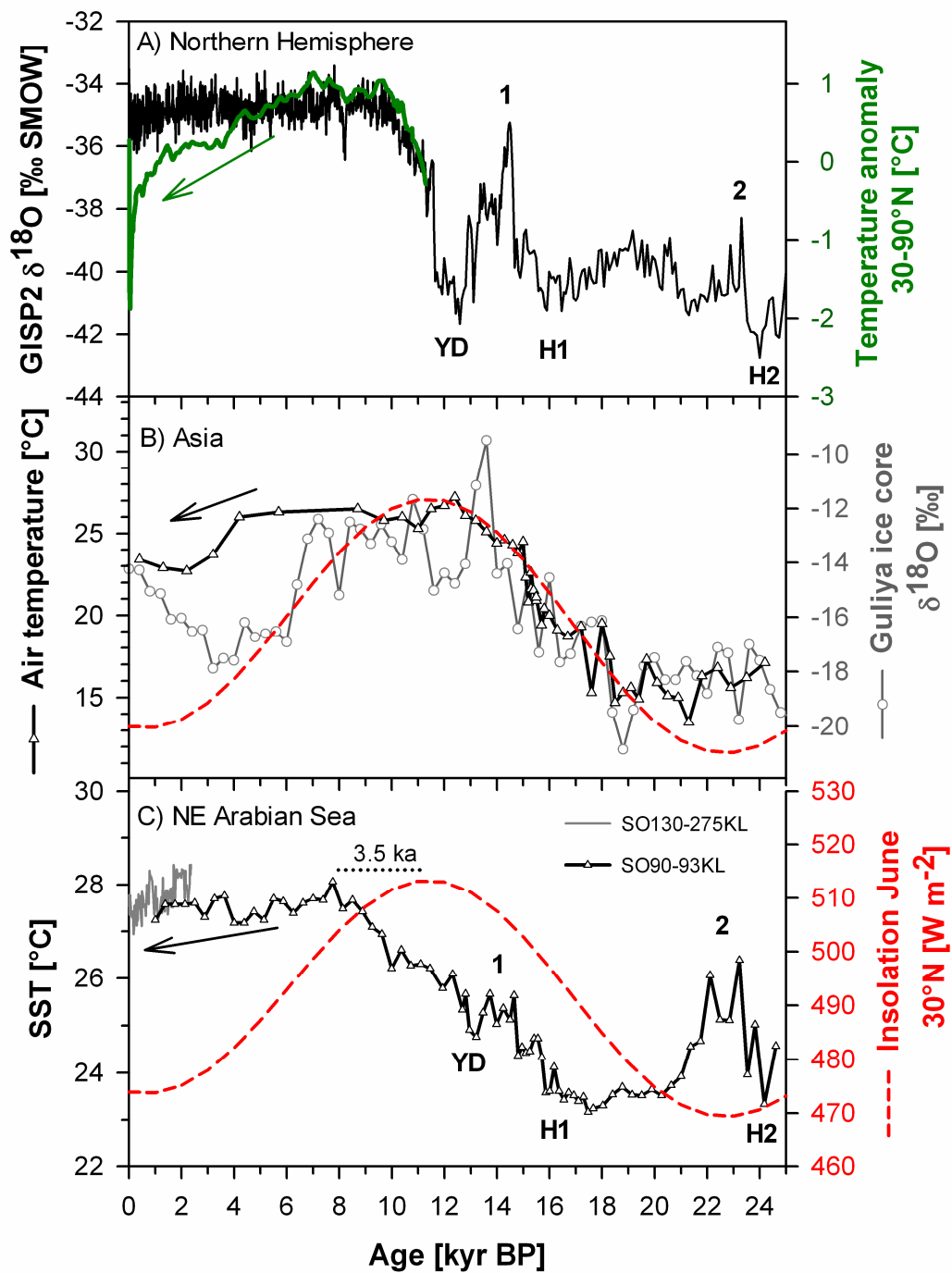
Figure 4.3: SST variations in the northeastern Arabian Sea over the last 25 ka compared to air temperature variations in Asia and the Northern Hemisphere. (a) temperature reconstructions for the North Atlantic (GISP2 ice core; Grootes and Stuiver, 1997) (black line) and the extratropical Northern Hemisphere (30°N-90°N; Marcott et al., 2013) (green line), (b) record of continental air temperature for central China (black curve; Peterse et al., 2011) and the Tibetan Plateau (gray curve; Thompson et al., 1997) compared to Northern Hemisphere (NH) summer solar insolation (Berger and Loutre, 1991) (red curve; same scale as in 3c) and (c) alkenone-derived SST reconstructions of core 93KL (last 25 ka) and cores 39KG/275KL (last 2.5 ka; Böll et al., 2014) compared to NH summer solar insolation (red curve; Berger and Loutre, 1991).

Comparison of alkenone-SST from the northeastern Arabian Sea (core 275KL; Böll et al., 2014) with tree-ring-derived temperature anomalies (PAGES 2k Consortium, 2013) reveals similar century-long temperature trends over the last 1200 years (Figure 4.4a, b). Furthermore, temperature changes in China (Ge et al., 2013) compiled from different types of terrestrial proxies (ice cores, stalagmites, tree-rings, lake sediments and historical documents) agree very well with NE Arabian Sea SST variations on centennial time scales (Figure 4.4c). Over the past 2000 years increased (decreased) SSTs in the NE Arabian Sea coincided with warm (cold) temperature excursions in China. This relationship is less significant during time periods of small-scale temperature variability (e.g. 1.6 to 1.1 ka), but well pronounced during late Holocene climate periods, such as the Roman Warm Period (RWP), Medieval Warm Period (MWP) and Little Ice Age (LIA) (see dashed gray lines in Figure 4.4). In general, both regions exhibited relatively warm climate conditions during NH warm periods (RWP and MWP), as well as recent warming over the last 100 years. On the other hand, cold climatic conditions are registered in both records during the LIA from 0.55 to 0.1 ka (1400 to 1850 A.D.), whereas climate was more variable in China from 1.55 to 1.15 ka (400 to 800 A.D.). Supporting evidence for LIA cooling and medieval warming comes not only from China (Ge et al., 2013; Yang et al., 2002), but also from other regions in Asia such as the northwest Karakorum (western Asia; Esper et al., 2002), the Tibetan Plateau (Bao et al., 2003) and the entire temperate East Asian region (PAGES 2k Consortium, 2013).

These coherent temperature changes between the NE Arabian Sea and the Asian continent imply a strong linkage between land and ocean during the last two millennia by the Asian monsoon system. Low SSTs on the Pakistan Margin indicate times of strengthened NE monsoonal winds in winter and/or weaker SW monsoon in summer (see chapter 4.4.1). Most studies in the Asian monsoon domain show intensified SW monsoon activity during the warm MWP, but diminished SW monsoon (increased NE monsoon) conditions during the cold LIA (e.g., Anderson et al., 2010; Gupta et al., 2003; Zhang et al., 2008). Modelling studies suggest that low air temperatures over Pakistan, north-west India and beyond were associated with strong north-easterly monsoon winds, the advection of cold, dry air over the Arabian Sea and low SST in the northern Arabian Sea during boreal winter (Marathayil et al., 2013). Thus, cold climate conditions over land during the LIA (Figure 4.4a, c) (Esper et al., 2002; Ge et al., 2013; PAGES 2k Consortium, 2013; Yang et al., 2002) increased NE monsoonal wind strength over the NE Arabian Sea and caused low SST off the coast of Pakistan (Figure 4.4b). Decadal- to centennial scale variations in NE monsoon strength over the NE Arabian Sea

were thus directly influenced by Asian climate via atmospheric teleconnections over the last two millennia.
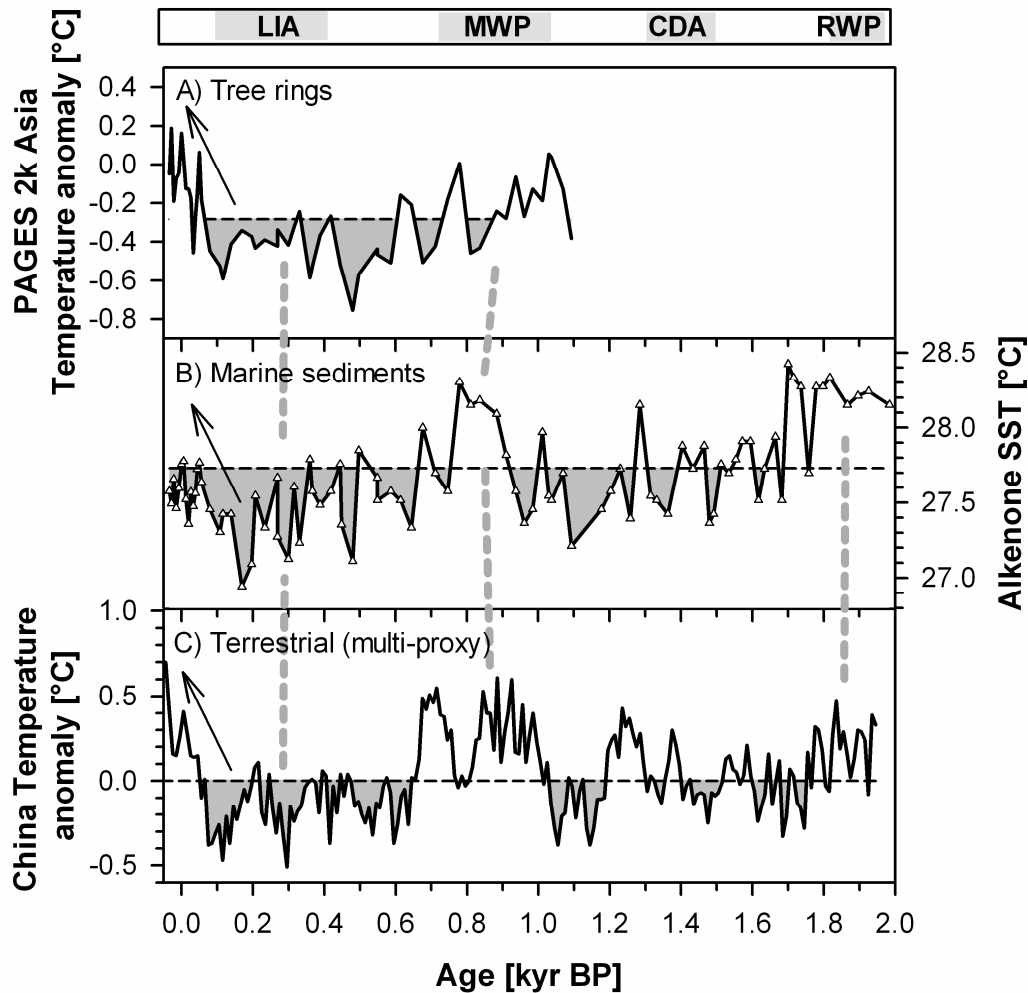
Figure 4.4: Temperature variability over the Asian monsoon domain during the last two millennia derived from (a) tree-rings (smoothed by calculating the respective mean value over the time interval which is represented by the alkenones) from PAGES 2k Consortium, (2013), (b) marine sediments from the northeastern Arabian Sea (alkenone-derived SST in cores 39KG/275KL; Böll et al., 2014), and (c) a combination of different continental proxy types (Ge et al., 2013). Dashed lines indicate the respective mean over the studied time interval. Dashed gray lines suggest correlations between the archives. Further illustrated are characteristic climate periods known from the Northern Hemisphere: Little Ice Age (LIA), Medieval Warm Period (MWP), Cold Dark Ages (CDA), and Roman Warm Period (RWP).

4.4.3. NE monsoon intensity and Northern Hemisphere climate change

Monsoon strength is closely coupled to North Atlantic climate over glacial/interglacial cycles, but Holocene millennial scale changes in NE monsoon intensity (core 93KL, Figure 4.3b) are not reflected in GISP2 ice core data (Grootes and Stuiver, 1997) that indicate relative stable climate conditions over the Holocene (Figure 4.3a). Nevertheless, a recently published multi-proxy temperature reconstruction from the extratropical NH (Marcott et al., 2013) exhibits gradual NH cooling since the beginning of the Holocene that parallels strengthening of NE monsoon intensity over the NE Arabian Sea (as indicated by lowered SST at site 93KL; Figure 4.3a, c). The NE monsoon weakened during the early Holocene when temperatures in the extratropical NH (30°N to 90°N) were high. On the other hand, decreasing temperatures in the NH from 5.5 to 0.1 ka match strengthened winter monsoon intensity over the northern Arabian Sea and East Asia (Yancheva et al., 2007). This linkage was also recognised in variations in summer monsoon strength and related to NH climate during the Holocene (e.g., Gupta et al., 2003; Hong et al., 2003; Wang et al., 2005b).

Similar features of the high-resolution SST record from core 275KL and NH temperature reconstructions suggest that the linkage between Asian climate variability and high-latitude climate change also exists on centennial time scales during the late Holocene (Figure 4.5). Variations in NE monsoon strength in the NE Arabian Sea (core 275KL; Figure 4.5d) are coeval and similar in sign as in air temperatures over Central Greenland (Figure 4.5b; Alley, 2000) and the entire NH (Figure 4.5a; Christiansen and Ljungqvist, 2012; Moberg et al., 2005), and track sea surface temperature (Sicre et al., 2008) and drift ice in the North Atlantic (Figure 4.5c; Bond et al., 2001). These expressions of high-latitude and North Atlantic climate coincide with climate variations (such as monsoon strength and temperature) of the Asian continent (Ge et al., 2013; PAGES 2k Consortium, 2013; Yang et al., 2002; Zhang et al., 2008). The linking mechanism is yet unclear, but may be related to solar activity. SST at site 275KL in the NE Arabian Sea gradually decrease over the past 2000 years, in accord with global SST cooling (PAGES/Ocean2k Working Group, 2012) and in response to decreasing NH summer insolation (Figure 4.5d). Thus, NE monsoon strength closely mirrors long-term as well as centennial scale variations in irradiance by responding to solar triggered feedback mechanisms such as the position of the ITCZ and Eurasian snow cover that determine the land-sea thermal contrast between the Asian continent and Indian Ocean.
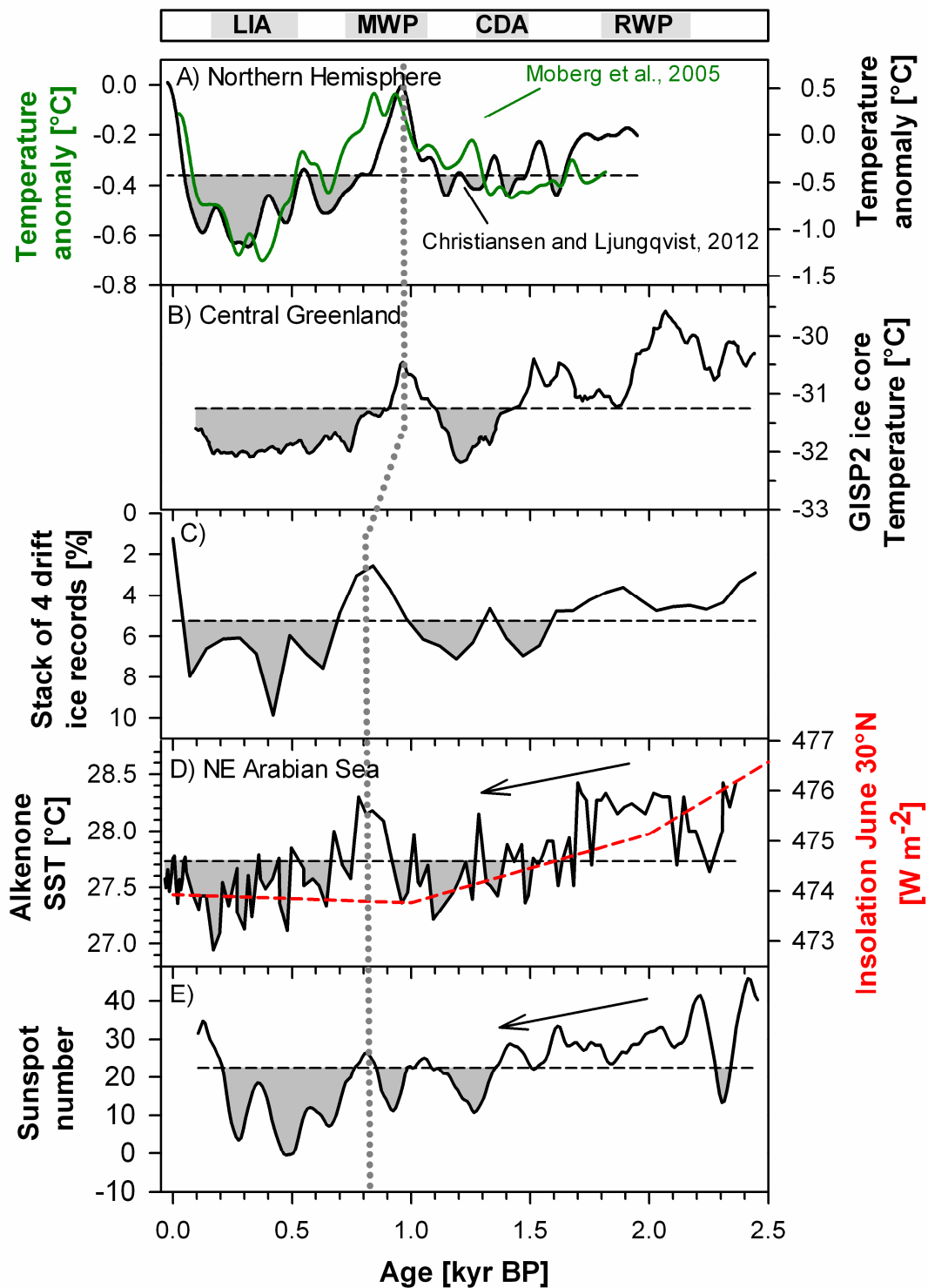
Figure 4.5: (a) Northern Hemisphere temperature reconstructions (Christiansen and Ljungqvist, 2012; Moberg et al., 2005), (b) Temperature record for Central Greenland from the GISP2 ice core (Alley, 2000), (c) Stack of 4 drift ice records from the North Atlantic (Bond et al., 2001), (d) Alkenone-SST record for cores 39KG/275KL from the northeastern Arabian Sea (black curve; Böll et al., 2014) compared to Northern Hemisphere summer solar insolation (red curve; Berger and Loutre, 1991), and (e) Sunspot numbers (smoothed by a 11-point running mean) as an indicator for changes in solar output (Solanki et al., 2004). Dashed lines indicate the respective mean over the studied time interval.

In-step cooling over the North Atlantic, Asia and the Tibetan Plateau (Feng and Hu, 2005) triggered by reduced solar insolation leads to expanded snow cover over Eurasia, a delayed warming in spring and a reduced pressure gradient between central Asia and the southern Indian Ocean (Meehl, 1994). The reduced land-sea thermal contrast causes the SW monsoon to weaken, so that annual mean SST in the NE Arabian Sea is shifted to lower temperatures. A physical mechanism linking North Atlantic SST and monsoonal climate was recently proposed by Goswami et al. (2006): Cold phases of the Atlantic Multidecadal Oscillation (AMO) result in a decrease of the meridional gradient of tropospheric temperature and thus to an early retreat of the SW monsoon, causing decreased monsoonal rainfall and cold atmospheric temperatures in Asia (Wang et al., 2013). As pointed out above, this would enhance the influence of NE monsoonal winds and lower SST off Pakistan. Although the exact teleconnection mechanism between climate variations of the high-latitude NH and the NE monsoon remains to be identified, SST in the northern Arabian Sea indicate that they are linked on orbital and shorter time scales during the Holocene.

4.5. Conclusions

Alkenone-based SST records from the NW Arabian Sea influenced by the summer monsoon (SST affected by upwelling processes) and from the NE Arabian Sea, where SST is mainly governed by the winter monsoon (no upwelling), depict the dynamic evolution of the SW and NE monsoon over last 25 ka. The strength of summer monsoon activity was inversely related to winter monsoon intensity over the Holocene. SW monsoon intensity began to increase at the start of the last deglaciation and reached maximum strength between 11 to 8 ka during the early Holocene climate optimum, as indicated by SST changes offshore northern Oman. This is to our knowledge the first alkenone-based SST record that provides sufficient temporal resolution to show an early Holocene intensification of SW monsoon induced upwelling that caused lower than today annual mean SSTs in the northern Arabian during this time. The NE monsoon on the other hand was strongest during the Last Glacial Maximum but diminished since ~17 ka. Throughout the middle to late Holocene, SW monsoon activity weakened while the NE monsoon gained strength again. This interplay between SW and NE monsoon strength was forced by a southward displacement of the Intertropical Convergence Zone throughout the Holocene.

Millennial to centennial scale monsoon dynamics over the northern Arabian Sea were linked to climate variations recorded on the Asian continent, such as variations in the East

Asian monsoon and changes in air temperature. The increase of SST in the NE Arabian Sea during the last deglaciation lagged that of NH summer solar insolation and of Asian air temperature for about 2 to 3 ka because monsoon intensity was still influenced by glacial boundary conditions during this time. However, a strong linkage between northeast monsoonal wind strength over the northern Arabian Sea (as indicated by SST changes), temperature variations in Asia and climate of the high-latitude NH exists over the last 2000 years. Colder climate conditions over land increase the strength of northeast monsoonal winds and lower SST in the NE Arabian Sea. These centennial scale variations in the strength of the northeast monsoon over the northern Arabian Sea seem to be coupled to solar changes over the last 2000 years.

CHAPTER 5

5. Spatial and temporal variability of the Arabian Sea oxygen minimum zone over the Holocene

Abstract

The northern Arabian Sea is one of the main oceanic regions with a permanent low oxygen layer at intermediate water depth that results in water column denitrification. While glacial/interglacial variations in the Arabian Sea oxygen minimum zone (OMZ) are relatively well studied, little is known about the spatial and temporal extent of mid-water oxygen throughout the Holocene. Here we analyzed parameters indicative of mid-water oxygenation together with records of southwest monsoon strength in two sediment cores from the northern Oman Margin to reconstruct the temporal variability of the Arabian Sea OMZ and its relation to changing SW monsoon activity over the Holocene. Comparison of $\delta^{15}N$ and Mn/Al records with other reconstructions of denitrification and oxygenation from the northern Arabian Sea reveals a Holocene shift in the location of the core OMZ from the northwest (early Holocene) to the northeast Arabian Sea (late Holocene). This shift was caused by the interplay of spatial differences in oxygen demand, caused by varying responses of primary productivity to SW monsoonal upwelling, and changes in mid-water ventilation due to sea level rise. Regional short-term (centennial scale) fluctuations in the oxygen inventory of the northern Arabian Sea were linked to variations in SW monsoon activity over the mid Holocene: Phases of strong wind intensity triggered intense upwelling in the coastal region of northern Oman that induced high rates of primary productivity and invigorated denitrification. Although it is unknown how the Arabian Sea OMZ will change in the future, our data infer that future short-term fluctuations in monsoonal wind strength might induce regional changes in mid-water oxygen.

5.1. Introduction

The Arabian Sea in the northern Indian Ocean exhibits one of the most pronounced oxygen minimum zones (OMZ) of the world's ocean. Permanent, year round low oxygen levels in Arabian Sea intermediate waters are accompanied by high rates of water column denitrification (Bange et al., 2000; Bulow et al., 2010; Codispoti et al., 2001; Ward et al., 2009), a process that removes biologically available nitrogen from the biosphere (Altabet et al., 1995). Moreover, nitrous oxide (N_2O), an important green house gas, is produced as a by-product of denitrification, thus making changes in the Arabian Sea OMZ a potential driver of climate change (Altabet et al., 2002; Bange et al., 2001; Naqvi et al., 1998).

The oceanic properties of the Arabian Sea that maintain the OMZ are closely coupled to the seasonal monsoon cycle. Differential land-ocean heating and the annual reversal of the atmospheric pressure gradient between central Asia and the southern Indian Ocean cause the seasonal reversal of low-level winds over the Arabian Sea (Clemens et al., 1991; Hastenrath and Lamb, 1979). The strong south-westerly winds of the summer monsoon induce upwelling and elevated primary production in the northwestern Arabian Sea (e.g., Haake et al., 1993; Nair et al., 1989; Rixen et al., 2000). Although mid-waters are faster replenished during this time of the year (Rixen et al., 2013), oxygen consumption during mineralization of sinking organic matter is the main, monsoon driven process in modulating OMZ intensity on seasonal to inter-decadal time scales.

Location, spatial extension and intensity of the mid-water oxygen minimum zone in the Arabian Sea was not stable through time, but varied in accordance with changes in southwest monsoon strength. Several studies report the existence of a pronounced OMZ and elevated denitrification during interstadials and interglacial stages, whereas the Arabian Sea was well ventilated and denitrification was suppressed during stadials and glacial stages (Altabet et al., 1999, 2002; Pichevin et al., 2007; Reichart et al., 1997; Schulte et al., 1999; Suthhof et al., 2001). This has been attributed to a reorganization of mid-water circulation (partly because of Red Sea water entrainment in reaction to sea level change) (Böning and Bard, 2009; Jung et al., 2009; Pichevin et al., 2007) combined with primary productivity changes due to varying SW monsoon intensity at glacial/interglacial transitions (Altabet et al., 2002). Changing denitrification rates indicated by $\delta^{15}N$ measurements further imply that Arabian Sea N_2O emissions may have contributed to past atmospheric N_2O fluctuations (e.g., Altabet et al., 1995). While the history of mid-water oxygenation in the Arabian Sea is well studied on longer time scales, relatively little is known about the spatial and temporal variability of the

Arabian Sea OMZ over the Holocene on sub-millennial time scales (e.g., Reichart et al., 2002b).

Here we present two new high-resolution records of $\delta^{15}N$ and Mn/Al from the northern Arabian Sea off northern Oman that offer insights into the regional history of mid-water oxygenation in two time slices from the mid and late Holocene. These new $\delta^{15}N$ and Mn/Al records were compared to published records of $\delta^{15}N$ and Mn/Al from different locations in the Arabian Sea (Pichevin et al., 2007), which together track short-term variations in the spatial and temporal extent of the Arabian Sea OMZ over the Holocene. The influence of SW monsoon activity on long-term (Holocene trends) and short-term (centennial scale fluctuations) variations in OMZ intensity was investigated by the reconstruction of monsoon driven parameters such as upwelling (alkenone-derived sea surface temperatures) and wind strength (Zr/Al), primary productivity changes (biogenic content of sediments) and the relative input of continental dust to our study site (accumulation of lithogenic material, Mg/Al, Ti/Al).
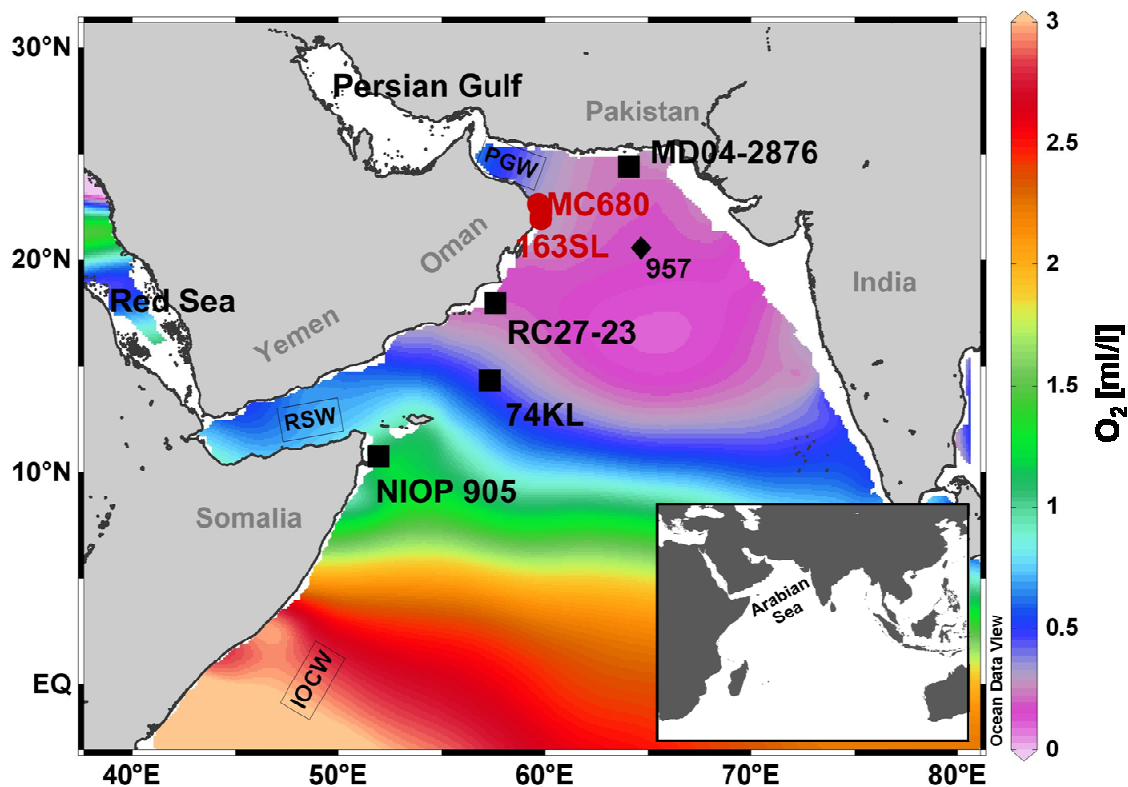
Figure 5.1: Study area of the Arabian Sea with core locations M74/1b-163SL and MC680 (red dots) and locations of cores discussed in the main text (black squares). Illustrated by color shading is the oxygen content in 300 m water depth indicating strongest oxygen deficiency in the northeastern basin. The main ventilation sources at intermediate water depth in the northern Arabian Sea are Indian Ocean Central Water (IOCW), Red Sea Water (RSW) and Persian Gulf Water (PGW). This map was produced by using Ocean Data View (Schlitzer, 2013).

5.2. The present-day OMZ in the northern Arabian Sea

Stable OMZ conditions in the northern Arabian Sea at water depths between 200 and 1200 m are maintained by the balanced interaction of oxygen demand (organic matter degradation) and oxygen supply (ventilation) (e.g., Olson et al., 1993; Sarma, 2002). The degradation of high sinking fluxes of organic matter from the mixed layer consumes oxygen and is the dominant oxygen sink. Primary productivity and particle flux in the northern Arabian Sea are highly seasonal and more than 50% of annual particle fluxes occur during the summer season, when strong southwest monsoon winds induce upwelling of cold, nutrient-rich water masses along the coast of Somalia and Oman (Haake et al., 1993; Nair et al., 1989; Rixen et al., 1996). The northeastern Arabian Sea off Pakistan is not influenced by upwelling. Here, vertical mixing through convection processes and upward transport of nutrients in winter sustain the main part of primary production. The northern Arabian Sea OMZ persists throughout the year, although primary production is highly variable and strongly impacted by the seasonal monsoon cycle.

The main sources of oxygen at intermediate water depth in the northern Arabian Sea are the outflows from the marginal seas in the north and Indian Ocean Central Water (IOCW) from the south (Olson et al., 1993). Persian Gulf Water (PGW, 200-400 m water depth) and Red Sea Water (RSW, 600-800 m water depth) have high salinities and are comparatively rich in oxygen, because they form at the surface and have atmospheric contact shortly before entering the Arabian Sea through the Strait of Hormuz (50 m sill depth) and Strait of Bab-el-Mandeb (137 m sill depth), respectively (Rohling and Zachariasse, 1996; Sarma, 2002; and references therein). IOCW combines Antarctic Intermediate Water, Subantarctic Mode Water and Indonesian Intermediate Water and is transported to the northern Arabian Sea from the southwest during the summer monsoon as part of the Somali current (You, 1998). Intermediate water from the southern sources is originally rich in oxygen, but becomes oxygen depleted (and nutrient rich) on its path to the Arabian Sea owing to oxygen loss during the mineralization of sinking organic matter. Further oxygen loss on its way through the Arabian Sea results in higher oxygen concentrations in the NW basin and lower oxygen concentrations in the NE basin of the Arabian Sea (Figure 5.1).

Oxygen concentrations at intermediate water depth restrict water column denitrification to the NE Arabian Sea, although particle flux from productivity is highest in the NW basin (e.g., Gaye-Haake et al., 2005). Denitrification that reduces nitrate to nitrite and gaseous nitrogen is triggered when oxygen concentration falls below 5µM O_2 (Devol, 1978). In general, oxygen deficient conditions enable denitrification below 100 m water depth (Figure

5.2). At our study site, intrusion of PGW that flows in southward direction along the coast of Oman can supply oxygen and occasionally suppresses denitrification, as was the case during the late SW monsoon 2007 between 250 and 400 m water depth (Gaye et al., 2013). Denitrification strongly fractionates nitrogen isotopes and the remaining nitrate is enriched in $\delta^{15}N$. Off Oman, SW monsoon upwelling forces nitrate deficient water masses to the surface, so that the high $\delta^{15}N$ signal of nitrate is effectively transported into the euphotic zone. The isotopically enriched nitrate is assimilated into particulate matter by phytoplankton and sinks through the water column to the seafloor. The signal of denitrification and OMZ intensity is thus preserved in marine sediments (Altabet et al., 1995; Gaye-Haake et al., 2005; Naqvi et al., 1998; Suthhof et al., 2001).
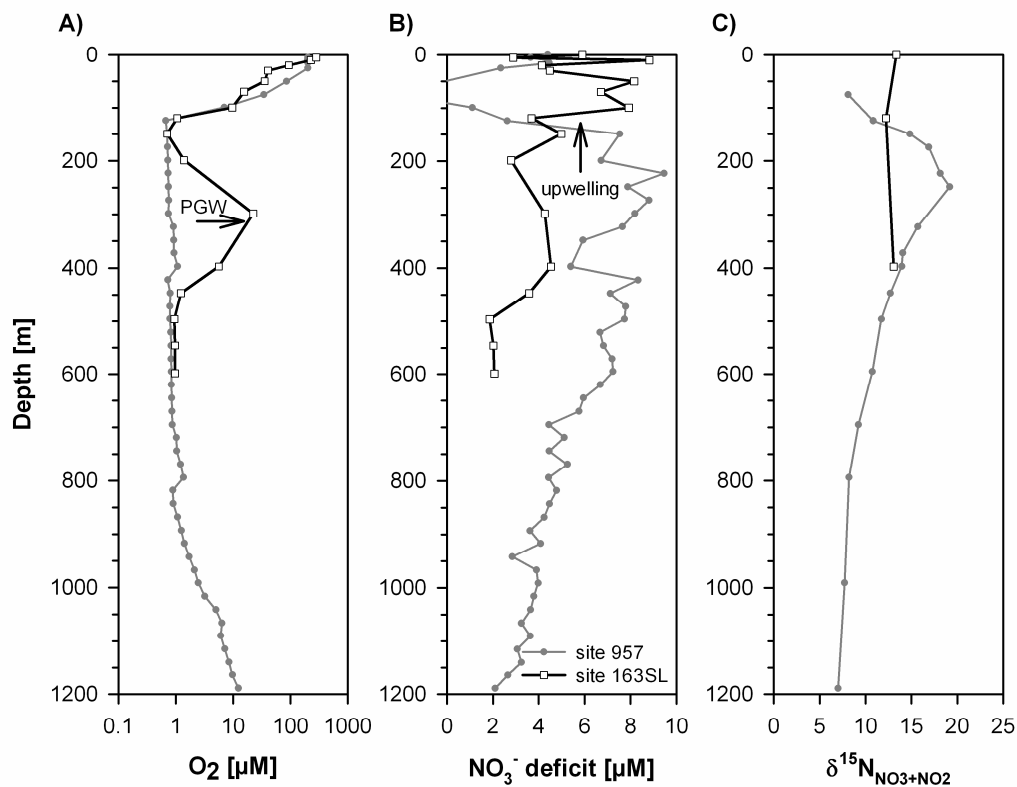
Figure 5.2: Water column profiles of (a) oxygen concentration, (b) NO_3^- deficit and (c) $\delta^{15}N$ at sites M74/1b-163SL (black) and #957 (gray) during the late SW monsoon 2007 (Gaye et al., 2013). Increase of oxygen between 250 and 400 m water depth indicate intrusion of Persian Gulf Water to our study site.

5.3. Methods

5.3.1. Sample collection

In this study, we analyzed the first 400 cm of gravity core 163SL and the first 50 cm of multicorer MC680. Core 163SL (21°55.97'N, 59°48.15'E, 650 m water depth) and multicorer MC680 (22°37.16'N, 59°41.50'E, 789 m water depth) both were retrieved in 2007 during Meteor cruise M74/1b within the OMZ on the continental margin off northern Oman. The first 400 cm of core 163SL were sampled in continuous 3 cm intervals (resolution of 10 to 50 years). We analyzed bulk parameters (TOC, carbonate, opal), alkenones and stable nitrogen isotopes ($\delta^{15}N$) in all sediment samples. The elemental composition of sediments was analyzed in 1 cm intervals for the upper part of the core (0-70 cm) and every third to forth sample in the lower part (70 to 400 cm). The elemental composition of MC680 was determined in 1 cm down-core resolution and $\delta^{15}N$ was analyzed in every second sample. All sediment samples were freeze-dried and homogenized prior to chemical treatment and analyses.

5.3.2. Bulk components

Total carbon and total organic carbon (TOC) were measured on a Carlo Erba 1500 elemental analyzer (Milan, Italy). Total organic carbon was analyzed after samples were treated with 1 molar hydrochloric acid (HCl) to eliminate inorganic carbon. Analytical precision for carbon was 0.02%. Carbonate carbon was calculated as the difference between total carbon and organic carbon.

Biogenic opal was determined photometrically after wet alkaline extraction of biogenic silica (BSi) using a modification of the DeMaster method (DeMaster, 1981). About 30 g sediment per sample was digested in 40 mL of 1% sodium carbonate solution (Na_2CO_3) in a shaking bath at 85°C. The neutralized supernatant (after treatment with 0.021 molar HCl) was analyzed after 3, 4 and 5 hours and the amount of BSi was estimated from the intercept of the line through the time course aliquots. This slope correction was used to prevent an overestimation of BSi by mineral dissolution at low BSi concentrations (Conley, 1998). Biogenic opal was determined by multiplying the BSi concentrations with a factor of 2.4. Duplicate measurement of samples resulted in a mean standard deviation of 0.13%.

The biogenic fraction of the sediments was calculated as the sum of TOC, carbonate and opal, and the lithogenic fraction was determined as follows: wt% lithogenic = 100 - wt% opal – wt% carbonate – (wt% TOC*1.8).

Mass accumulation rates (MAR) of the bulk components were calculated as the product of the dry bulk densities of the sediments (measured at the Department of Geosciences – University of Tübingen), linear sedimentation rates and the weight fraction of the respective bulk component. All bulk components are presented as weight percent.

5.3.3. Stable nitrogen isotopes

The ratio of the two stable isotopes of nitrogen ($^{15}N/^{14}N$) is expressed as $\delta^{15}N$, which is the per mil deviation from the N-isotope composition of atmospheric N_2 ($\delta^{15}N = 0‰$): $\delta^{15}N = [(R_{Sample}-R_{Standard})/R_{Standard}]*1000$, where R_{Sample} is the $^{15}N/^{14}N$ ratio of the sample and $R_{Standard}$ is the $^{15}N/^{14}N$ ratio of atmospheric N_2. $\delta^{15}N$ values were determined using a Finnigan MAT 252 gas isotope mass spectrometer after high-temperature flash combustion in a Carlo Erba NA-2500 elemental analyzer at 1100°C. Pure tank N_2 calibrated against the International Atomic Energy Agency reference standards IAEA-N-1 and IAEA-N-2, which were, in addition to an internal sediment standard, also used as working standards. Replicate measurements of a reference standard resulted in an analytical precession better than 0.1‰. The mean standard deviation based on duplicate measurements of samples is 0.07‰.

5.3.4. Alkenones

Purified lipid extracts of between 1.5 to 5 g freeze-dried and homogenized sediment samples were analyzed for alkenones using an Agilent 6850 gas chromatograph (GC) equipped with a split-splitless inlet system, a silica column (30 m x 0.25 µm film thickness x 0.32 mm ID; HP-1; Agilent) and a flame ionisation detector (310°C). Sample preparation and detailed analytical procedure for alkenone identification is described in Böll et al. (2014). Alkenones were translated into sea surface temperature using the core top calibration for the Indian Ocean of Sonzogni et al. (1997b): SST=(U^{K}_{37} -0.043)/0.033, with U^{K}_{37} =$C_{37:2}$/($C_{37:2}$ + $C_{37:3}$). All lipid extracts were analyzed twice resulting in a mean standard deviation of 0.2°C. The mean standard deviation of estimated SST based on replicate extraction and measurement of a working sediment standard is 0.5°C.

5.3.5. Major and trace element analysis

Bulk chemical sediment analyses were performed with X-ray fluorescence (XRF) using Philips PW 2400 and PW 1480 wavelength dispersive spectrometers at the Federal Institute for Geosciences and Natural Resources in Hannover. Concentrations of 42 major and trace elements were quantitatively analyzed after fusion of the samples with lithium metaborate at 1200°C for 20 minutes (sample/LiBO$_2$ = 1/5). Quality of the results was controlled with certified reference materials (i.e., BCR, Community Bureau of Reference, Brussels). The precision for major elements was generally better than ±0.5% and better than 5% for trace elements.
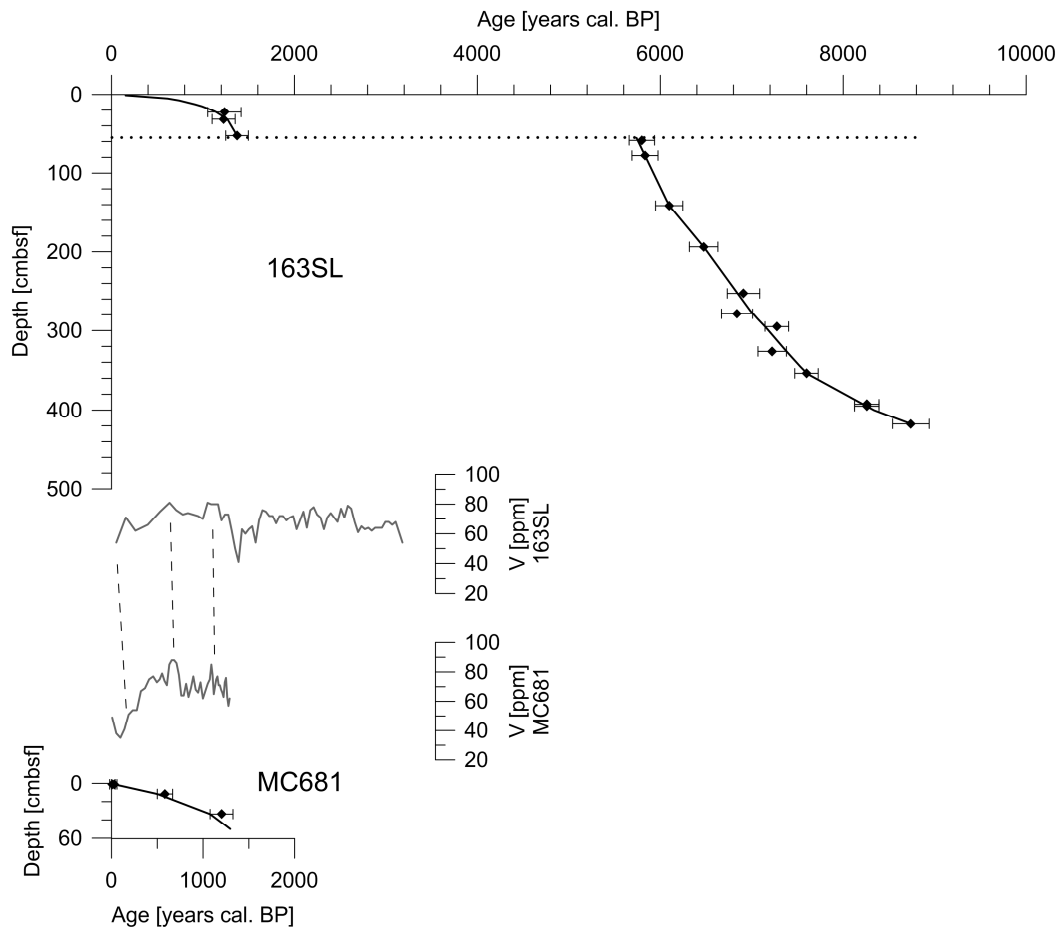
Figure 5.3: Age-depth dependency of core 163SL and MC681 of the same station. MC681 was tied to 163SL by correlating Vanadium levels between both cores. The stratigraphic framework of each core was established by ^{14}C accelerator mass spectrometry datings (diamond symbols, with age uncertainties). Stippled line indicates a sedimentary hiatus at 56 cm core depth.

5.4. Age model

Age models of both cores are based on nineteen (163SL; Figure 5.3) and four (MC680; Figure 5.4) AMS ^{14}C datings from different core depths, measured at Beta Analytics, Miami/FL, the Leibniz Laboratory in Kiel and the Ion Beam Physics Laboratory at ETH Zurich (Table 5.1). Depending on the availability of sufficient foraminiferal shells, ^{14}C was either measured in carbon from monospecific samples of *Neogloboquadrina dutertrei*, from mixed planktonic foraminifera, or from the sedimentary bulk organic carbon fraction. To exclude a potential bias by the use of different methodologies and carbon compounds, one sample was dated twice using two different techniques (see Table 5.1). Both measurements revealed almost the same radiocarbon age, and thus comparability of ages obtained from planktonic foraminiferal calcite and the bulk organic carbon fraction. The uppermost 15 cm of 163SL were correlated with multicorer MC681 from the same station by the visual matching of variations in element concentrations (Figure 5.3). Due to the higher temporal resolution and lower probability of sediment compaction, MC681 was given priority for age dating of deposits near the sediment-water-interface.
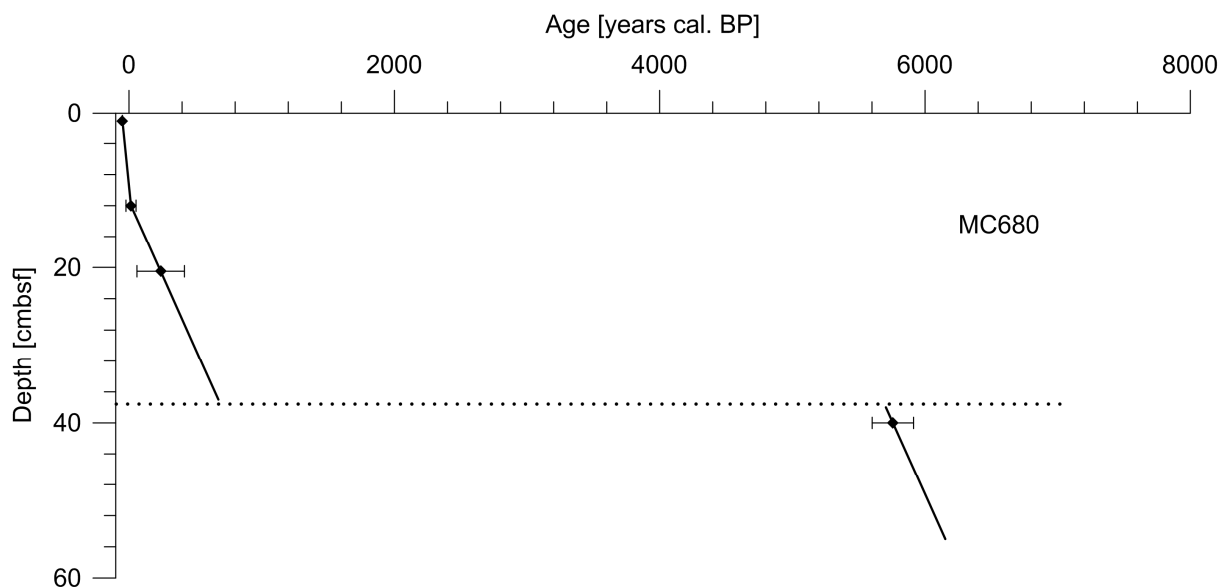
Figure 5.4: Chronology of core MC680, established by four ^{14}C AMS datings (diamond symbols, with age uncertainties). A sedimentary hiatus (stippled line) was located at 37 cm, by a sharp increase of heavy mineral element ratios (see chapter 5.4).

Table 5.1: Results of radiocarbon AMS datings. Beta refers to Beta Analytics, Miami, FL/USA, KIA to the Leibniz Laboratory, Kiel/Germany and ETH to the ETH Laboratory of Ion Beam Physics, Zurich/Switzerland

Core	Depth (cmbsf)	Lab Code	Material	Conventional 14C age (yr BP)	Reservoir corrected calibrated age (cal BP)
MC680	1 ± 1	Beta340286	mixed planktics	80 ± 30	post 1950
MC680	12 ± 2	Beta357279	N.dutertrei	600 ± 30	15 ± 38
MC680	20.5 ± 1.5	Beta357280	mixed planktics	810 ± 30	239 ± 179
MC680	40 ± 1	Beta357281	mixed planktics	5600 ± 40	5758 ± 156
MC681	1 ± 1	Beta342813	mixed planktics	650 ± 30	30 ± 30
MC681	1 ± 1	Beta342812	bulk organic fraction	630 ± 30	10 ± 30
MC681	11.5 ± 0.5	Beta342814	bulk organic fraction	1300 ± 30	584 ± 84
MC681	33.5 ± 0.5	Beta342815	bulk organic fraction	1960 ± 30	1202 ± 125
163SL	22.5 ± 0	ETH	N.dutertrei	1996 ± 67	1234.5 ± 182.5
163SL	31.5 ± 0.5	Beta346602	bulk organic fraction	1980 ± 30	1226 ± 126
163SL	52.5 ± 0.5	Beta346603	bulk organic fraction	2100 ± 30	1372.5 ± 123.5
163SL	58.5 ± 0.5	Beta346604	bulk organic fraction	5740 ± 30	5798 ± 139
163SL	77.75 ± 1.25	KIA47119	N.dutertrei	5760 ± 30	5832.5 ± 142.5
163SL	141.25 ± 1.25	Beta319751	N.dutertrei	5990 ± 30	6097 ± 149
163SL	193.75 ± 1.25	Beta319752	N.dutertrei	6350 ± 40	6474 ± 156
163SL	252.75 ± 2.75	KIA47120	N.dutertrei	6715 ± 35	6909.5 ± 177.5
163SL	278.75 ± 1.25	Beta319753	N.dutertrei	6670 ± 40	6839 ± 170
163SL	295 ± 0	Beta319754	N.dutertrei	7030 ± 40	7274 ± 129
163SL	326.25 ± 1.25	Beta319755	N.dutertrei	6990 ± 40	7223.5 ± 155.5
163SL	353.75 ± 1.25	KIA47121	N.dutertrei	7420 ± 40	7598 ± 128
163SL	392.5 ± 0	KIA47122	N.dutertrei	8090 ± 40	8257.5 ± 133.5
163SL	395 ± 0	Beta319756	N.dutertrei	8090 ± 40	8257.5 ± 133.5
163SL	417.5 ± 0	Beta342816	N.dutertrei	8500 ± 40	8740 ± 200

Conventional ^{14}C ages were calibrated to calendar ages using the CALIB 7.0 software (Stuiver and Reimer, 1993) with the MARINE09 calibration dataset (Reimer et al., 2009). One sample with a negative radiocarbon age was corrected with the postbomb calibration curve of Northern Hemisphere Zone 3 (Hua and Barbetti, 2004). Reservoir ages in surface water masses in the western Arabian Sea are older than the global reservoir age due to admixture of intermediate waters by strong upwelling (Southon et al., 2002). For the slightly northward location of MC680, we assume a regional reservoir correction of $\Delta R=200\pm62$ years, which is the weighted mean of the 10 closest ΔR determination points from the Marine Reservoir Correction database (http://calib.qub.ac.uk/marine/), but ignoring the highest and

lowest values. The core site of 163SL is under the influence of a highly productive coastal upwelling zone. Therefore, we applied a comparatively high reservoir correction of $\Delta R=297\pm51$ years from Southon et al. (2002) that was determined from the station closest to the core site. This correction factor is consistent with the corrected age of our undisturbed surface sample of MC681 (Table 5.1).

Both cores have a conspicuous sedimentation hiatus around 5700 years BP (Figures 5.3 and 5.4), indicated by the dense succession of dating points. In core MC680 the hiatus was positioned at 37 cm, and is expressed by a sharp increase of Zr/Al and Ti/Al ratios, suggesting an erosional surface. The missing sedimentary sequence in core 163SL is 1.5 m thick (1.9 m for MC680), based on the accumulation rates above and below the unconformity.

5.5. Results

5.5.1. Indicators for OMZ variability ($\delta^{15}N$, Mn/Al)

Variations in the intensity of the OMZ over the Holocene are expressed in stable nitrogen isotope ratios ($\delta^{15}N$ values) and Mn/Al ratios. $\delta^{15}N$ ranges from 7.4 to 9.4‰ in core 163SL (Figures 5.6 and 5.8) and is indicative of water column denitrification associated with suboxic conditions in Arabian Sea intermediate waters (e.g., Altabet et al., 1999; Gaye-Haake et al., 2005). Core top values of 8.9‰ (163SL) and 8.0‰ (MC680) are well within the range of modern surface sediment $\delta^{15}N$ values for this region (Gaye-Haake et al., 2005). $\delta^{15}N$ values (7.4 to 8.5‰) in the early to middle Holocene age interval (from 8 to 5.8 ka) are about 1‰ lower than the $\delta^{15}N$ values (8.9 to 9.4‰) of the late Holocene section of core 163SL. The increase in $\delta^{15}N$ is further evident in MC680 that show mid Holocene $\delta^{15}N$ values of about 7‰ compared to late Holocene values of ~8.5‰ (Figure 5.8). This suggests elevated denitrification due to more intense OMZ conditions off northern Oman during the late Holocene, which is in line with results from the NE Arabian Sea off Pakistan (Pichevin et al., 2007), but in contrast to decreasing $\delta^{15}N$ in the NW Arabian Sea over the same time period (Ivanochko et al., 2005; Suthhof et al., 2001).

Decreased oxygen levels of intermediate water during the late Holocene relative to mid Holocene conditions are further traced by decreasing Mn/Al ratios in cores 163SL and MC680. Manganese deposition in marine sediments is highly redox sensitive. Under suboxic bottom water conditions (when the OMZ impinges on the continental slope) insoluble Mn (IV) oxyhydroxides are reduced to soluble Mn (II), which is mobilized and removed from the sediments (e.g., Calvert and Pedersen, 1993; Schnetger et al., 2000). Relatively lower

sedimentary Mn/Al ratios in the late Holocene intervals of cores 163SL and MC680 (Figure 5.8, note reversed y axis) thus indicate less oxygenated bottom waters and imply a more intense OMZ in this sector of the Arabian Sea compared to the mid Holocene.
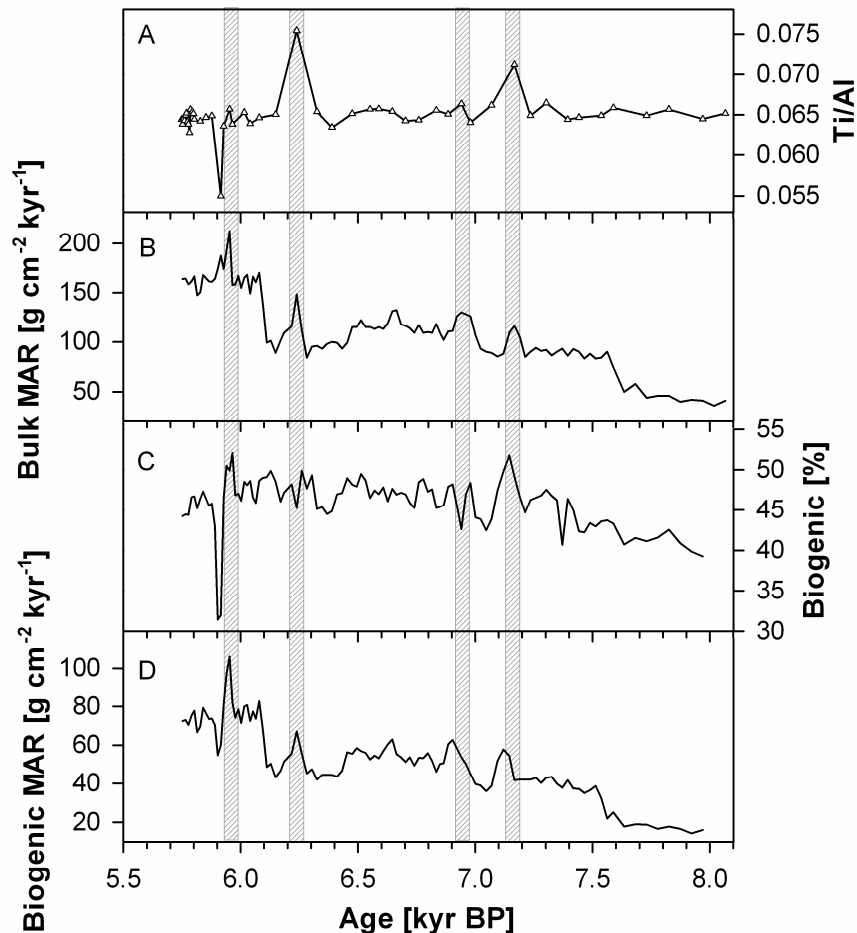
Figure 5.5: Sedimentary records of core M74/1b-163SL over the mid Holocene. (a) Ti/Al as a tracer for the input of lithogenic material, (b) bulk mass accumulation rates (MAR), (c) biogenic content of sediments, and (d) mass accumulation of the biogenic sediment fraction. The shaded areas indicate phases of increased eolian input.

5.5.2. Marine primary productivity changes (biogenic content)

To track Holocene changes in primary productivity off Oman we used the sedimentary fraction of biogenic material. The biogenic fraction was calculated as the sum of organic carbon, opal (diatoms) and carbonate (coccolithophores) and thus accounts for past changes or shifts in the primary producer community. Similar patterns of wt% biogenic and bulk MAR imply that the biogenic fraction of sediments is not affected by dilution (Figure 5.5), although

mass accumulation rates at our coring sites are strongly influenced by the input of lithogenic material (see chapter 5.5.3.).

The biogenic fraction in core 163SL ranges from 31 to 52%. Primary productivity decreased from the middle to late Holocene as indicated by relatively higher biogenic contents in the mid Holocene fraction of core 163SL (Figure 5.6). Short-term primary productivity fluctuations on decadal to centennial time scales correlate well with SST and $\delta^{15}N$ patterns over the mid Holocene and suggest that short-term variations in OMZ intensity are coupled to upwelling induced primary productivity changes during this time (Figure 5.7).

5.5.3. Continental aridity, dust input (Mg/Al, Zr/Al, lithogenic MAR)

To examine the role of varying SW monsoon strength on OMZ conditions we investigated the input of eolian material to our sediments. Dust deposited on the Oman Margin is primarily transported from Arabia by the Northwesterlies that overlie the low-level winds of the SW monsoon (Sirocko et al., 1991). In this region the input of eolian material is characterized by Mg-bearing minerals such as palygorskite and dolomite that are transported with dust plumes from Arabia to the northern Arabian Sea (Sirocko et al., 2000, 1991). Since titanium is preferentially incorporated into heavy minerals and concentrated in the coarse-grained sediment fraction (and is not affected by early diagenesis), Mg/Al and Ti/Al ratios in Arabian Sea sediments trace the input of eolian dust from the Arabian Peninsula and Somalia (Shimmield and Mowbray, 1991). Zr/Al ratios (parallel to Ti/Al) can be used as an indirect tracer for wind strength, because zirconium is usually enriched in heavy minerals such as zircon that is associated with the coarse grained sediment fraction and thus could only be transported at vigorous wind speeds (Shimmield and Mowbray, 1991; Sirocko et al., 2000). This interpretation is supported by a study from Deplazes et al. (2014), which found that the Zr/Al ratio is well correlated with grain size in a sediment core from the Pakistan continental margin. Furthermore, the input of lithogenic material (46 to 67%) at site 163SL determines sediment mass accumulation rates and correlates closely with bulk MAR and Ti/Al (Figure 5.5). Terrigenous matter deposited on the Oman Margin is almost exclusively of eolian origin due to the absence of river systems in this region, and we argue that lithogenic mass accumulation rates in core SL163 reflect the changing input of dust near the coast of northern Oman.

Deposition of dust in Arabian Sea sediments intensified over the Holocene as a direct result of increased continental aridity due to diminishing SW monsoon strength (Prins et al.,

2000; Sirocko et al., 2000). Lithogenic MAR at site 163SL started to increase at about 7.6 ka (23 g cm^{-2} kyr^{-1}) to values of up to 126 g cm^{-2} kyr^{-1} at 5.9 ka (Figure 5.7), in line with continental aridification on the Arabian Peninsula (e.g., Berger et al., 2012; Fleitmann et al., 2007; Fuchs and Buerkert, 2008). Moreover, the steep increase in lithogenic MAR at 6.1 ka closely mirrors the moisture history of northern Oman, where the transition from more humid to arid conditions was not gradual but occurred relative abruptly at around 6 ka (Bray and Stokes, 2004; Fleitmann et al., 2007). Aridification continued until the late Holocene as shown by high Mg/Al ratios in the late Holocene section of core 163SL (Figure 5.6).

Superimposed on the long-term trend were several short-term events of high eolian activity (high lithogenic MAR and high Ti/Al) at 7.15 ka, 6.25 ka and 5.95 ka (Figures 5.5 and 5.7). Increased upwelling (low SST) and elevated Zr/Al ratios suggest that these were times of intensified wind strength.

5.5.4. Sea surface temperatures

Alkenone-derived SST estimates in our record vary between 23.8 and 27.8°C (Figure 5.6) and fluctuated around the modern annual mean value of 26.2°C (Levitus and Boyer, 1994) during the late Holocene and from 8 to 6.6 ka. In contrast, SSTs were almost constantly below modern values in the period from 6.5 to 5.7 ka. The close correlation between small scale SST changes and variations in $\delta^{15}N$ (increased denitrification) implicates that upwelling processes are the main driver for short-term SST fluctuations in this region (Figure 5.7). Decreasing SSTs from 6.5 to 5.7 ka thus most likely reflect a regional strengthening of upwelling at the coast of northern Oman.
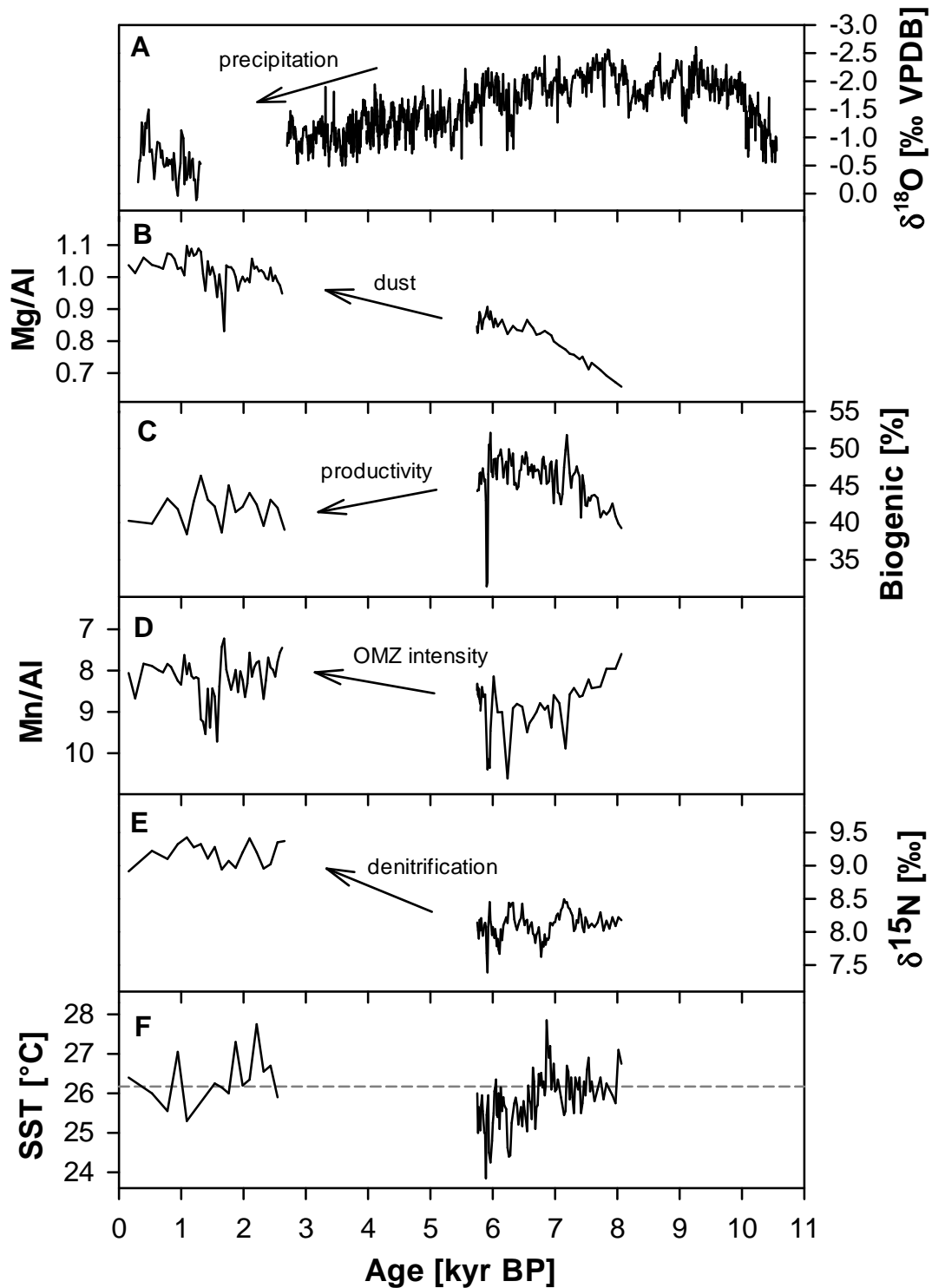
Figure 5.6: Monsoon reconstruction of core M74/1b-163SL showing strongest southwest monsoon activity during the mid to early Holocene. (a) speleothem $\delta^{18}O$ of Qunf Cave in Southern Oman (Fleitmann et al., 2007), (b) Mg/Al as an indicator for continental dust input, (c) biogenic content of sediments, (d) Mn/Al as a tracer for oxygen variability, (e) sedimentary $\delta^{15}N$, and (f) alkenone-derived SST estimates for core M74/1b-163SL. Dashed line indicates modern SST of 26.2°C (Levitus and Boyer, 1994).

5.6. Discussion

5.6.1. OMZ variability at the northern Oman Margin and SW monsoon strength

In today's situation, low mid-water oxygen levels in the NE Arabian Sea are maintained by the interplay between oxygen consumption below the mixed layer and low oxygen supply caused by sluggish replenishment of intermediate waters (Olson et al., 1993; Sarma, 2002; Wyrtki, 1962).

One controlling factor for OMZ variability in the Arabian Sea thus are variations in SW monsoon activity that result in variable rates of primary productivity, particle export from the euphotic zone and oxygen demand below the mixed layer (Altabet et al., 1999, 2002; Reichart et al., 1998, 1997; Schulte et al., 1999; Suthhof et al., 2001). Our records of summer monsoon strength and OMZ intensity shed light on the relative importance of the two factors during the Holocene.

5.6.1.1. Mid Holocene versus late Holocene

The long-term development of local OMZ intensity on the northern Oman Margin is not primary governed by varying SW monsoon strength. When comparing the mid Holocene time slice with that from the late Holocene in core 163SL, stronger SW monsoon activity (intense upwelling, high primary production and relatively low dust input) is indicated during the middle Holocene, whereas most intense OMZ conditions occurred during the late Holocene (Figure 5.6). This mismatch suggests that intermediate water ventilation must have been stronger during the middle than during the late Holocene off northern Oman. Other studies from the northern Arabian Sea also report an overriding role of ventilation changes in modulating glacial to interglacial OMZ variability (Böning and Bard, 2009; Jung et al., 2009; Pichevin et al., 2007; Schulte et al., 1999).
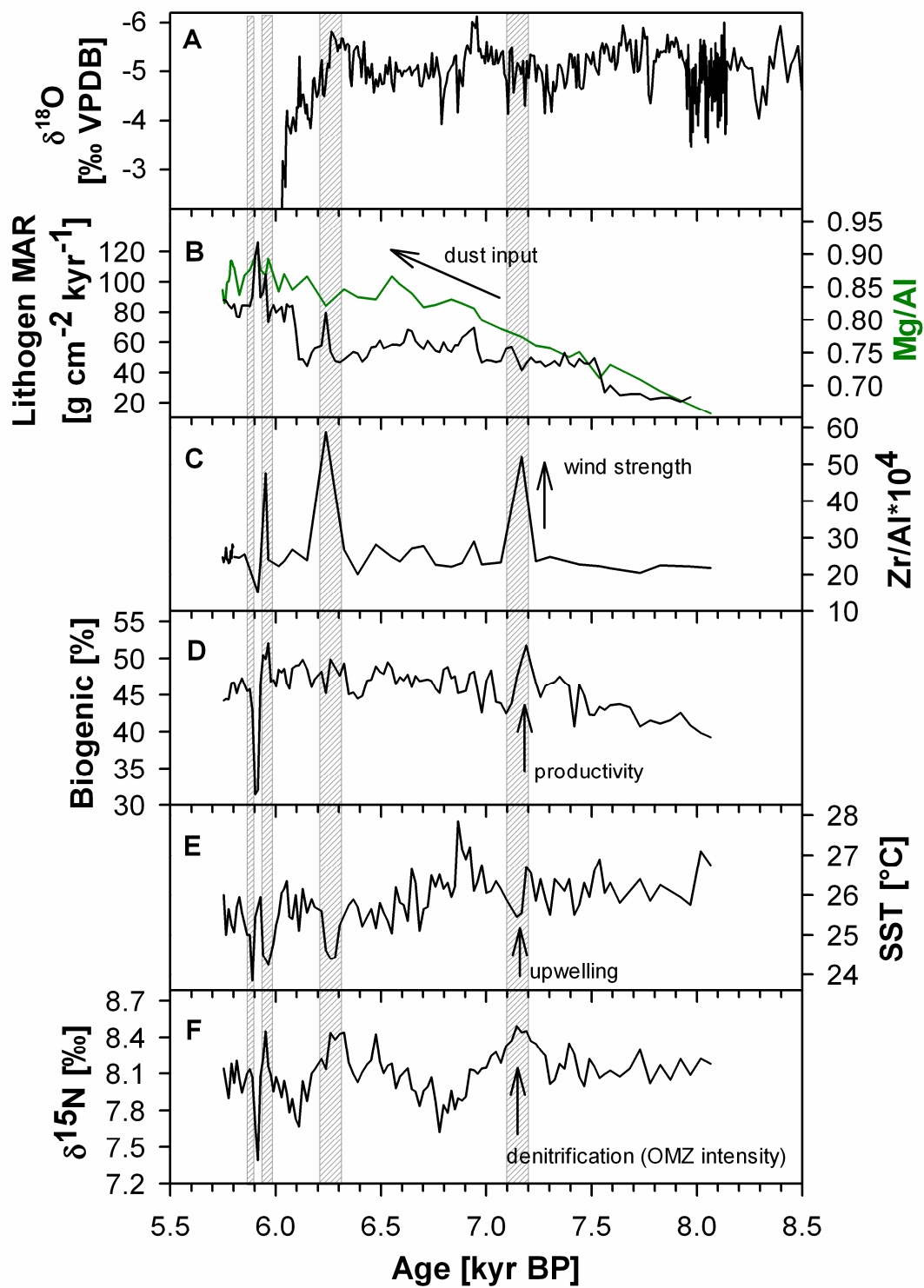
Figure 5.7: Short-term climate variability at site M74/1b-163SL over the middle Holocene. (a) speleothem $\delta^{18}O$ of Hoti Cave (Northern Oman) as an indicator for precipitation (Neff et al., 2001), (b) mass accumulation of lithogenic material (black) compared to Mg/Al ratios (green) in core 163SL, (c) record of Zr/Al as an indirect tracer for wind strength, (d) biogenic content of sediments (productivity tracer), (e) alkenone-derived SST estimates, and (f) sedimentary $\delta^{15}N$ of core 163SL. Short-term events of strong wind intensity trigger intense upwelling that is accompanied by high primary productivity and elevated denitrification (shaded areas).

5.6.1.2. Short-term control on local OMZ intensity during the mid Holocene

Regional short-term fluctuations in the oxygen inventory of the northern Arabian Sea were linked to variations in SW monsoon activity over the middle Holocene (Figure 5.7). This suggests that the centennial scale variability of oceanic properties on the northern Oman Margin was significantly controlled by atmospheric processes (and that ventilation changes probably only played a minor role in modulating regional short-term oxygen levels). Core 163SL recorded several events of intensified wind velocity during the mid Holocene, dated around 7.15 ka, 6.25 ka and 5.95 ka. Increased wind strengths during these events strengthened the upwelling of cold, nutrient-rich waters near the coast of Oman that in turn enhanced regional biological productivity, as evidenced by negative SST excursions and high sedimentary contents of biogenic matter. Periods of low SST were essentially anti-correlated with $\delta^{15}N$ indicating that invigorated upwelling increased oxygen consumption and denitrification during mineralization of elevated organic matter fluxes. Phases of most intense oxygen deficient conditions in the coastal region off northern Oman thus were coupled to elevated wind strength over the northern Arabian Sea throughout the mid Holocene.

Strong winds, furthermore, enable the entrainment of dust to our study area as indicated by high Ti/Al ratios (Figure 5.5) and elevated accumulation of lithogenic matter during times of increased wind velocities (Figure 5.7). Although the increased input of dust to Arabian Sea sediments is attributed to decreased SW monsoon activity over longer time scales (e.g., Deplazes et al., 2014; Prins et al., 2000; Sirocko et al., 2000, 1991), the short-term events of high eolian activity observed here most likely reflect times of elevated SW monsoon activity. Sirocko et al. (1991) stated that dust transported to the NW Arabian Sea is mainly controlled by continental aridity together with wind strength. Clemens and Prell (1990) showed that lithogenic MAR mainly reflects source area aridity, whereas lithogenic grain size (which is tightly linked to Zr/Al (Deplazes et al., 2014)) is indicative of SW monsoon wind strength. The gradual increase of lithogenic MAR at our study site thus reflects a long-term trend of SW monsoon weakening over the Holocene and is in line with cave records (recorders of continental aridity; Fleitmann et al., 2007, 2003) and other studies from the northern Arabian Sea (e.g., Gupta et al., 2003; Overpeck et al., 1996; Sirocko et al., 1993).

5.6.2. Spatial and temporal variability of the Arabian Sea OMZ during the Holocene

The comparison of $\delta^{15}N$ and Mn/Al records throughout the northern Arabian Sea helps to decipher changes in the spatial and temporal development of the Arabian Sea OMZ over the

Holocene (Figure 5.8). Variations in the sedimentary $\delta^{15}N$ signal are not only caused by changing denitrification rates and thus oxygen availability, but also by other processes that influence the absolute $\delta^{15}N$ signal in the sedimentary record such as (1) $\delta^{15}N$ reduction through N_2 fixation (Karl et al., 2002), (2) isotopic fractionation during incomplete nitrogen uptake (Schäfer and Ittekkot, 1993), (3) input of terrigenous matter with a reduced $\delta^{15}N$ signature (Gaye-Haake et al., 2005), (4) $\delta^{15}N$ increase with distance from the upwelling center ('Rayleigh-type fractionation'; Altabet and Francois, 1994) and (5) diagenetic alteration in the sediment (Gaye-Haake et al., 2005; Möbius et al., 2011). In Arabian Sea sediments from the continental slope $\delta^{15}N$ values are not primarily driven by diagenesis (Möbius et al., 2011) and for the $\delta^{15}N$ records considered here a $\delta^{15}N$ bias through terrigenous organic matter input by river runoff is unlikely, because sediment cores were not obtained in the proximity of large river mouths. Moreover, nitrate is completely utilized by phytoplankton on an annual basis in the NW Arabian Sea (Schäfer and Ittekkot, 1993). We thus assume that $\delta^{15}N$ is primary modulated by mid-water oxygen availability. This interpretation is strengthened by the good agreement of $\delta^{15}N$ with the records of Mn/Al (Figure 5.8). The Mn/Al ratio is the result of complex redox dynamics at the boundary of the OMZ. Within the OMZ Mn (II) is mobilized and removed from the sediment, so that lowered sedimentary Mn/Al ratios reflect more intense oxygen deficient conditions (see also chapter 5.5.1.; cores MC680 and 163SL). On the other hand, strong OMZ conditions are reflected in enriched manganese concentrations in sediments deposited below the OMZ (cores 74KL and NIOP 905). Extension of the OMZ would result in mobilization of Mn that was previously deposited in sediments below the OMZ, lateral transportation of the released Mn (II) and reoxidation and transformation of Mn (II) to particulate Mn (IV) outside the OMZ (Schnetger et al., 2000; Suthhof et al., 2001). Sedimentary $\delta^{15}N$ together with changes in Mn/Al thus indicate spatial and temporal variations of mid-water oxygenation in the Arabian Sea (that will be discussed below).

5.6.2.1. Early Holocene (11-8 ka)

The northern Arabian Sea was well oxygenated during the Younger Dryas and last glaciation, but oxygen deficient conditions developed in the northern Arabian Sea during the early Holocene (Altabet et al., 1999, 2002; Suthhof et al., 2001). Deglacial lowering of the oxygen inventory in Arabian Sea intermediate waters was caused by (1) high production of organic matter induced by strong southwest monsoonal upwelling (e.g., Altabet et al., 2002), (2) decreased northward intrusion of intermediate waters from the south (e.g. Antarctic

Intermediate Water) due to sea level rise and increased influence of highly saline waters from the marginal seas (RSW and PGW) (Böning and Bard, 2009; Jung et al., 2009; Pichevin et al., 2007; Schulte et al., 1999) and (3) thermocline ventilation due to deep convective winter mixing in the northeastern part of the Arabian Sea (Reichart et al., 2002a).

OMZ conditions were most intense in the NW Arabian Sea during the early Holocene as shown by enhanced denitrification off Somalia and Oman (Figure 5.8; period 1). Sea level at this time was about 40 m below present level (Figure 5.8; Bard et al., 1996; Siddall et al., 2003) and inflow of RSW and PGW was still weaker than under modern conditions (Lambeck, 1996; Rohling and Zachariasse, 1996). Instead, oxygen was probably supplied to the northeastern basin by IOCW, which represents southern intermediate water sources and enters the northern Arabian Sea at the southwestern boundary with the Somali current. Advection of this intermediate water mass weakened the OMZ in the NE Arabian Sea (Böning and Bard, 2009; Pichevin et al., 2007). This scenario further implies better ventilation of the NW basin (inferred from the modern flowing path of IOCW), and in consequence OMZ intensity in the NW Arabian Sea should have been low. But a comparison of different δ^{15}N and Mn/Al records from the NW basin (Altabet et al., 2002; Ivanochko et al., 2005; Ivanochko, 2004a; Suthhof et al., 2001) and the NE basin of the Arabian Sea (Pichevin et al., 2007) shows that the O_2 deficit was most pronounced in the northwestern part of the Arabian Sea (Figure 5.8). We argue that O_2 loss and build up of intensely oxygen deficient conditions in the NW Arabian Sea was caused by an increased demand of oxygen due to elevated primary production and associated mineralization of sinking organic matter in the upwelling regions off Somalia and Oman. SST records from these regions reveal that upwelling during this time was much more vigorous than today (Böll et al., submitted; Huguet et al., 2006) driven by a contemporaneous maximum in SW monsoon strength during the early Holocene (Fleitmann et al., 2003; Overpeck et al., 1996; Sirocko et al., 1993). Upwelling processes trigger high rates of primary productivity off Somalia (Ivanochko et al., 2005) as well as off Oman (Gupta et al., 2003; Naidu and Malmgren, 1996).

Modern SST patterns show no indication of upwelling in reaction to the SW monsoon on the Pakistan Margin (Levitus and Boyer, 1994), and sediment trap studies indicate higher productivity during the NE monsoon season in winter (Andruleit et al., 2000; Schulz et al., 2002b). Von Rad et al. (1999b) indeed found evidence of reduced primary production together with oxygenated bottom water conditions off Pakistan between 10.5 to 7 ka. Strengthened SW monsoon winds during the early Holocene thus only slightly impacted the NE Arabian Sea productivity. Although northern Arabian Sea intermediate water was better

ventilated from southern sources during the early Holocene than today, the increased rain rate of organic matter due to strong SW monsoonal upwelling caused pronounced oxygen deficiency in the NW Arabian Sea, where most intense OMZ conditions are today observed in the NE basin.

5.6.2.2. Early- to mid Holocene (8-6 ka)

Organic matter production as the main control on oxygen levels at intermediate water depth probably declined with gradual weakening of SW monsoon strength (e.g., Fleitmann et al., 2007; Gupta et al., 2003) over the early to middle Holocene. Changes in intermediate water ventilation became more important than productivity and oxygen demand as driving factors for mid-water oxygen levels. In consequence, the west-east gradient of the Arabian Sea OMZ decreased, and the OMZ intensified in the NE Arabian Sea and weakened in the NW Arabian Sea (Figure 5.8; period 2). Gradual reduction of SW monsoon intensity is well documented at site 163SL where increasing amounts of dust signalling continental aridification were deposited between 8 to 6 ka (Berger et al., 2012; Fleitmann et al., 2007; Fuchs and Buerkert, 2008). Upwelling intensity decreased and lowered surface ocean productivity in the NW Arabian Sea (Gupta et al., 2003; Ivanochko et al., 2005), so that oxygen concentrations at intermediate water depths increased and denitrification was reduced (see Figure 5.8). On the other hand, increased inflow of PGW and RSW due to rising sea level (Lambeck, 1996; Rohling and Zachariasse, 1996) constricted intrusion of IOCW to the NE basin (Pichevin et al., 2007), whereas the NW basin continued to receive intermediate water of southern provenance. This leads to a stabilization of the OMZ and a continuous expansion of oxygen deficiency in the NE Arabian Sea, whereas the NW Arabian Sea remained ventilated.
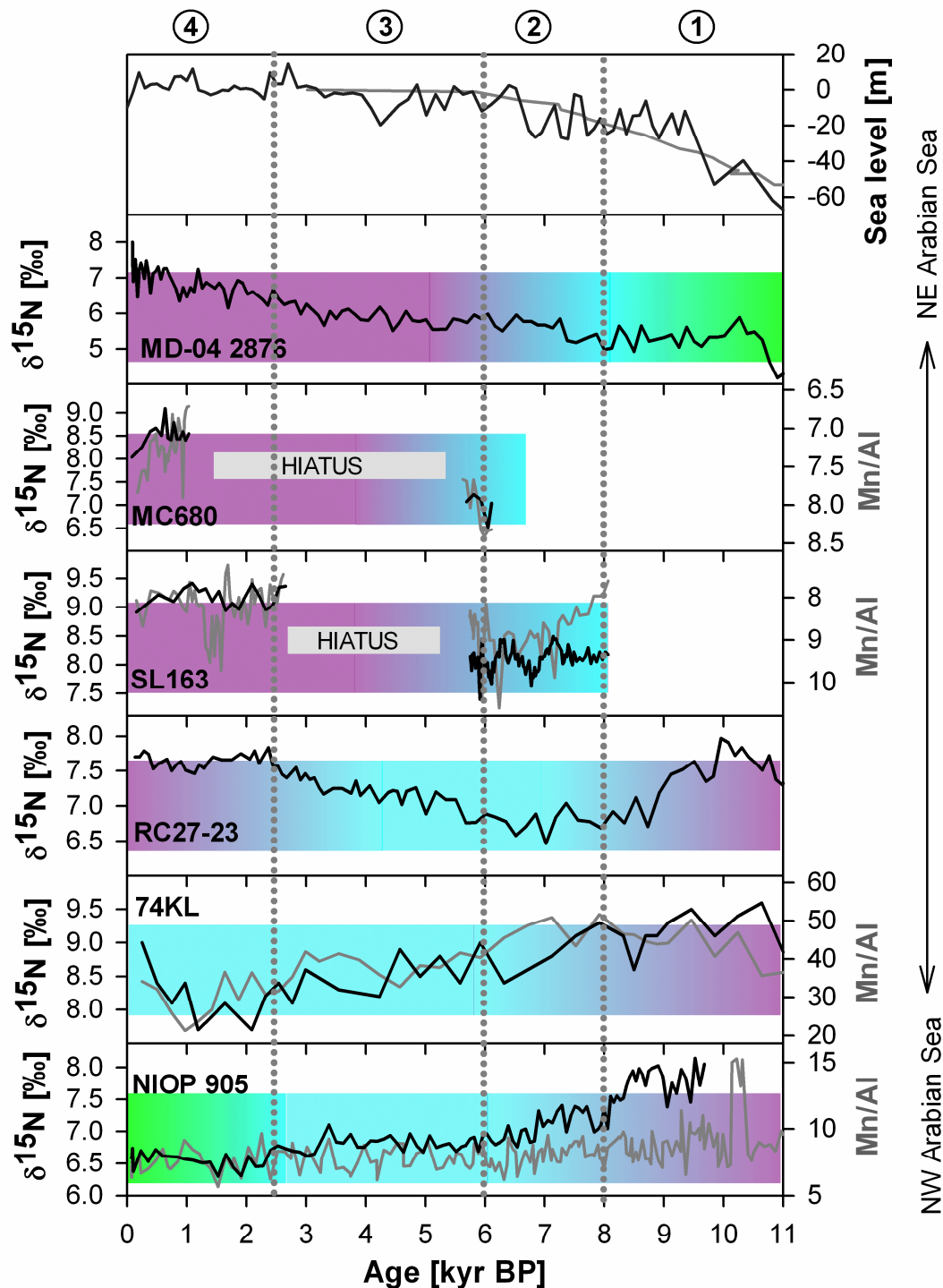
Figure 5.8: Comparison of $\delta^{15}N$ and Mn/Al (when available) records of several cores obtained from the northern Arabian Sea. From the bottom up: NIOP 905 off Somalia (Ivanochko et al., 2005; Ivanochko, 2004), SO42-74KL (Suthhof et al., 2001) and RC27-23 from the Oman Margin (Altabet et al., 2002), M74/1b-163SL and MC680 off northern Oman (this study) and MD04-2876 off Pakistan (Pichevin et al., 2007). The comparison allows the reconstruction of the temporal and spatial variability of the Arabian Sea oxygen minimum zone over the Holocene (indicated by color shading). Further illustrated is the relative Holocene sea level change reconstructed by Siddall et al. (2003) (black curve) and Bard et al. (1996) (gray curve). Numbers indicate climate periods discussed in the main text.

5.6.2.3. Mid Holocene (6-2.5 ka)

Present sea level was reached shortly before 6 ka (Bard et al., 1996; Siddall et al., 2003) and thermocline circulation over the middle Holocene most likely was similar to modern conditions. Detailed comparison of denitrification patterns for the northern Arabian Sea points to a gradual southward retreat of intermediate water ventilation from southern sources (IOCW) until modern circulation patterns were established around 2.5 ka before present (Figure 5.8; period 3). While denitrification and thus oxygen deficiency increased again on the Oman Margin since ~6 ka (site RC27-23; Altabet et al., 2002), ongoing water column oxygenation is indicated by the contemporaneous decline of $\delta^{15}N$ and Mn/Al at southern stations (site 74KL (Suthhof et al., 2001) and site NIOP 905 (Ivanochko, 2004)). Oxygen supply by IOCW probably plays a substantial role for mid-water ventilation south of about 15°N, whereas its influence diminished in the northern part of the Arabian Sea at the coast of northern Oman and Pakistan. Our spatial comparison of $\delta^{15}N$ data suggests that the OMZ expanded from the northeastern basin of the Arabian Sea to the northwest resulting in a reversal of the early Holocene west-east gradient of OMZ intensity throughout the middle Holocene.

5.6.2.4. Late Holocene (since 2.5 ka)

The modern OMZ, which is characterized by permanent low oxygen concentrations and associated high denitrification rates in the NE Arabian Sea and weaker OMZ conditions in the NW Arabian Sea, was established at about 2.5 ka (Figure 5.8; period 4). Maximum primary production (northwestern upwelling regions) and intense denitrification (northeastern basin) were spatially decoupled over the late Holocene. Thus, low oxygen levels and increased denitrification in the NE Arabian Sea can not primarily be attributed to enhanced production and subsequent loss of oxygen due to mineralization of sinking organic matter. SW monsoon activity at site 163SL off northern Oman was relatively low during the late Holocene compared to early Holocene conditions, as indicated by weak upwelling intensities (higher SST) and decreased primary production and an increased input of continental dust to the 163SL sedimentary record (Figure 5.6). The gradual weakening of Arabian Sea upwelling is concurrent with other SST reconstructions that show a sea surface warming tendency throughout the Holocene (Böll et al., submitted; Huguet et al., 2006). At the coast of Pakistan, where oceanic processes are mainly controlled by winter monsoon activity, SST decreased and primary productivity increased over the late Holocene (imaging a long-term trend of NE

monsoon strengthening) (Böll et al., 2014). Low mid-water oxygen concentrations in this region thus must be coupled to increased productivity caused by strong NE monsoonal winds. Nevertheless, spatial differences in the late Holocene oxygen deficiency in the northern Arabian Sea were significantly governed by weak ventilation at intermediate water depth that is minimal in the northeastern part of the Arabian Sea.

5.6.3. Present development of the Arabian Sea OMZ and implications for future climate change

Climate models (Matear and Hirst, 2003) predict a decrease of dissolved oxygen concentrations in the oceans and expanding oxygen minimum zones under global warming conditions. Measurements of dissolved oxygen over the last 50 years show more divergent results, but indicate an overall oxygen decline in the tropical oceans, while oxygen concentrations generally increased in the subtropical oceans (Keeling et al., 2010; Stramma et al., 2012). Ocean 'deoxygenation' in response to global warming is mainly attributed to lower oxygen solubility in warmer waters and to an increase of upper ocean stratification (Keeling et al., 2010; and references therein). Since the Arabian Sea is one of the main denitrification regions of the world's ocean (e.g., Bange et al., 2000; Codispoti et al., 2001) and significantly contributes to the oceanic loss of N_2O to the atmosphere (Bange et al., 2001), changes in the Arabian Sea OMZ would have implications for future climate change. A study by Levitus et al. (2005) revealed that the Indian Ocean has warmed since the mid-1960s (see Figure 5.9b) and the question arises if and how this warming has effected the present development of the Arabian Sea OMZ. Stable nitrogen isotopic measurements spanning the period from 1950 to 1990 A.D. from the NE Arabian Sea (Böll et al., 2014) indicate a slight increase of denitrification over this time interval, in line with a regional sea surface warming tendency (that is also reflected in air temperature measurements from this region; Figure 5.9a). This regional increase of denitrification at the coast of Pakistan thus may be a consequence of a recently observed expansion of the Arabian Sea denitrification zone (Rixen et al., 2013). Recent and ongoing warming further strengthen the southwest monsoonal winds and are expected to enhance primary productivity in the Arabian Sea (Goes et al., 2005). In analogy with the patterns observed over the Holocene, we expect an intensified mid-water oxygen minimum due to enhanced oxygen demand below the thermocline. Interestingly, Banse et al. (2014) found no clear trend in the NO_2^- distribution of the Arabian Sea between 1959 and 2004 A.D. that would signal enhanced denitrification and intensified OMZ conditions. Also a

global compilation of oceanic dissolved oxygen measurements for the last 50 years shows no substantial change in the Indian Ocean OMZ (Stramma et al., 2008). Thus, the future development of the Arabian Sea OMZ remains an open question that needs to be further studied, especially since denitrification in the Arabian Sea accounts for a significant part of global N_2O emissions.
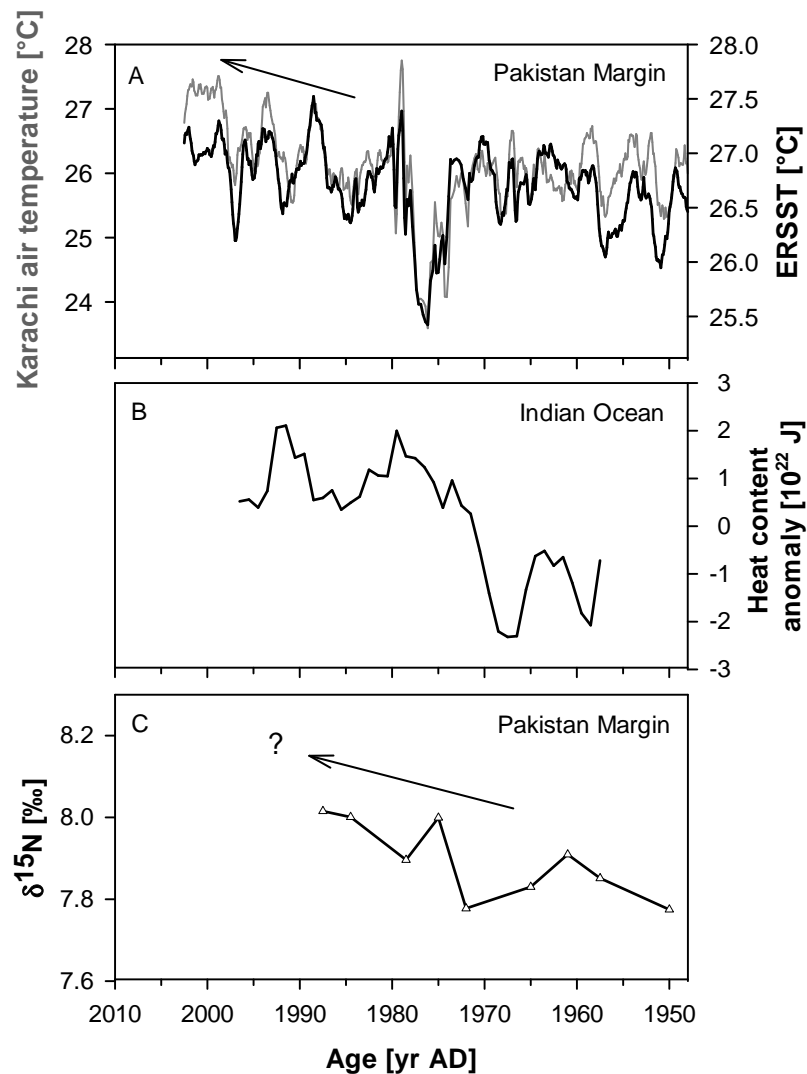
Figure 5.9: (a) Air temperature of Karachi (Pakistan) (gray curve; data from Deutscher Wetterdienst) and ERSST (extended reconstructed sea surface temperatures derived from in situ observations and improved statistical methods; Smith and Reynolds, 2003) for the Pakistan continental margin (black curve), (b) Heat content anomaly of the Indian Ocean for the period 1955-2003 (Levitus et al., 2005) and (c) $\delta^{15}N$ of core SO130-275KL from the northeastern Arabian Sea (Böll et al., 2014).

5.7. Conclusions

The joint examination of our $\delta^{15}N$ and Mn/Al records together with published reconstructions (Altabet et al., 2002; Ivanochko et al., 2005; Ivanochko, 2004; Pichevin et al., 2007; Suthhof et al., 2001) indicative of mid-water oxygenation reveal new insights into the spatial and temporal variability of the Arabian Sea OMZ over the Holocene. Oxygen concentrations in Arabian Sea intermediate waters varied not only in intensity but experienced spatial changes in the regional location of strongest oxygen deficiency. Unlike today, when oxygen levels are lowest in the NE Arabian Sea, core OMZ conditions with elevated denitrification occurred in the northwestern part of the Arabian Sea over the early Holocene. This regional shift was caused by a changing interplay of mid-water ventilation (oxygen supply) and primary productivity (oxygen sink): Strong SW monsoon activity during the early Holocene drives upwelling and high rates of primary productivity at the coast of Oman and Somalia while SW monsoon driven primary productivity was comparable weak in the NE Arabian Sea. On the other hand, low sea level (Bard et al., 1996; Siddall et al., 2003) and reduced inflow from the marginal seas in the north enable IOCW to replenish oxygen at intermediate water depth from the south farther to the northeast. Better ventilation of the northeast basin together with spatial differences in oxygen demand causes an early Holocene OMZ, being most intense in the NW Arabian Sea. Over the middle Holocene, SW monsoon activity weakened and the influence of primary production on maintaining OMZ conditions decreased. This was accompanied by a gradual retreat of mid-water ventilation from southern sources due to sea level rise and increased inflow of warm and saline PGW and RSW. Oxygen supply to the northeast Arabian Sea declined while the NW Arabian Sea was still well ventilated, so that most severe oxygen minimum conditions developed in the northeastern basin over the late Holocene. The shift from the northeast to the northwest of the core OMZ implied a spatial decoupling of regions with highest primary productivity and lowest mid-water oxygen concentrations (highest denitrification), as evident in modern observations from the Arabian Sea (Gaye-Haake et al., 2005).

Mid Holocene short-term fluctuations in mid-water oxygen at the northern Oman Margin were mainly governed by atmospheric forcing related to SW monsoon activity. Intensified wind strength drives coastal upwelling that induces phases of high primary production, elevated loss of oxygen at intermediate water depth and increased water column denitrification.

Until now, it is unclear if and how the OMZ of the Arabian Sea may respond to future climate change. Our high-resolution reconstruction of the middle Holocene, however, shows

that regional variations of mid-water oxygen in the Arabian Sea are sensitive to short-term fluctuations in monsoon wind strength. A predicted increase in global temperature may strengthen the land-sea thermal contrast that drives the low-level winds of the SW monsoon (Goes et al., 2005), with possible consequences for the Arabian Sea OMZ.

CHAPTER 6

6. Conclusions and Outlook

6.1. Conclusions

The analysis of different sediment cores from two regions in the northern Arabian Sea that are differentially impacted by the summer and winter monsoon, respectively, was successfully used to disentangle signals of summer and winter monsoon strength. While summer monsoon winds drive intense upwelling and high rates of primary productivity in the northwestern Arabian Sea, the influence of the winter monsoon is most pronounced in the northeastern Arabian Sea off Pakistan, where north-easterly winds induce convective winter mixing and high primary productivity during the winter season.

My high-resolution reconstruction of primary productivity and alkenone-derived SST variability from the NE Arabian Sea provides a unique record of winter monsoon variability for the late Holocene, a climate period from which information about winter monsoon strength is scarce. Winter monsoon activity intensified over the last 2400 years and was strongest during the LIA from 1400 to 1900 A.D. The decadal to centennial scale variability in winter monsoon strength reported here supports the growing body of evidence that significant climate variability occurs not only on time scales of several hundred of thousand years but also throughout the late Holocene.

Comparison of my alkenone-SST reconstructions from the NW and NE Arabian Sea confirms an antagonistic relationship of summer and winter monsoon strength over the Holocene, which was so far only reported for glacial/interglacial cycles (Rostek et al., 1997; Schulz et al., 1998). Summer monsoon activity was strongest during the early Holocene climate optimum as indicated by low SST and strong upwelling offshore Oman. Winter monsoon activity, on the other hand, was diminished during this time (high SST off Pakistan) but increased again since the early to mid Holocene. This reversed relationship of summer

and winter monsoon strength did not only exist on millennial time scales throughout the Holocene, but was also evidenced in the centennial scale monsoon variability of the last two millennia, as indicated by the comparison of my late Holocene winter monsoon record with records of summer monsoon strength. The dynamical interplay between summer and winter monsoon strength over the Arabian Sea was most likely caused by solar triggered shifts in the long-term latitudinal position of the ITCZ. The northern Arabian Sea is located in a sensitive region at the northern latitudinal boundary of the ITCZ: A southward displacement of the ITCZ due to low solar insolation would have shortened the duration of the summer monsoon season and strengthened the influence of northeast monsoonal winds over the northern Arabian Sea.

Holocene monsoon activity in the northern Arabian Sea varied in line with Northern Hemisphere climate change. A general picture emerged of increased winter monsoon strength corresponding to colder climate conditions on the Northern Hemisphere (LGM and LIA) and strong summer monsoon activity correlating with periods of comparatively warmer climate conditions (early Holocene and MWP). Their likely driving forces might be related to insolation changes. Climate variability in the high and low-latitudes probably was either directly (and thus simultaneously) influenced by varying solar activity or was linked through solar triggered internal climate feedback mechanisms, such as movements in the position of the ITCZ or snow cover that determines the land-sea thermal contrast between the Asian continent and the southern Indian Ocean. The data of this thesis show that the monsoon climate of the low-latitudes has responded to short-term (decadal to centennial) changes in global climate variability over the last 2000 years.

The Arabian Sea hosts one of the main OMZ of the world's ocean, which make monsoon induced changes in the Arabian Sea OMZ a potential driver of climate change. Reconstruction of mid-water oxygenation and monsoon intensity from the northern Oman Margin and its comparison to other records indicative of mid-water oxygenation from the northern Arabian Sea shows that the Arabian Sea OMZ has varied in intensity and location (northwest to northeast shift) over the Holocene. This variability was most likely caused by changes in intermediate water ventilation due to sea level rise combined with spatial differences in the response of primary productivity to varying monsoon strength. While monsoon activity thus was not the only driver for millennial scale variations in OMZ intensity, strong southwest monsoon winds were significantly linked to regionally low oxygen levels (increased denitrification) at intermediate water depth over decadal to centennial time scales during the middle Holocene. My high-resolution record of the mid Holocene infers that regional future

changes in mid-water oxygen might be sensitive to short-term fluctuations in monsoon wind strength.

6.2. Outlook

The data presented in this PhD thesis show that changing monsoon activity have played a substantial role in modulating mid-water oxygen in the northern Arabian Sea over the Holocene. Although the spatial comparison of $\delta^{15}N$ records from the northern Arabian Sea suggests that changes in mid-water ventilation might have been of equal importance for the development of the OMZ, direct data reflecting mid-water ventilation from the northern Arabian Sea are lacking. For instance, further investigation of $\delta^{13}C$ on benthic foraminifers in different sediment cores, spanning a transect from the northwestern to the northeastern Arabian Sea, could be used to trace past variations in the pathway of IOCW. This could provide further information about the extent of the northward intrusion of IOCW into the northern Arabian Sea (which, unlike today, might have reached the northeastern basin of the Arabian Sea during the early Holocene). Since mid-water ventilation most likely was coupled to sea level change over the Holocene this analysis might further help to evaluate the role of sea level on OMZ intensity in the northern Arabian Sea.

This PhD thesis presents a high-resolution record of decadal to centennial scale variations in NE monsoon strength over the last 2400 years. The comparison of this record with published records of SW monsoon strength from the northwestern Arabian Sea provides some insights into the dynamical interplay between NE and SW monsoon strength over the late Holocene. Previous late Holocene reconstructions indicative of SW monsoon strength, however, are often of lower resolution and are based on different proxies (which might be influenced by different monsoon-unrelated factors) than our NE monsoon reconstruction. It would thus be beneficial to locate new coring stations in the northwestern Arabian Sea that would provide undisturbed sedimentation and high sedimentation rates to enable the reconstruction of SW monsoon activity in comparable high resolution. The analysis of the same SST (alkenones) and primary productivity proxies ($\delta^{15}N$, bulk components) in cores from the northwestern Arabian Sea in similar resolution and its comparison to the NE monsoon record could help to identify SW and NE monsoon dynamics in more detail on time scales of societal relevance.

An issue that could not be addressed in this study, but that needs further investigation is the future development of the monsoon system and its influence on the Arabian Sea oceanic environment. A predicted increase in global temperature might intensify the strength of SW monsoon winds with implication for SST, primary productivity and OMZ intensity (and associated emission of N_2O) in the Arabian Sea. The investigation of new high-resolution sediment cores that would cover the recent 30 years (which are missing in the sediment cores investigated in this thesis) might be able to capture a possible signal of global warming in the Arabian Sea.

List of Figures

Figure 5.1: Study area of the Arabian Sea with core locations M74/1b-163SL and MC680 (red dots) and locations of cores discussed in the main text (black squares). Illustrated by color shading is the oxygen content in 300 m water depth indicating

List of Tables

List of Abbreviations

ACD	aragonite compensation depth
A.D.	Anno Domini
AMO	Atlantic Multidecadal Oscillation
AMS	accelerator mass spectrometry
AM-SST	annual mean sea surface temperature
B/A	Bølling/Allerød epoch
B.C.	Before Christ
BMBF	Bundesministerium für Bildung und Forschung
BP	Before Present
BSi	biogenic silica
CAME	Central Asia and Tibet: Monsoon dynamics and geo-ecosystems
CARIMA	Natural versus anthropogenic controls of past monsoon variability in central Asia recorded in marine archives
CDA	Cold Dark Ages
DCM	methylene chloride
EPT-2	Eastern PAKOMIN sediment trap station 2
GC	gas chromatograph
GISP	Greenland Ice Sheet Project
H1, H2	Heinrich event 1 und 2
HCl	hydrochlorid acid
IAEA	International Atomic Energy Agency
ID	inner diameter
IOCW	Indian Ocean Central Water
IS	Interstadial
ITCZ	Intertropical Convergence Zone
ka	kiloannus (thousand years)
KG	box core
KL	kasten lot
KOH	potassium hydroxide
kyr	thousand years

LGM	Last Glacial Maximum
LIA	Little Ice Age
MAR	mass accumulation rates
MARUM	Zentrum für Marine Umweltwissenschaften
MC	multicorer
MWP	Medieval Warm Period
NE	northeast
NH	Northern Hemisphere
NIOP	Netherlands Indian Ocean Programme
NW	northwest
OM	organic matter
OMZ	oxygen minimum zone
PGW	Persian Gulf Water
R	isotope ratio
RSW	Red Sea Water
RWP	Roman Warm Period
SL	gravity core
SR	sedimentation rate
SST	sea surface temperature
SW	southwest
TOC	total organic carbon
XRF	X-ray fluorescence
YD	Younger Dryas

References

Agnihotri, R., Bhattacharya, S.K., Sarin, M.M., Somayajulu, B.L.K., 2003. Changes in surface productivity and subsurface denitrification during the Holocene: a multiproxy study from the eastern Arabian Sea. The Holocene 13, 701–713. doi:10.1191/0959683603hl656rp.

Agnihotri, R., Dutta, K., Bhushan, R., Somayajulu, B.L.K., 2002. Evidence for solar forcing on the Indian monsoon during the last millennium. Earth Planet. Sci. Lett. 198, 521–527.

Agnihotri, R., Kurian, S., Fernandes, M., Reshma, K., D'Souza, W., Naqvi, S.W.A., 2008. Variability of subsurface denitrification and surface productivity in the coastal eastern Arabian Sea over the past seven centuries. The Holocene 18, 755–764. doi:10.1177/0959683608091795.

Alley, R.B., 2000. The Younger Dryas cold interval as viewed from central Greenland. Quat. Sci. Rev. 19, 213–226.

Altabet, A., Murray, D.W., Prell, W.L., 1999. Climatically linked oscillation in Arabian Sea denitrification over the past 1 m.y.: Implications for the marine N cycle. Paleoceanography 14, 732–743.

Altabet, M.A., Francois, R., 1994. Sedimentary nitrogen isotopic ratio as a recorder for surface ocean nitrate utilization. Global Biogeochem. Cycles 8, 103–116.

Altabet, M.A., Francois, R., Murray, D.W., Prell, W.L., 1995. Climate-related variations in denitrification in the Arabian Sea from sediment ^{15}N/^{14}N ratios. Nature 373, 506–509.

Altabet, M.A., Higginson, M.J., Murray, D.W., 2002. The effect of millennial-scale changes in Arabian Sea denitrification on atmospheric CO_2. Nature 415, 159–162.

Anand, P., Kroon, D., Singh, A.D., Ganeshram, R.S., Ganssen, G., Elderfield, H., 2008. Coupled sea surface temperature-seawater δ^{18}O reconstructions in the Arabian Sea at the millennial scale for the last 35 ka. Paleoceanography 23, PA4207. doi:10.1029/2007PA001564.

Anderson, D.M., Baulcomb, C.K., Duvivier, A.K., Gupta, A.K., 2010. Indian summer monsoon during the last two millennia. J. Quat. Sci. 25, 911–917. doi:10.1002/jqs.1369.

Anderson, D.M., Overpeck, J.T., Gupta, A.K., 2002. Increase in the Asian Southwest Monsoon during the past Four Centuries. Science 297, 596–599.

Andruleit, H., Rogalla, U., Stäger, S., 2004. From living communities to fossil assemblages: origin and fate of coccolithophores in the northern Arabian Sea. Micropaleontology 50, 5–21.

Andruleit, H.A., von Rad, U., Bruns, A., Ittekkot, V., 2000. Coccolithophore fluxes from sediment traps in the northeastern Arabian Sea off Pakistan. Mar. Micropaleontol. 38, 285–308.

Bange, H.W., Andreae, M.O., Lal, S., Law, C.S., Naqvi, S.W.A., Patra, P.K., Rixen, T., Upstill-Goddard, R.C., 2001. Nitrous oxide emissions from the Arabian Sea: A synthesis. Atmos. Chem. Phys. 1, 61–71. doi:10.5194/acpd-1-167-2001.

Bange, H.W., Rixen, T., Johansen, A.M., Siefert, R.L., Ramesh, R., Ittekkot, V., Hoffmann, M.R., Andreae, M.O., 2000. A revised nitrogen budget for the Arabian Sea. Global Biogeochem. Cycles 14, 1283–1297.

Banse, K., McClain, C.R., 1986. Winter blooms of phytoplankton in the Arabian Sea as observed by the Coastal Zone Color Scanner. Mar. Ecol. - Prog. Ser. 34, 201–211.

Banse, K., Naqvi, S.W.A., Narvekar, P. V., Postel, J.R., Jayakumar, D.A., 2014. Oxygen minimum zone of the open Arabian Sea: variability of oxygen and nitrite from daily to decadal timescales. Biogeosciences 11, 2237–2261. doi:10.5194/bg-11-2237-2014.

Bao, Y., Bräuning, A., Yafeng, S., 2003. Late Holocene temperature fluctuations on the Tibetan Plateau. Quat. Sci. Rev. 22, 2335–2344. doi:10.1016/S0277-3791(03)00132-X.

Bard, E., Hamelin, B., Arnold, M., Montaggioni, L., Cabioch, G., Faure, G., Rougerie, F., 1996. Deglacial sea-level record from Tahiti corals and the timing of global meltwater discharge. Nature 382, 241–244.

Bard, E., Raisbeck, G., Yiou, F., Jouzel, J., 2000. Solar irradiance during the last 1200 years based on cosmogenic nuclides. Tellus 52B, 985–992. doi:10.1034/j.1600-0889.2000.d01-7.x.

Berger, A., Loutre, M.F., 1991. Insolation values for the climate of the last 10 million years. Quat. Sci. Rev. 10, 297–317.

Berger, J.-F., Bravard, J.-P., Purdue, L., Benoist, A., Mouton, M., Braemer, F., 2012. Rivers of the Hadramawt watershed (Yemen) during the Holocene: Clues of late functioning. Quat. Int. 266, 142–161. doi:10.1016/j.quaint.2011.10.037.

Berger, W.H., Herguera, J.C., Lange, C.B., Schneider, R., 1994. Paleoproductivity: Flux proxies versus nutrient proxies and other problems concerning the quaternary productivity record, in: Zahn, R., Pedersen, T.F., Kaminski, M.A., Labeyrie, L. (Eds.), Carbon Cycling in the Glacial Ocean: Constraints on the Ocean's Role in Global Change. NATO ASI Series. Springer-Verlag, Berlin-Heiderlberg, New York, pp. 385-412.

Berkelhammer, M., Sinha, A., Mudelsee, M., Cheng, H., Edwards, R.L., Cannariato, K.G., 2010. Persistent multidecadal power of the Indian Summer Monsoon. Earth Planet. Sci. Lett. 290, 166–172. doi:10.1016/j.epsl.2009.12.017.

Black, D.E., Abahazi, M.A, Thunell, R.C., Kaplan, A., Tappa, E.J., Peterson, L.C., 2007. An 8-century tropical Atlantic SST record from the Cariaco Basin: Baseline variability,

twentieth-century warming, and Atlantic hurricane frequency. Paleoceanography 22, PA4204. doi:10.1029/2007PA001427.

Böll, A., Lückge, A., Munz, P., Forke, S., Schulz, H., Ramaswamy, V., Rixen, T., Gaye, B., Emeis, K.-C., 2014. Late Holocene primary productivity and sea surface temperature variations in the northeastern Arabian Sea: implications for winter monsoon variability. Paleoceanography 29, 778-794. doi:10.1002/2013PA002579.

Böll, A., Schulz, H., Munz, P., Rixen, T., Gaye, B., Emeis, K.-C., 2014. Contrasting sea surface temperature of summer and winter monsoon variability in the northern Arabian Sea over the last 25 ka. submitted to Palaeogeogr. Palaeoclimatol. Palaeoecol.

Bond, G., Kromer, B., Beer, J., Muscheler, R., Evans, M.N., Showers, W., Hoffmann, S., Lotti-Bond, R., Hajdas, I., Bonani, G., 2001. Persistent Solar Influence on North Atlantic Climate During the Holocene. Science 294, 2130–2136. doi:10.1126/science.1065680.

Böning, P., Bard, E., 2009. Millennial/centennial-scale thermocline ventilation changes in the Indian Ocean as reflected by aragonite preservation and geochemical variations in Arabian Sea sediments. Geochim. Cosmochim. Acta 73, 6771–6788. doi:10.1016/j.gca.2009.08.028.

Brassell, S.C., Eglinton, G., Marlowe, I.T., Pflaumann, U., Sarnthein, M., 1986. Molecular stratigraphy: a new tool for climate assessment. Nature 320, 129–133.

Bray, H.E., Stokes, S., 2004. Temporal patterns of arid-humid transitions in the south-eastern Arabian Peninsula based on optical dating. Geomorphology 59, 271–280. doi:10.1016/j.geomorph.2003.07.022.

Broccoli, A.J., Dahl, K.A., Stouffer, R.J., 2006. Response of the ITCZ to Northern Hemisphere cooling. Geophys. Res. Lett. 33, L01702. doi:10.1029/2005GL024546.

Broerse, A.T.C., Brummer, G.-J.A., Van Hinte, J.E., 2000. Coccolithophore export production in response to monsoonal upwelling off Somalia (northwestern Indian Ocean). Deep Sea Res. II 47, 2179–2205. doi:10.1016/S0967-0645(00)00021-7.

Bulow, S.E., Rich, J.J., Naik, H.S., Pratihary, A.K., Ward, B.B., 2010. Denitrification exceeds anammox as a nitrogen loss pathway in the Arabian Sea oxygen minimum zone. Deep Sea Res. I 57, 384–393. doi:10.1016/j.dsr.2009.10.014.

Burns, S.J., Fleitmann, D., Mudelsee, M., Neff, U., Matter, A., Mangini, A., 2002. A 780-year annually resolved record of Indian Ocean monsoon precipitation from a speleothem from south Oman. J. Geophys. Res. 107, 4434. doi:10.1029/2001JD001281.

Calvert, S., Pedersen, T., 1993. Geochemistry of Recent oxic and anoxic marine sediments: Implications for the geological record. Mar. Geol. 113, 67–88. doi:10.1016/0025-3227(93)90150-T.

Chauhan, O.S., Vogelsang, E., Basavaiah, N., Kader, U.S.A., 2010. Reconstruction of the variability of the southwest monsoon during the past 3 ka, from the continental margin of the southeastern Arabian Sea. J. Quat. Sci. 25, 798–807.

Christiansen, B., Ljungqvist, F.C., 2012. The extra-tropical Northern Hemisphere temperature in the last two millennia: reconstructions of low-frequency variability. Clim. Past 8, 765–786. doi:10.5194/cp-8-765-2012.

Clemens, S., Prell, W.L., Murray, D.W., Shimmield, G., Weedon, G., 1991. Forcing mechanisms of the Indian Ocean monsoon. Nature 353, 720–725.

Clemens, S.C., Prell, W.L., 1990. Late Pleistocene variability of Arabian Sea summer monsoon winds and continental aridity: Eolian records from the lithogenic component of deep-sea sediments. Paleoceanography 5, 109–145.

Clemens, S.C., Prell, W.L., 2003. A 350,000 year summer-monsoon multi-proxy stack from the Owen Ridge, Northern Arabian Sea. Mar. Geol. 201, 35–51. doi:10.1016/S0025-3227(03)00207-X.

Clemens, S.C., Prell, W.L., Sun, Y., 2010. Orbital-scale timing and mechanism driving Late Pleistocene Indo-Asian summer monsoons: Reinterpreting cave speleothem δ^{18}O. Paleoceanography 25, doi:10.1029/2010PA001926.

Clift, P.D., Plumb, R.A., 2008. The Asian Monsoon: Causes, History and Effects. Cambridge University Press, New York.

Codispoti, L.A., Brandes, J.A.Y.A., Christensen, J.P., Devol, A.H., 2001. The oceanic fixed nitrogen and nitrous oxide budgets: Moving targets as we enter the anthropocene? Sci. Mar. 65, 85–105.

Conley, D.J., 1998. An interlaboratory comparison for the measurement of biogenic silica in sediments. Mar. Chem. 63, 39–48. doi:10.1016/S0304-4203(98)00049-8.

Conte, M.H., Sicre, M.-A., Rühlemann, C., Weber, J.C., Schulte, S., Schulz-Bull, D., Blanz, T., 2006. Global temperature calibration of the alkenone unsaturation index (U_{37}^{K}) in surface waters and comparison with surface sediments. Geochemistry, Geophys. Geosystems 7, Q02005. doi:10.1029/2005GC001054.

Cowie, G.L., Calvert, S.E., Pedersen, T.F., Schulz, H., von Rad, U., 1999. Organic content and preservational controls in surficial shelf and slope sediments from the Arabian Sea (Pakistan margin). Mar. Geol. 161, 23–38.

Dahl, K.A., Oppo, D.W., 2006. Sea surface temperature pattern reconstructions in the Arabian Sea. Paleoceanography 21, PA1014. doi:10.1029/2005PA001162.

Dansgaard, W., Johnsen, S.J., Clausen, H.B., Dahl-Jensen, D., Gundestrup, N., Hammer, C.U., Hvidberg, C.S., Steffensen, J.P., Sveinbjörnsdottir, A.E., Jouzel, J., Bond, G., 1993. Evidence for general instability of past climate from a 250-kyr ice-core record. Nature 364, 218–220.

DeMaster, D.J., 1981. The supply and accumulation of silica in the marine environment. Geochim. Cosmochim. Acta 45, 1715–1732. doi:10.1016/0016-7037(81)90006-5.

DeMenocal, P., 2000. Coherent High- and Low-Latitude Climate Variability During the Holocene Warm Period. Science 288, 2198–2202. doi:10.1126/science.288.5474.2198.

Deplazes, G., Lückge, A., Stuut, J.-B.W., Pätzold, J., Kuhlmann, H., Husson, D., Fant, M., Haug, G.H., 2014. Weakening and strengthening of the Indian monsoon during Heinrich events and Dansgaard-Oeschger oscillations. Paleoceanography 29, 99–114. doi:10.1002/2013PA002509.

Devol, A.H., 1978. Bacterial oxygen uptake kinetics as related to biological processes in oxygen deficient zones of the oceans. Deep Sea Res. 25, 137–146.

Doose-Rolinski, H., Rogalla, U., Scheeder, G., Lückge, A., von Rad, U., 2001. High-resolution temperature and evaporation changes during the late Holocene in the northeastern Arabian Sea. Paleoceanography 16, 358–367.

Dykoski, C., Edwards, R., Cheng, H., Yuan, D., Cai, Y., Zhang, M., Lin, Y., Qing, J., An, Z., Revenaugh, J., 2005. A high-resolution, absolute-dated Holocene and deglacial Asian monsoon record from Dongge Cave, China. Earth Planet. Sci. Lett. 233, 71–86. doi:10.1016/j.epsl.2005.01.036.

Emeis, K.-C., Anderson, D.M., Doose-Rolinski, H., Kroon, D., Schulz-Bull, D., 1995. Sea-Surface Temperatures and the History of Monsoon Upwelling in the Northwest Arabian Sea during the Last 500,000 Years. Quat. Res. 43, 355–361.

Emeis, K.-C., Struck, U., Schulz, H.-M., Rosenberg, R., Bernasconi, S., Erlenkeuser, H., Sakamoto, T., Martinez-Ruiz, F., 2000. Temperature and salinity variations of Mediterranean Sea surface waters over the last 16,000 years from records of planktonic stable oxygen isotopes and alkenone unsaturation ratios. Palaeogeogr. Palaeoclimatol. Palaeoecol. 158, 259–280.

Esper, J., Schweingruber, F.H., Winiger, M., 2002. 1300 years of climate history for Western Central Asia inferred from tree-rings. The Holocene 12, 267–277.

Feng, S., Hu, Q., 2005. Regulation of Tibetan Plateau heating on variation of Indian summer monsoon in the last two millennia. Geophys. Res. Lett. 32, L02702. doi:10.1029/2004GL021246.

Findlater, J., 1969. A major low-level air current near the Indian Ocean during the northern summer. Q. J. R. Meteorol. Soc. 95, 362–380. doi:10.1002/qj.49709540409.

Fleitmann, D., Burns, S.J., Mangini, A., Mudelsee, M., Kramers, J., Villa, I., Neff, U., Al-Subbary, A.A., Buettner, A., Hippler, D., Matter, A., 2007. Holocene ITCZ and Indian monsoon dynamics recorded in stalagmites from Oman and Yemen (Socotra). Quat. Sci. Rev. 26, 170–188. doi:10.1016/j.quascirev.2006.04.012.

Fleitmann, D., Burns, S.J., Mudelsee, M., Neff, U., Kramers, J., Mangini, A., Matter, A., 2003. Holocene Forcing of Indian Monsoon Recorded in a Stalagmite from Southern Oman. Science 300, 1737–1739.

Fleitmann, D., Burns, S.J., Neff, U., Mudelsee, M., Mangini, A., Matter, A., 2004. Palaeoclimatic interpretation of high-resolution oxygen isotope profiles derived from annually laminated speleothems from Southern Oman. Quat. Sci. Rev. 23, 935–945.

Fuchs, M., Buerkert, A., 2008. A 20 ka sediment record from the Hajar Mountain range in N-Oman, and its implication for detecting arid–humid periods on the southeastern Arabian Peninsula. Earth Planet. Sci. Lett. 265, 546–558. doi:10.1016/j.epsl.2007.10.050.

Ganeshram, S., Pedersen, F., Calvert, E., McNeill, W., Fontugne, M.R., 2000. Glacial-interglacial variability in denitrification in the world's oceans: Causes and consequences. Paleoceanography 15, 361–376.

Gaye, B., Nagel, B., Dähnke, K., Rixen, T., Emeis, K.-C., 2013. Evidence of parallel denitrification and nitrite oxidation in the ODZ of the Arabian Sea from paired stable isotopes of nitrate and nitrite. Global Biogeochem. Cycles 27, 1059–1071. doi:10.1002/2011GB004115.

Gaye-Haake, B., Lahajnar, N., Emeis, K.-C., Unger, D., Rixen, T., Suthhof, A., Ramaswamy, V., Schulz, H., Paropkari, A.L., Guptha, M.V.S., Ittekkot, V., 2005. Stable nitrogen isotopic ratios of sinking particles and sediments from the northern Indian Ocean. Mar. Chem. 96, 243–255. doi:10.1016/j.marchem.2005.02.001.

Ge, Q., Hao, Z., Zheng, J., Shao, X., 2013. Temperature changes over the past 2000 yr in China and comparison with the Northern Hemisphere. Clim. Past 9, 1153–1160. doi:10.5194/cp-9-1153-2013.

Goes, J.I., Thoppil, P.G., Gomes, H. do R., Fasullo, J.T., 2005. Warming of the Eurasian Landmass is Making the Arabian Sea More Productive. Science 308, 545–547.

Goswami, B.N., Madhusoodanan, M.S., Neema, C.P., Sengupta, D., 2006. A physical mechanism for North Atlantic SST influence on the Indian summer monsoon. Geophys. Res. Lett. 33, L02706. doi:10.1029/2005GL024803.

Grootes, P.M., Stuiver, M., 1997. Oxygen 18/16 variability in Greenland snow and ice with 10^{-3}- to 10^{5}-year time resolution. J. Geophys. Res. 102, 26455–26470.

Gupta, A.K., Anderson, D.M., Overpeck, J.T., 2003. Abrupt changes in the Asian southwest monsoon during the Holocene and their links to the North Atlantic Ocean. Nature 421, 354–356.

Gupta, A.K., Das, M., Anderson, D.M., 2005. Solar influence on the Indian summer monsoon during the Holocene. Geophys. Res. Lett. 32, L17703. doi:10.1029/2005GL022685.

Gupta, A.K., Mohan, K., Sarkar, S., Clemens, S.C., Ravindra, R., Uttam, R.K., 2011. East–West similarities and differences in the surface and deep northern Arabian Sea records during the past 21 Kyr. Palaeogeogr. Palaeoclimatol. Palaeoecol. 301, 75–85. doi:10.1016/j.palaeo.2010.12.027.

Haake, B., Ittekkot, V., Rixen, T., Ramaswamy, V., Nair, R.R., Curry, W.B., 1993. Seasonality and interannual variability of particle fluxes to the deep Arabian Sea. Deep Sea Res. I 40, 1323–1344.

Hastenrath, S., Lamb, P.J., 1979. Climate Atlas of the Indian Ocean, Volume 1: Surface Climate and Atmospheric Circulation. University of Wisconsin Press, Madison.

Haug, G.H., Hughen, K.A., Sigman, D.M., Peterson, L.C., Röhl, U., 2001. Southward migration of the intertropical convergence zone through the Holocene. Science 293, 1304–1308. doi:10.1126/science.1059725.

Herbert, T.D., 2003. Alkenone Paleotemperature Determinations, in: Holland, H.D., Turekian, K.K. (Ed.), Treatise on Geochemistry, Volume 6: The Oceans and Marine Geochemistry. Elsevier, New York, pp. 391–432.

Herzschuh, U., 2006. Palaeo-moisture evolution in monsoonal Central Asia during the last 50,000 years. Quat. Sci. Rev. 25, 163–178. doi:10.1016/j.quascirev.2005.02.006.

Hoefs, J., 2009. Stable Isotope Geochemistry, 6th ed. Springer.

Hong, Y.T., Hong, B., Lin, Q.H., Zhu, Y.X., Shibata, Y., Hirota, M., Uchida, M., Leng, X.T., Jiang, H.B., Xu, H., Wang, H., Yi, L., 2003. Correlation between Indian Ocean summer monsoon and North Atlantic climate during the Holocene. Earth Planet. Sci. Lett. 211, 371–380.

Hua, Q., Barbetti, M., 2004. Review of tropospheric bomb ^{14}C data for carbon cycle modeling and age calibration purposes. Radiocarbon 46, 1273–1298.

Huguet, C., Kim, J.-H., Sinninghe Damsté, J.S., Schouten, S., 2006. Reconstruction of sea surface temperature variations in the Arabian Sea over the last 23 kyr using organic proxies (TEX$_{86}$ and U$_{37}^{K'}$). Paleoceanography 21, PA3003, doi:10.1029/2005PA001215.

Ivanochko, T., Ganeshram, R.S., Brummer, G.-J.A., Ganssen, G., Jung, S.J.A., Moreton, S.G., Kroon, D., 2005. Variations in tropical convection as an amplifier of global climate change at the millennial scale. Earth Planet. Sci. Lett. 235, 302–314. doi:10.1016/j.epsl.2005.04.002.

Ivanochko, T.S., 2004. Sub-orbital variations in the intensity of the Arabian Sea monsoon. Ph.D. thesis. 230 pp. University of Edinburgh.

Jung, S.J.A., Kroon, D., Ganssen, G., Peeters, F., Ganeshram, R., 2009. Enhanced Arabian Sea intermediate water flow during glacial North Atlantic cold phases. Earth Planet. Sci. Lett. 280, 220–228. doi:10.1016/j.epsl.2009.01.037.

Jung, S.J.A., Davies, G.R., Ganssen, G., Kroon, D., 2004. Synchronous Holocene sea surface temperature and rainfall variations in the Asian monsoon system. Quat. Sci. Rev. 23, 2207–2218.

Kallel, N., Labeyrie, L.D., Juillet-Leclerc, A., Duplessy, J.C., 1988. A deep hydrological front between intermediate and deep-water masses in the glacial Indian Ocean. Nature 333, 651–655.

Karl, D., Michaels, A., Bergman, B., Capone, D., Carpenter, E., Letelier, R., Lipschultz, F., Paerl, H., Sigman, D., Stal, L., 2002. Dinitrogen fixation in the world's oceans. Biogeochemistry 57, 47–98.

Keeling, R.E., Körtzinger, A., Gruber, N., 2010. Ocean deoxygenation in a warming world. Ann. Rev. Mar. Sci. 2, 199–229. doi:10.1146/annurev.marine.010908.163855.

Keigwin, L.D., 1996. The Little Ice Age and Medieval Warm Period in the Sargasso Sea. Science 274, 1504–1508.

Keil, R.G., Cowie, G.L., 1999. Organic matter preservation through the oxygen-deficient zone of the NE Arabian Sea as discerned by organic carbon:mineral surface area ratios. Mar. Geol. 161, 13–22. doi:10.1016/S0025-3227(99)00052-3.

Kessarkar, P.M., Rao, V.P., Naqvi, S.W.A., Karapurkar, S.G., 2013. Variation in the Indian summer monsoon intensity during the Bølling-Ållerød and Holocene. Paleoceanography 28, 413-425. doi:10.1002/palo.20040.

Labeyrie, L., Waelbroeck, C., Cortijo, E., Michel, E., Duplessy, J.-C., 2005. Changes in deep water hydrology during the Last Deglaciation. Comptes Rendus Geosci. 337, 919–927. doi:10.1016/j.crte.2005.05.010.

Lambeck, K., 1996. Shoreline reconstructions for the Persian Gulf since the last glacial maximum. Earth Planet. Sci. Lett. 142, 43–57. doi:10.1016/0012-821X(96)00069-6.

Levitus, S., Antonov, J., Boyer, T., 2005. Warming of the world ocean, 1955–2003. Geophys. Res. Lett. 32, L02604. doi:10.1029/2004GL021592.

Levitus, S., Boyer, T., 1994. World Ocean Atlas, Volume 4: Temperature. NOAA Atlas NESDIS, U.S. department of Commerce, Washington, D.C.

Lézine, A.-M., Tiercelin, J.-J., Robert, C., Saliège, J.-F., Cleuziou, S., Inizan, M.-L., Braemer, F., 2007. Centennial to millennial-scale variability of the Indian monsoon during the early Holocene from a sediment, pollen and isotope record from the desert of Yemen. Palaeogeogr. Palaeoclimatol. Palaeoecol. 243, 235–249. doi:10.1016/j.palaeo.2006.05.019

Liu, X., Dong, H., Yang, X., Herzschuh, U., Zhang, E., Stuut, J.-B.W., Wang, Y., 2009. Late Holocene forcing of the Asian winter and summer monsoon as evidenced by proxy records from the northern Qinghai–Tibetan Plateau. Earth Planet. Sci. Lett. 280, 276–284. doi:10.1016/j.epsl.2009.01.041.

Locarnini, R.A., Mishonov, A.V., Antonov, J.I., Boyer, T.P., Garcia, H.E., Baranova, O.K., Zweng, M.M., Johnson, D.R., 2010. World Ocean Atlas 2009, Volume 1: Temperature, in: Levitus, S. (Ed.), NOAA Atlas NESDIS 68. U.S. Government Printing Office, Washington, D.C., p. 184.

Lückge, A., Doose-Rolinski, H., Khan, A.A., Schulz, H., von Rad, U., 2001. Monsoonal variability in the northeastern Arabian Sea during the past 5000 years: geochemical evidence from laminated sediments. Palaeogeogr. Palaeoclimatol. Palaeoecol. 167, 273–286.

Lückge, A., Reinhardt, L., Andruleit, H., Doose-Rolinski, H., von Rad, U., Schulz, H., Treppke, U., 2002. Formation of varve-like laminae off Pakistan: decoding 5 years of sedimentation. Geol. Soc. London, Spec. Publ. 195, 421–431.

Madhupratap, M., Prasanna Kumar, S., Bhattathiri, P.M.A., Dileep Kumar, M., Raghukumar, S., Nair, K.K.C., Ramaiah, N., 1996. Mechanism of the biological response to winter cooling in the northeastern Arabian Sea. Nature 384, 549–552.

Mann, M.E., Zhang, Z., Rutherford, S., Bradley, R.S., Hughes, M.K., Shindell, D., Ammann, C., Faluvegi, G., Ni, F., 2009. Global Signatures and Dynamical Origins of the Little Ice Age and Medieval Climate Anomaly. Science 326, 1256–1260. doi:10.1126/science.1177303

Marathayil, D., Turner, A.G., Shaffrey, L.C., Levine, R.C., 2013. Systematic winter sea-surface temperature biases in the northern Arabian Sea in HiGEM and the CMIP3 models. Environ. Res. Lett. 8, 014028. doi:10.1088/1748-9326/8/1/014028.

Marcott, S.A., Shakun, J.D., Clark, P.U., Mix, A.C., 2013. A Reconstruction of Regional and Global Temperature for the Past 11,300 Years. Science 339, 1198–1201. doi:10.1126/science.1228026

Matear, R.J., Hirst, A.C., 2003. Long-term changes in dissolved oxygen concentrations in the ocean caused by protracted global warming. Global Biogeochem. Cycles 17, 1125. doi:10.1029/2002GB001997.

Meehl, G.A., 1994. Influence of the Land Surface in the Asian Summer Monsoon: External Conditions versus Internal Feedbacks. J. Clim. 7, 1033–1049.

Moberg, A., Sonechkin, D.M., Holmgren, K., Datsenko, N.M., Karlén, W., 2005. Highly variable Northern Hemisphere temperatures reconstructed from low- and high-resolution proxy data. Nature 433, 613–617. doi:10.1038/nature03298.1.

Möbius, J., Gaye, B., Lahajnar, N., Bahlmann, E., Emeis, K.-C., 2011. Influence of diagenesis on sedimentary $\delta^{15}N$ in the Arabian Sea over the last 130 kyr. Mar. Geol. 284, 127-138. doi: 10.1016/j.margeo.2011.03.013.

Müller, P.J., Suess, E., 1979. Productivity, sedimentation rate, and sedimentary organic matter in the oceans-I. Organic carbon preservation. Deep Sea Res. 26A, 1347–1362.

Naidu, P.D., Malmgren, A., 1996. A high-resolution record of late Quaternary upwelling along the Oman Margin, Arabian Sea based on planktonic foraminifera. Palaeogeography 11, 129–140. doi:10.1029/95PA03198.

Naidu, P.D., Malmgren, B.A., 2005. Seasonal sea surface temperature contrast between the Holocene and last glacial period in the western Arabian Sea (Ocean Drilling Project Site 723A): Modulated by monsoon upwelling. Paleoceanography 20, PA1004, doi:10.1029/2004PA001078.

Nair, R.R., Ittekkot, V., Manganini, S.J., Ramaswamy, V., Haake, B., Degens, E.T., Desai, B.N., Honjo, S., 1989. Increased particle flux to the deep ocean related to monsoons. Nature 338, 749–751.

Naqvi, S.W.A., Yoshinari, T., Jayakumar, D.A., Altabet, M.A., Narvekar, P.V., Devol, A.H., Brandes, J.A., Codispoti, L.A., 1998. Budgetary and biogeochemical implications of N_2O isotope signatures in the Arabian Sea. Nature 394, 462–464.

Neff, U., Burns, S.J., Mangini, A., Mudelsee, M., Fleitmann, D., Matter, A., 2001. Strong coherence between solar variability and the monsoon in Oman between 9 and 6 kyr ago. Nature 411, 290–293. doi:10.1038/35077048.

Olson, D.B., Hitchcock, G.L., Fine, R.A., Warren, B.A., 1993. Maintenance of the low-oxygen layer in the central Arabian Sea. Deep Sea Res. II 40, 673–685.

Oppo, D.W., Rosenthal, Y., Linsley, B.K., 2009. 2,000-year-long temperature and hydrology reconstructions from the Indo-Pacific warm pool. Nature 460, 1113–1116. doi:10.1038/nature08233.

Overpeck, J., Anderson, D., Trumbore, S., Prell, W., 1996. The southwest Indian Monsoon over the last 18 000 years. Clim. Dyn. 12, 213–225. doi:10.1007/BF00211619.

PAGES 2k Consortium, 2013. Continental-scale temperature variability during the past two millennia. Nat. Geosci. 6, 339–346. doi:10.1038/NGEO1797.

PAGES/Ocean2k Working Group, 2012. Synthesis of marine sediment-derived SST records for the past 2 millennia: First-order results from the PAGES/Ocean2k project. AGU Fall Meet. abstr. PP1.

Paropkari, A.L., Babu, C.P., Mascarenhas, A., 1992. A critical evaluation of depositional parameters controlling the variability of organic carbon in Arabian Sea sediments. Mar. Geol. 107, 213–226.

Peterse, F., Prins, M.A., Beets, C.J., Troelstra, S.R., Zheng, H., Gu, Z., Schouten, S., Sinninghe Damsté, J.S., 2011. Decoupled warming and monsoon precipitation in East Asia over the last deglaciation. Earth Planet. Sci. Lett. 301, 256–264. doi:10.1016/j.epsl.2010.11.010.

Pichevin, L., Bard, E., Martinez, P., Billy, I., 2007. Evidence of ventilation changes in the Arabian Sea during the late Quaternary: Implication for denitrification and nitrous oxide emission. Global Biogeochem. Cycles 21, GB4008. doi:10.1029/2006GB002852.

Prahl, F.G., Dymond, J., Sparrow, M.A., 2000. Annual biomarker record for export production in the central Arabian Sea. Deep Sea Res. II 47, 1581–1604. doi:10.1016/S0967-0645(99)00155-1.

Prahl, F.G., Popp, B.N., Karl, D.M., Sparrow, M.A., 2005. Ecology and biogeochemistry of alkenone production at Station ALOHA. Deep Sea Res. I 52, 699–719. doi:10.1016/j.dsr.2004.12.001.

Prahl, F.G., Wakeham, S.G., 1987. Calibration of unsaturation patterns in long-chain ketone compositions for palaeotemperature asessment. Nature 330, 367–369.

Prasanna Kumar, S., Prasad, T.G., 1996. Winter cooling in the northern Arabian Sea. Curr. Sci. 71, 834–841.

Prasanna Kumar, S., Ramaiah, N., Gauns, M., Sarma, V.V.S.S., Muraleedharan, P.M., Raghukumar, S., Dileep Kumar, M., Madhupratap, M., 2001. Physical forcing of

biological productivity in the Northern Arabian Sea during the Northeast Monsoon. Deep Sea Res. II 48, 1115–1126. doi:10.1016/S0967-0645(00)00133-8.

Prell, W.L., Kutzbach, J.E., 1992. Sensitivity of the Indian monsoon to forcing parameters and implications for its evolution. Nature 360, 647–652.

Prins, M., Postma, G., Weltje, G., 2000. Controls on terrigenous sediment supply to the Arabian Sea during the late Quaternary: the Makran continental slope. Mar. Geol. 169, 351–371. doi:10.1016/S0025-3227(00)00087-6.

Ramaswamy, V., Gaye, B., 2006. Regional variations in the fluxes of foraminifera carbonate, coccolithophorid carbonate and biogenic opal in the northern Indian Ocean. Deep Sea Res. I 53, 271–293. doi:10.1016/j.dsr.2005.11.003.

Reichart, G.J., den Dulk, M., Visser, H.J., van der Weijden, C.H., Zachariasse, W.J., 1997. A 225 kyr record of dust supply, paleoproductivity and the oxygen minimum zone from the Murray Ridge (northern Arabian Sea). Palaeogeogr. Palaeoclimatol. Palaeoecol. 134, 149–169. doi:10.1016/S0031-0182(97)00071-0.

Reichart, G.J., Lourens, L.J., Zachariasse, W.J., 1998. Temporal variability in the northern Arabian Sea Oxygen Minimum Zone (OMZ) during the last 225,000 years. Paleoceanography 13, 607–621. doi:10.1029/98PA02203.

Reichart, G.J., Nortier, J., Versteegh, G., Zachariasse, W.J., 2002a. Periodical breakdown of the Arabian Sea oxygen minimum zone caused by deep convective mixing. Geol. Soc. London, Spec. Publ. 195, 407–419. doi:10.1144/GSL.SP.2002.195.01.22.

Reichart, G.J., Schenau, S.J., de Lange, G.J., Zachariasse, W.J., 2002b. Synchroneity of oxygen minimum zone intensity on the Oman and Pakistan Margins at sub-Milankovitch time scales. Mar. Geol. 185, 403–415. doi:10.1016/S0025-3227(02)00184-6.

Reimer, P.J., Baillie, M.G.L., Bard, E., Bayliss, A., Beck, J.W., Blackwell, P.G., Bronk Ramsey, C., Buck, C.E., Burr, G.S., Edwards, R.L., Friedrich, M., Grootes, P.M., Guilderson, T.P., Hajdas, I., Heaton, T.J., Hogg, A.G., Hughen, K.A., Kaiser, K.F., Kromer, B., McCormac, F.G., Manning, S.W., Reimer, R.W., Richards, D.A., Southon, J.R., Talamo, S., Turney, C.S.M., van der Plicht, J., Weyhenmeyer, C.E., 2009. IntCal09 and Marine09 radiocarbon age calibration curves, 0-50,000 years cal BP. Radiocarbon 51, 1111–1150.

Reynolds, R.W., Rayner, N.A., Smith, T.M., Stokes, D.C., Wang, W., 2002. An Improved In Situ and Satellite SST Analysis for Climate. J. Clim. 15, 1609–1625.

Rixen, T., Baum, A., Gaye, B., Nagel, B., 2013. Seasonal and interannual variations of the nitrogen cycle in the Arabian Sea. Biogeosciences Discuss. 10, 19541–19570. doi:10.5194/bgd-10-19541-2013.

Rixen, T., Guptha, M.V.S., Ittekkot, V., 2005. Deep ocean fluxes and their link to surface ocean processes and the biological pump. Prog. Oceanogr. 65, 240–259. doi:10.1016/j.pocean.2005.03.006.

Rixen, T., Haake, B., Ittekkot, V., Guptha, M.V.S., Nair, R.R., Schlüssel, P., 1996. Coupling between SW monsoon-related surface and deep ocean processes as discerned from continuous particle flux measurements and correlated satellite data. J. Geophys. Res. 101, 569–582.

Rixen, T., Ittekkot, V., Haake-Gaye, B., Schäfer, P., 2000. The influence of the SW monsoon on the deep-sea organic carbon cycle in the Holocene. Deep Sea Res. II 47, 2629–2651.

Rohling, E.J., Zachariasse, W.J., 1996. Red Sea outflow during the last glacial maximum. Quat. Int. 31, 77–83. doi:10.1016/1040-6182(95)00023-C.

Rosell-Melé, A., Prahl, F.G., 2013. Seasonality of $U^{K'}_{37}$ temperature estimates as inferred from sediment trap data. Quat. Sci. Rev. 72, 128–136. doi:10.1016/j.quascirev.2013.04.017.

Rostek, F., Bard, E., Beaufort, L., Sonzogni, C., Ganssen, G., 1997. Sea surface temperature and productivity records for the past 240 kyr in the Arabian Sea. Deep Sea Res. II 44, 1461–1480.

Russell, J.M., Johnson, T.C., 2005. Late Holocene climate change in the North Atlantic and equatorial Africa: Millennial-scale ITCZ migration. Geophys. Res. Lett. 32, L17705. doi:10.1029/2005GL023295.

Saher, M.H., Jung, S.J.A., Elderfield, H., Greaves, M.J., Kroon, D., 2007a. Sea surface temperatures of the western Arabian Sea during the last deglaciation. Paleoceanography 22, PA2208. doi:10.1029/2006PA001292.

Saher, M.H., Peeters, F.J.C., Kroon, D., 2007b. Sea surface temperatures during the SW and NE monsoon seasons in the western Arabian Sea over the past 20,000 years. Palaeogeogr. Palaeoclimatol. Palaeoecol. 249, 216–228. doi:10.1016/j.palaeo.2007.01.014.

Sanwal, J., Kotlia, B.S., Rajendran, C., Ahmad, S.M., Rajendran, K., Sandiford, M., 2013. Climatic variability in Central Indian Himalaya during the last 1800 years: Evidence from a high resolution speleothem record. Quat. Int. 304, 183-192. doi:10.1016/j.quaint.2013.03.029.

Saraswat, R., Lea, D.W., Nigam, R., Mackensen, A., Naik, D.K., 2013. Deglaciation in the tropical Indian Ocean driven by interplay between the regional monsoon and global teleconnections. Earth Planet. Sci. Lett. 375, 166–175. doi:10.1016/j.epsl.2013.05.022.

Sarma, V.V.S.S., 2002. An evaluation of physical and biogeochemical processes regulating perennial suboxic conditions in the water column of the Arabian Sea. Global Biogeochem. Cycles 16, 1082. doi:10.1029/2001GB001461.

Schäfer, P., Ittekkot, V., 1993. Seasonal Variability of $\delta^{15}N$ in Settling Particles in the Arabian Sea and Its Palaeogeochemical Significance. Naturwissenschaften 80, 511–513.

Schlitzer, R., 2013. Ocean Data View. (Available at http://odv.awi-bremerhaven.de)

Schnetger, B., Brumsack, H.-J., Schale, H., Hinrichs, J., Dittert, L., 2000. Geochemical characteristics of deep-sea sediments from the Arabian Sea: a high-resolution study. Deep Sea Res. II 47, 2735–2768. doi:10.1016/S0967-0645(00)00047-3.

Schott, F.A., McCreary, J.P., 2001. The monsoon circulation of the Indian Ocean. Prog. Oceanogr. 51, 1–123.

Schulte, S., Müller, P., 2001. Variations of sea surface temperature and primary productivity during Heinrich and Dansgaard-Oeschger events in the northeastern Arabian Sea. Geo-Marine Lett. 21, 168–175. doi:10.1007/s003670100080.

Schulte, S., Rostek, F., Bard, E., Rullkötter, J., Marchal, O., 1999. Variations of oxygen-minimum and primary productivity recorded in sediments of the Arabian Sea. Earth Planet. Sci. Lett. 173, 205–221. doi:10.1016/S0012-821X(99)00232-0.

Schulz, H., Emeis, K.-C., Erlenkeuser, H., von Rad, U., Rolf, C., 2002a. The Toba Volcanic Event and Interstadial/Stadial Climates at the Marine Isotopic Stage 5 to 4 Transition in the Northern Indian Ocean. Quat. Res. 57, 22–31.

Schulz, H., von Rad, U., Erlenkeuser, H., 1998. Correlation between Arabian Sea and Greenland climate oscillations of the past 110,000 years. Nature 393, 54–57.

Schulz, H., von Rad, U., Ittekkot, V., 2002b. Planktic foraminifera, particle flux and oceanic productivity off Pakistan, NE Arabian Sea: modern analogues and application to the palaeoclimatic record. Geol. Soc. London, Spec. Publ. 195, 499–516. doi:10.1144/GSL.SP.2002.195.01.27.

Schulz, H., von Rad, U., von Stackelberg, U., 1996. Laminated sediments from the oxygen-minimum zone of the northeastern Arabian Sea. Geol. Soc. London, Spec. Publ. 116, 185–207. doi:10.1144/GSL.SP.1996.116.01.16.

Seki, O., Nakatsuka, T., Kawamura, K., Saitoh, S.-I., Wakatsuchi, M., 2007. Time-series sediment trap record of alkenones from the western Sea of Okhotsk. Mar. Chem. 104, 253–265. doi:10.1016/j.marchem.2006.12.002.

Shimmield, G.B., Mowbray, S.R., 1991. The inorganic geochemical record of the northwest Arabian Sea: A history of productivity variation over the last 400 k.y. from sites 722 and 724. Proc. Ocean Drill. Program, Sci. Results 117, 409–420.

Sicre, M.-A., Jacob, J., Ezat, U., Rousse, S., Kissel, C., Yiou, P., Eiríksson, J., Knudsen, K.L., Jansen, E., Turon, J.-L., 2008. Decadal variability of sea surface temperatures off North Iceland over the last 2000 years. Earth Planet. Sci. Lett. 268, 137–142. doi:10.1016/j.epsl.2008.01.011.

Siddall, M., Rohling, E.J., Almogi-Labin, A., Hemleben, C., Meischner, D., Schmelzer, I., Smeed, D.A., 2003. Sea-level fluctuations during the last glacial cycle. Nature 423, 853–858. doi:10.1038/nature01687.1.

Sigman, D.M., Altabet, M.A., McCorkle, D.C., Francois, R., Fischer, G., 2000. The $\delta^{15}N$ of nitrate in the Southern Ocean: Nitrogen cycling and surface circulation in the ocean interior. J. Geophys. Res. 105, 19599–19614.

Sinha, A., Berkelhammer, M., Stott, L.D., Mudelsee, M., Cheng, H., Biswas, J., 2011a. The leading mode of Indian Summer Monsoon precipitation variability during the last millennium. Geophys. Res. Lett. 38, L15703. doi:10.1029/2011GL047713.

Sinha, A., Cannariato, K.G., Stott, L.D., Cheng, H., Edwards, R.L., Yadava, M.G., Ramesh, R., Singh, I.B., 2007. A 900-year (600 to 1500 A.D.) record of the Indian summer monsoon precipitation from the core monsoon zone of India. Geophys. Res. Lett. 34, L16707. doi:10.1029/2007GL030431.

Sinha, A., Stott, L.D., Berkelhammer, M., Cheng, H., Edwards, R.L., Buckley, B., Aldenderfer, M., Mudelsee, M., 2011b. A global context of megadroughts in monsoon Asia during the past millennium. Quat. Sci. Rev. 30, 47–62.

Sirocko, F., Garbe-Schönberg, D., Devey, C., 2000. Processes controlling trace element geochemistry of Arabian Sea sediments during the last 25,000 years. Glob. Planet. Change 26, 217–303.

Sirocko, F., Sarnthein, M., Erlenkeuser, H., Lange, H., Arnold, M., Duplessy, J.C., 1993. Century-scale events in monsoonal climate over the past 24,000 years. Nature 364, 322–324.

Sirocko, F., Sarnthein, M., Lange, H., Erlenkeuser, H., 1991. Atmospheric Summer Circulation and Coastal Upwelling in the Arabian Sea during the Holocene and the Last Glaciation. Quat. Res. 36, 72–93.

Skinner, L.C., Shackleton, N.J., 2005. An Atlantic lead over Pacific deep-water change across Termination I: implications for the application of the marine isotope stage stratigraphy. Quat. Sci. Rev. 24, 571–580. doi:10.1016/j.quascirev.2004.11.008.

Smith, T.M., Reynolds, R.W., 2003. Extended Reconstruction of Global Sea Surface Temperatures Based on COADS Data (1854–1997). J. Clim. 16, 1495–1510.

Solanki, S.K., Usoskin, I.G., Kromer, B., Schüssler, M., Beer, J., 2004. Unusual activity of the Sun during recent decades compared to the previous 11,000 years. Nature 431, 1084–1087. doi:10.1038/nature02995.

Sonzogni, C., Bard, E., Rostek, F., 1998. Tropical sea-surface temperatures during the last glacial period: a view based on alkenones in Indian Ocean sediments. Quat. Sci. Rev. 17, 1185–1201.

Sonzogni, C., Bard, E., Rostek, F., Dollfus, D., Rosell-Melé, A., Eglinton, G., 1997a. Temperature and Salinity Effects on Alkenone Ratios Measured in Surface Sediments from the Indian Ocean. Quat. Res. 47, 344–355.

Sonzogni, C., Bard, E., Rostek, F., Lafont, R., Rosell-Melé, A., Eglinton, G., 1997b. Core-top calibrations of the alkenone index vs sea surface temperature in the Indian Ocean. Deep Sea Res. II 44, 1445–1460.

Southon, J., Kashgarian, M., Fontugne, M., Metivier, B., Yim, W.W.-S., 2002. Marine reservoir corrections for the Indian Ocean and Southeast Asia. Radiocarbon 44, 167–180.

Stramma, L., Johnson, G.C., Sprintall, J., Mohrholz, V., 2008. Expanding oxygen-minimum zones in the tropical oceans. Science 320, 655–658. doi:10.1126/science.1153847.

Stramma, L., Oschlies, A., Schmidtko, S., 2012. Mismatch between observed and modeled trends in dissolved upper-ocean oxygen over the last 50 yr. Biogeosciences 9, 4045–4057. doi:10.5194/bg-9-4045-2012.

Stuiver, M., Reimer, P.J., 1993. Extended ^{14}C data base and revised CALIB 3.0 ^{14}C age calibration program. Radiocarbon 35, 215–230.

Suthhof, A., Ittekkot, V., Gaye-Haake, B., 2001. Millennial-scale oscillation of denitrification intensity in the Arabian Sea during the late Quaternary and its potential influence on atmospheric N_2O and global climate. Global Biogeochem. Cycles 15, 637–649. doi:10.1029/2000GB001337.

Suthhof, A., Jennerjahn, T.C., Schäfer, P., Ittekkot, V., 2000. Nature of organic matter in surface sediments from the Pakistan continental margin and the deep Arabian Sea: amino acids. Deep. Res. II 47, 329–351.

Thompson, L.G., Yao, T., Davis, M.E., Henderson, K.A., Mosley-Thompson, E., Lin, P.-N., Beer, J., Synal, H.-A., Cole-Dai, J., Bolzan, J.F., 1997. Tropical Climate Instability: The Last Glacial Cycle from a Qinghai-Tibetan Ice Core. Science 276, 1821–1825. doi:10.1126/science.276.5320.1821.

van der Weijden, C.H., Reichart, G.J., Visser, H.J., 1999. Enhanced preservation of organic matter in sediments deposited within the oxygen minimum zone in the northeastern Arabian Sea. Deep Sea Res. I 46, 807–830. doi:10.1016/S0967-0637(98)00093-4.

Van Rampelbergh, M., Fleitmann, D., Verheyden, S., Cheng, H., Edwards, L., De Geest, P., De Vleeschouwer, D., Burns, S.J., Matter, A., Claeys, P., Keppens, E., 2013. Mid- to late Holocene Indian Ocean Monsoon variability recorded in four speleothems from Socotra Island, Yemen. Quat. Sci. Rev. 65, 129–142. doi:10.1016/j.quascirev.2013.01.016.

von Rad, U., Burgarth, K.-P., Pervaz, M., Schulz, H., 2002a. Discovery of the Toba Ash (c. 70 ka) in a high-resolution core recovering millennial monsoonal variability off Pakistan. Geol. Soc. London, Spec. Publ. 195, 445–461. doi:10.1144/GSL.SP.2002.195.01.25.

von Rad, U., Delisle, G., Lückge, A., 2002b. Comment - On the formation of laminated sediments on the continental margin off Pakistan. Mar. Geol. 192, 425–429.

von Rad, U., Khan, A.A., Berger, W.H., Rammlmair, D., Treppke, U., 2002c. Varves, turbidites and cycles in upper Holocene sediments (Makran slope, northern Arabian Sea). Geol. Soc. London, Spec. Publ. 195, 387–406. doi:10.1144/GSL.SP.2002.195.01.21.

von Rad, U., Schaaf, M., Michels, K.H., Schulz, H., Berger, W.H., Sirocko, F., 1999a. A 5000-yr Record of Climate Change in Varved Sediments from the Oxygen Minimum Zone off Pakistan, Northeastern Arabian Sea. Quat. Res. 51, 39–53.

von Rad, U., Schulz, H., Riech, V., den Dulk, M., Berner, U., Sirocko, F., 1999b. Multiple monsoon-controlled breakdown of oxygen-minimum conditions during the past 30,000

years documented in laminated sediments off Pakistan. Palaeogeogr. Palaeoclimatol. Palaeoecol. 152, 129–161.

von Rad, U., Schulz, H., SONNE 90 Scientific Party, 1995. Sampling the oxygen minimum zone off Pakistan: glacial-interglacial variations of anoxia and productivity (preliminary results, SONNE 90 cruise). Mar. Geol. 125, 7–19.

Waelbroeck, C., Levi, C., Duplessy, J., Labeyrie, L., Michel, E., Cortijo, E., Bassinot, F., Guichard, F., 2006. Distant origin of circulation changes in the Indian Ocean during the last deglaciation. Earth Planet. Sci. Lett. 243, 244–251. doi:10.1016/j.epsl.2005.12.031.

Wakeham, S.G., Peterson, M.L., Hedges, J.I., Lee, C., 2002. Lipid biomarker fluxes in the Arabian Sea, with a comparison to the equatorial Pacific Ocean. Deep Sea Res. II 49, 2265–2301. doi:10.1016/S0967-0645(02)00037-1.

Wang, J., Yang, B., Ljungqvist, F.C., Zhao, Y., 2013. The relationship between the Atlantic Multidecadal Oscillation and temperature variability in China during the last millennium. J. Quat. Sci. 28, 653-658. doi:10.1002/jqs.2658.

Wang, P., Clemens, S.C., Beaufort, L., Braconnot, P., Ganssen, G., Zhimin, J., Kershaw, P., Sarnthein, M., 2005a. Evolution and variability of the Asian monsoon system: state of the art and outstanding issues. Quat. Sci. Rev. 24, 595–629.

Wang, Y., Cheng, H., Edwards, R.L., He, Y., Kong, X., An, Z., Wu, J., Kelly, M.J., Dykoski, C.A., Li, X., 2005b. The Holocene Asian Monsoon: Links to Solar Changes and North Atlantic Climate. Science 308, 854–857. doi:10.1126/science.1106296.

Wang, Y.J., Cheng, H., Edwards, R.L., An, Z.S., Wu, J.Y., Shen, C.C., Dorale, J.A., 2001. A high-resolution absolute-dated late Pleistocene Monsoon record from Hulu Cave, China. Science 294, 2345–2348. doi:10.1126/science.1064618.

Ward, B.B., Devol, A.H., Rich, J.J., Chang, B.X., Bulow, S.E., Naik, H., Pratihary, A., Jayakumar, A., 2009. Denitrification as the dominant nitrogen loss process in the Arabian Sea. Nature 461, 78–81. doi:10.1038/nature08276.

Webster, P.J., 1987. The Elementary Monsoon, in: Fein, J.S., Stephens, P.L. (Eds.), Monsoons. John Wiley, New York, pp. 3–32.

Wen, R., Xiao, J., Chang, Z., Zhai, D., Xu, Q., Li, Y., Itoh, S., 2010. Holocene precipitation and temperature variations in the East Asian monsoonal margin from pollen data from Hulun Lake in northeastern Inner Mongolia, China. Boreas 39, 262–272. doi:10.1111/j.1502-3885.2009.00125.x.

Wyrtki, K., 1962. The oxygen minima in relation to ocean circulation. Deep Sea Res. 9, 11–23. doi:10.1016/0011-7471(62)90243-7.

Wyrtki, K., 1973. Physical Oceanography of the Indian Ocean, in: Zeitzschel, B. (Ed.), The Biology of the Indian Ocean. Springer, Berlin, pp. 18–36.

Yancheva, G., Nowaczyk, N.R., Mingram, J., Dulski, P., Schettler, G., Negendank, J.F.W., Liu, J., Sigman, D.M., Peterson, L.C., Haug, G.H., 2007. Influence of the intertropical

convergence zone on the East Asian monsoon. Nature 445, 74–77. doi:10.1038/nature05431.

Yang, B., Bräuning, A., Johnson, K.R., Yafeng, S., 2002. General characteristics of temperature variation in China during the last two millennia. Geophys. Res. Lett. 29, doi:10.1029/2001GL014485.

You, Y., 1998. Intermediate water circulation and ventilation of the Indian Ocean derived from water-mass contributions. J. Mar. Res. 56, 1029–1067. doi:10.1357/002224098765173455.

Zhang, P., Cheng, H., Edwards, R.L., Chen, F., Wang, Y., Yang, X., Liu, J., Tan, M., Wang, X., Liu, J., An, C., Dai, Z., Zhou, J., Zhang, D., Jia, J., Jin, L., Johnson, K.R., 2008. A Test of Climate, Sun, and Culture Relationships from an 1810-Year Chinese Cave Record. Science 322, 940–942.

Curriculum vitae

Anna Böll

Born:	02.08.1985 in Hamburg
Nationality:	German
Home address:	Redingskamp 113, 22523 Hamburg

Education

Since May 2011	Ph.D. student, Institute of Geology (section Biogeochemistry) University of Hamburg Thesis subject: Reconstruction of the Holocene monsoon climate variability in the Arabian Sea based on alkenone sea surface temperature, primary productivity and denitrification proxies
Oct 2009 – Jan 2011	Studies of Marine Environmental Sciences (Master of Science) University of Oldenburg Emphasis on Geochemistry Master thesis: Bestimmung des terrestrischen Eintrags von organischem Material in die oberflächennahen Sedimente der Nordsee anhand von Archaeen- und Bakterienlipiden
Oct 2005 – Sep 2009	Studies of Environmental Sciences (Bachelor of Science) University of Oldenburg Emphasis on Environmental Chemistry Bachelor thesis: Dynamik und Zusammensetzung von Bakteriengemeinschaften im Tidezyklus im Wattenmeer
2005	Abitur at Graf Anton Günther Gymnasium Oldenburg

List of Publications

Böll, A., Lückge, A., Munz, P., Forke, S., Schulz, H., Ramaswamy, V., Rixen, T., Gaye, B., Emeis, K.-C., 2014. Late Holocene primary productivity and sea surface temperature variations in the northeastern Arabian Sea: implications for winter monsoon variability. Paleoceanography 29, 778-794. doi:10.1002/2013PA002579.

Böll, A., Schulz, H., Munz, P., Rixen, T., Gaye, B., Emeis, K.-C., submitted 2014. Contrasting sea surface temperature of summer and winter monsoon variability in the northern Arabian Sea over the last 25 ka. submitted to Palaeogeography, Palaeoclimatology, Palaeoecology.

Böll, A., Munz, P., Lückge, A., Schulz, H., Gaye, B., Emeis, K.-C., submitted 2014. Spatial and temporal variability of the Arabian Sea oxygen minimum zone over the Holocene. submitted to Quaternary Science Reviews.

Acknowledgements

I would like to thank Prof. Dr. Kay-Christian Emeis for the supervision of my thesis and for his constant support during the writing process of my manuscripts which greatly improved the quality of this thesis. I also thank for enabling the financial support during the last part of my work that helped me to complete this thesis.

I thank Dr. Birgit Gaye for the opportunity to write this thesis, for supervision, many fruitful scientific discussions and her encouragement, guidance and constant support. I very much appreciate that she were always open for questions and willing to listen to the little problems that emerged during my scientific work. I thank for providing the opportunity to participate in international conferences which offered valuable experiences and provided first insight into the scientific world.

Frauke Langenberg, Sabine Beckmann and Dr. Niko Lahajnar are thanked for their assistance during my laboratory work and analytical measurements.

I thank all my colleagues from the Institute of Geology (formerly Institute of Biogeochemistry and Marine Chemistry) and from the CARIMA project for the nice working atmosphere, their help, discussion and diversion.

I would like to thank the members of the CARIMA project for the good collaboration, data exchange and scientific discussion. A special thanks goes to Dr. Hartmut Schulz and Dr. Andreas Lückge for providing additional sample material and for sample analyses.

Funding of this project by the BMBF is gratefully acknowledged.

Finally I thank all my friends, my boyfriend and family for their consistent support and diversion during the last years.

Eidesstattliche Erklärung

Hiermit erkläre ich an Eides statt, dass ich die vorliegende Dissertationsschrift selbst verfasst

und keine anderen als die angegebenen Quellen und Hilfsmittel benutzt habe.

Hamburg, den _____

                                                           Anna Böll